CORA Cork Open Research Archive
Cartlann Taighde Oscailte Chorcaí

Title	Quantum control of many-particle systems via shortcuts to adiabaticity
Authors	Dowdall, Tom
Publication date	2020-06-19
Original Citation	Dowdall, T. 2020. Quantum control of many-particle systems via shortcuts to adiabaticity. PhD Thesis, University College Cork.
Type of publication	Doctoral thesis
Rights	© 2020, Tom Dowdall. - https://creativecommons.org/licenses/by-nc-nd/4.0/
Download date	2023-05-07 18:02:43
Item downloaded from	http://hdl.handle.net/10468/10493

UCC
University College Cork, Ireland
Coláiste na hOllscoile Corcaigh

University College Cork

University College Cork, Ireland
Coláiste na hOllscoile Corcaigh

Doctoral Thesis

Quantum Control of Many-Particle Systems via Shortcuts to Adiabaticity

Author:

Tom Dowdall

Supervisor:

Dr. Andreas Ruschhaupt

A thesis submitted in fulfillment of the requirements

for the degree of Doctor of Philosophy

in the

Department of Physics

Head of Department: Prof. John McInerney

June 19, 2020

Declaration of Authorship

I, Tom Dowdall, declare that this thesis titled, "Quantum Control of Many-Particle Systems via Shortcuts to Adiabaticity" and the work presented in it are my own. I confirm that:

- This work was done wholly or mainly while in candidature for a research degree at this University.
- Where any part of this thesis has previously been submitted for a degree or any other qualification at this University or any other institution, this has been clearly stated.
- Where I have consulted the published work of others, this is always clearly attributed.
- Where I have quoted from the work of others, the source is always given. With the exception of such quotations, this thesis is entirely my own work.
- I have acknowledged all main sources of help.
- Where the thesis is based on work done by myself jointly with others, I have made clear exactly what was done by others and what I have contributed myself.

Signed:

_____

Date:

_____

"*None so fitted to break the chains as they who wear them, none so well equipped to decide what is a fetter* "

- James Connolly

Abstract

A major barrier for the development of new quantum technologies is fast and robust methods for preparing and manipulating complex quantum states. To date preparation and manipulation of quantum systems has primarily been done using adiabatic processes. These adiabatic processes while robust have significant disadvantages such as their requiring long process times, a further drawback is that the system-environment interaction over these these long process times can lead to loss of coherence of the state of the system. A new area of study to achieve the robustness of adiabatic schemes but in time-scales much shorter is "Shortcuts to Adiabaticity" (STA). These STA techniques provide new methods for the manipulation of quantum systems that achieve high-fidelity state transfers in much shorter times. The aim of this thesis is to use STA and related methods for many particle systems. A method for manipulating a gas of fermions is developed using Pauli blocking and it's robustness in the presence of temperature and different particle number investigated. A novel method for trapping and cooling particles using atom-diode and reflecting atomic mirror is investigated, both the classical and quantum cases are simulated. A method for transporting atoms and condensates across an optical lattice using invariant based inverse engineering is developed. Finally we look at non-hermitian potentials and design particular potentials that result in desirable asymmetries in the transmission and reflection of incident particles.

Acknowledgements

First and foremost I would like to thank my supervisor Dr. Andreas Ruschhaupt for being a constant source of guidance and help, certainly much of this work would not have been completed without him pushing me along. I would like to thank the entire quantum optics gruop in UCC for their encouragement and company over the years, my experience would not quite have been the same without scones with David Rea and the conversations in the main rest with Chris, Guido, Anthony, Imo and Manuel. Further i want to thank my collaborators over the years, a special thanks to Thomas Busch for my visit to OIST and a thanks to the friends i made along the way. Of course I must thank my parents Eileen and Paul for their support, never failing to encourage me through difficult problems and times. I must give special thanks to Megan for her support throughout the PhD and the many happy memories we've shared throughout this time. I thank all my friends for their encouragement and the much needed distraction from academic matters at times. Thank you to my examiners Bryan Kelleher and Verònica Ahufinger. Finally I would like to thank my part time editor and full time cat Lenny who loved to sit on top of my keyboard and notebooks as i wrote the thesis and completed the corrections.

List of Publications

The work in this thesis is based on the following publications

- Tom Dowdall, Albert Benseny, Thomas Busch and Andreas Ruschhaupt,
  Fast and robust quantum control based on Pauli blocking,
  Phys. Rev. A **96**, 043601 (2017)

- T. Dowdall and A. Ruschhaupt,
  Trapping and cooling particles using a moving atom diode and an atomic mirror,
  Phys. Rev. A **97**, 013412 (2018)

- T. Dowdall and A. Ruschhaupt
  Fast and robust moving of atoms through an optical lattice.
  In preperation

- A. Ruschhaupt, T. Dowdall, M. A. Simón and J. G. Muga
  Asymmetric scattering by non-Hermitian potentials,
  EPL **120** 20001 (2017)

Contents

Chapter 1

Introduction

At small scales interesting phenomena occur that are indescribable by classical physics. At this scale the theory of quantum mechanics replaces classical mechanics as a model of particle behaviour, and the quantum nature of objects at this scale gives rise to new opportunities both scientific and technological. In the past forty years there has been immense progress in the ability to isolate and probe quantum mechanics systems, advances range from manipulation and trapping of neutral atoms in optical traps or lattices [1] to Nobel prizes in physics to Eric A. Cornell, Wolfgang Ketterle and Carl E. Wieman [2] for achieving Bose-Einstein condensation in dilute gases, or to Sarge Haroche and David Wineland [3] for ground breaking experimental methods for measuring and manipulating individual quantum systems. These experiments have enabled both the study of fundamental physics such as that of Bose-Einstein condensates, and the development of new techniques of state manipulation that could be used to create new technologies.

Of particular interest for quantum technologies is the quantum computer and quantum simulations [4]. First discussed by Feynmann [5] as a means of simulating quantum systems, quantum computation has grown into a vibrant field. However despite its rapid growth to date there remains many unsolved problems with realising the potential of quantum computers. The advantage of building such a quantum computer is that it will be able to solve certain problems much

quicker than modern classical computers. A necessary requirement for building a quantum computer is the ability to prepare and manipulate complex quantum systems in a robust manner in a short time scale. To achieve the desired robust state preparation and manipulation for quantum computing typically adiabatic protocols have been used examples include manipulating the internal states of an atom using STIRAP [6] or spatial states using SAP [7]. However while adiabatic techniques are stable and enable high fidelities they also take long times to achieve and as such through system-environment interaction the quantum system can decohere losing its quantum properties.

These problems motivate the development of Shortcuts to Adiabaticity (STA) [8, 9]. STA are a number of methods and techniques to speed up preparation and manipulation of quantum states while ensuring the manipulation remains robust and with high fidelity. These STA techniques are advantageous over the ubiquitous adiabatic techniques as they do not have the associated longer process times. Due to the widespread use of adiabatic protocols across many areas of physics, STA has a wide range of applicability.

In this thesis I will apply the Shortcuts to Adiabaticity and related control techniques to achieve a variety of manipulations of many particle systems.

In chapter 2 I will discuss the background theory required for the remainder of the thesis. I will review some common techniques of Shortcuts to Adiabaticity before discussing some of the physics of identical particles and finally I will review the relevant numerical techniques used to obtain the results in this thesis.

In chapter 3, I will develop a method for manipulating large populations of identical fermions in a harmonic trap using the Pauli exclusion principle as a sort of insulation for lower energy fermions in an ensemble. In particular we shall

investigate settings where applying traditional STA methods is difficult such as an anharmonic trapping potential. We study the stability of the scheme versus particle number and temperature effects.

In chapter 4, I will move to considering an atom catcher device, based on earlier research into an atom-diode we proposed a method for trapping and cooling particles. The atom catcher device is a combination of a moving atom-diode with a moving atomic mirror. Particles can enter the atom-diode and mirror from one direction but once confined within it slow down through collisions with the two reflecting walls. This scheme is simulated to demonstrate cooling.

In chapter 5, I look again at STA methods for many particle systems. In particular a scheme for transporting a Bose-Eisntein condensate across an optical lattice using an external harmonic trapping potential is developed. We investigate different shortcut protocols for achieving transport from one lattice site to the next. In one protocol we require both the trap frequency and trap centre to be tuneable and in the other protocol we solely require control of the trap center position.

In chapter 6, we look to develop devices that have asymettric transmission and reflection coefficients. To achieve this we consider non-local non-Hermitian Hamiltonians in one dimension. We derive possible scattering regimes and discuss a variety devices that could be made by designing different potentials for these Hamiltonians.

Finally, in chapter 7, I will provide a summary of the thesis and an outlook for extensions and future work.

Chapter 2

Review of Background Theory

For the control of many particle quantum systems we must first discuss the details of the physics. In this chapter we will review shortcuts to adiabaticity, the underlying physics of many particle systems and the computational techniques that are used in this thesis.

2.1 Shortcuts to Adiabaticity

Our task is the control of quantum systems and we will use the techniques of shortcuts to adiabaticity (STA) to achieve this. Shortcuts to adiabaticity are a collection of techniques to achieve the same fidelities as adiabatic methods but in much shorter times.

Shortcuts to Adiabaticity were first applied to systems such as the manipulation of harmonic traps of single atoms avoiding final excitation [8]; they have has since been applied in many different contexts such as quantum computing [10] and transport or expansion of condensates [11, 12]. First we will outline the adiabatic theorem before discussing the Shortcuts to Adiabaticity technique of inverse engineering via Lewis-Riesenfeld invariants. A more thorough and complete review of Shortcuts to Adiabaticity techniques and applications can be found in [8] and [9].

2.1.1 Adiabatic Theorem

In this section we will discuss the adiabatic theorem of quantum mechanics. Originally discovered by Born and Fock in [13] the theorem states a quantum mechanical system will remain in the instantaneous eigenstate of the system Hamiltonian provided the parameters of the Hamiltonian are varied over sufficiently long timescales allowing the energy gap between close lying states to remain large.

Here we will provide a sketch of the proof of the adiabatic theorem. A more general discussion for Hamiltonians with degenerate spectra is given in [14]. We assume that we have a Hamiltonian $H(t)$ with a discrete and non-degenerate spectrum. Then the eigenstates of the Hamiltonian at any time during the evolution are given by the eigenvalue equation

$$H(t)|\phi_n(t)\rangle = E_n(t)|\phi_n(t)\rangle. \tag{2.1}$$

Throughout the variation of the system's parameters the state evolves according to the time-dependent Schrödinger equation

$$i\hbar\partial_t|\psi(t)\rangle = H(t)|\psi(t)\rangle. \tag{2.2}$$

We can expand the time dependent wavefunction in terms of the of eigenstates the time dependent Hamiltonian in the form $|\psi(t)\rangle = \sum_{n=0}^{\infty} c_n(t)|\phi_n(t)\rangle e^{i\theta_n(t)}$ with $\theta_n(t) = -\frac{1}{\hbar}\int_0^t E_n(t')dt'$ and normalisation $\sum_n |c_n(t)|^2 = 1$. Plugging this into Eq. (2.2) we obtain

$$i\hbar\sum_{n=0}^{\infty}\left[\dot{c}_n(t)|\phi_n(t)\rangle + c_n(t)|\dot{\phi}_n(t)\rangle + ic_n(t)|\phi_n(t)\rangle\dot{\theta}_n(t)\right]e^{i\theta_n} = \sum_{n=0}^{\infty} H(t)c_n(t)|\phi_n(t)\rangle e^{i\theta_n(t)}. \tag{2.3}$$

Combining $\dot{\theta}_n(t) = -\frac{E_n(t)}{\hbar}$ and Eq. (2.1), the $\dot{\theta}_n(t)$ term cancels with the right hand side of Eq (2.3) and then we obtain

$$i\hbar \sum_{n=0}^{\infty} (\dot{c}_n(t)|\phi_n(t)\rangle + c_n(t)|\dot{\phi}_n(t)\rangle) e^{i\theta_n} = 0. \tag{2.4}$$

Now applying $\langle\phi_m(t)|$ to Eq. (2.4) and we obtain

$$\sum_{n=0}^{\infty} \dot{c}_n(t) \underbrace{\langle\phi_m(t)|\phi_n(t)\rangle}_{\delta_{nm}} e^{i\theta_n} = -\sum_{n=0}^{\infty} c_n(t)\langle\phi_m(t)|\dot{\phi}_n(t)\rangle e^{i\theta_n},$$

$$\Rightarrow \dot{c}_m(t) = -\sum_{n=0}^{\infty} c_n(t)\langle\phi_m(t)|\dot{\phi}_n(t)\rangle e^{i(\theta_n-\theta_m)}. \tag{2.5}$$

We can calculate the $\langle\phi_m(t)|\dot{\phi}_n(t)\rangle$ term using Eq. (2.1) and obtain $\langle\phi_m|\dot{H}(t)|\phi_n(t)\rangle + E_m(t)\langle\phi_m|\dot{\phi}_n(t)\rangle = E_n\langle\phi_m(t)|\dot{\phi}_n(t)\rangle$ for $m \neq n$. Plugging this into Eq. (2.5) we obtain

$$\dot{c}_m(t) = -c_m(t)\langle\phi_m(t)|\dot{\phi}_m(t)\rangle + \sum_{n\neq m} c_n \frac{\langle\phi_m(t)|\dot{H}(t)\phi_n(t)\rangle}{E_n - E_m} e^{i(\theta_n-\theta_m)}. \tag{2.6}$$

This result is exact. It can be shown that the second term on the right hand side in Eq. (2.6) vanishes in the limit of $t \to \infty$ i.e. if the parameters of the Hamiltonian $H(t)$ are varied infinitely slowly. The adiabatic approximation is now that we can ignore this second term in Eq. (2.6) so that we are left with

$$\begin{aligned} \dot{c}_m(t) &\approx -c_m\langle\phi_m(t)|\dot{\phi}_m(t)\rangle \\ \Rightarrow c_m(t) &\approx c_m(0)e^{i\gamma_m(t)}, \end{aligned} \tag{2.7}$$

where $\gamma_n(t) = i\int_0^t \langle\phi_m(t')|\dot{\phi}_m(t')\rangle dt'$ is the geometric phase. Now consider we start in the ground state of $H(0)$ and then we have the initial state $|\psi(0)\rangle = |\phi_0(0)\rangle$ where $|\phi_0(0)\rangle$ is the ground state of $H(0)$. Then the solution of the time

dependent Schrödinger equation Eq. (2.2) at time t is $|\psi(t)\rangle \approx e^{i\gamma_0(t)}e^{i\theta_0(t)}|\phi_0(t)\rangle$; we can see that we remain in the instantaneous ground state $|\phi_0(t)\rangle$ of the Hamiltonian $H(t)$ up to a geometric and dynamical phase.

Control techniques based on using the Adiabatic Approximation/Theorem through slow changes of parameters are ubiquitous in quantum control processes, one famous example of the utility of these adiabatic techniques is Stimulated Raman Adiabatic Passage (STIRAP)[6]. However adiabatic methods have some drawbacks, to satisfy the adiabatic approximation the Hamiltonian must vary slowly; not only does this put constraints on how fast we can manipulate a system, it also has the added risk of losing the coherence of the system through interactions with the surrounding environment over the course of the long process times. In the following subsections we will discuss the strengths of the Shortcuts to Adiabaticity method in contrast to adiabatic techniques.

2.1.2 Lewis-Riesenfeld Invariants

As a starting point for Shortcuts to Adiabaticity, let us look at Lewis-Riesenfeld invariants. Consider a system evolving with Hermitian time-dependent Hamiltonian $H(t)$, a Lewis-Riesenfeld invariant [15] is a Hermitian operator $I(t)$ that satisfies the following equation,

$$\frac{dI(t)}{dt} = i\hbar\frac{\partial I(t)}{\partial t} - [H(t), I(t)] = 0. \tag{2.8}$$

We will show in the following that the eigenvalues of this operator $I(t)$ are time independent. Let

$$I(t)|\varphi_n(t)\rangle = \lambda_n|\varphi_n(t)\rangle \tag{2.9}$$

with $\langle\varphi_m|\varphi_n\rangle = \delta_{m,n}$. Now differentiate Eq. (2.9) with respect to t

$$\partial_t I(t)|\varphi_n\rangle + I\partial_t|\varphi_n\rangle = \partial_t\lambda_n|\varphi_n\rangle + \lambda_n\partial_t|\varphi_n\rangle. \tag{2.10}$$

We now take the inner product of this expression with $\langle\varphi_n|$

$$\langle\varphi_n|\partial_t I(t)\varphi_n\rangle + \lambda_n\langle\varphi_n|\partial_t\varphi_n\rangle = \partial_t\lambda_n\langle\varphi_n|\varphi_n\rangle + \lambda_n\langle\varphi_n|\partial_t\varphi_n\rangle.$$

So we obtain the expression

$$\partial_t\lambda_n = \langle\varphi_n|\partial_t I(t)\varphi_n\rangle.$$

Now operating on Eq. (2.8) with $|\varphi_n\rangle$ from the right

$$i\hbar\partial_t I(t)|\varphi_n\rangle - H(t)I(t)|\varphi_n\rangle + I(t)H(t)|\varphi_n\rangle = 0.$$

Taking the inner product with $\langle\varphi_n|$ from the left we obtain

$$\begin{aligned}\langle\varphi_n|\partial_t I(t)\varphi_n\rangle - \langle\varphi_n|H(t)I(t)|\varphi_n\rangle + \langle\varphi_n|I(t)H(t)|\varphi_n\rangle = \\ \langle\varphi_n|\partial_t I(t)\varphi_n\rangle - E_n\langle\varphi_n|I(t)\varphi_n\rangle + E_n\langle\varphi_n|I(t)\varphi_n\rangle\end{aligned}$$

$$\langle\varphi_n|\partial_t I(t)\varphi_n\rangle = \partial_t\lambda_n = 0$$

It follows the above Eq. (2.8) that the eigenvalues of $I(t)$ are time independent and we can write

$$\Rightarrow i\hbar\partial_t(I(t)|\psi\rangle) = H(I(t)|\psi\rangle).$$

Further we can write arbitrary solutions of the time-dependent Schrödinger equation Eq. (2.2) using orthonormal states of the invariant $I(t)$

$$|\Psi(t)\rangle = \sum_{n=0}^{\infty} c_n|\psi_n(t)\rangle, \qquad |\psi_n(t)\rangle = e^{i\alpha_n(t)}|\varphi_n(t)\rangle$$

with

$$I(t) = \sum_{n=0}^{\infty} |\varphi_n(t)\rangle\lambda_n\langle\varphi_n(t)|.$$

The c_n are time independent amplitudes, λ_n are real valued and the $\alpha_n(t)$ is the Lewis-Riesenfeld phase given by

$$\alpha_n(t) = \frac{1}{\hbar}\int_0^t \langle\phi_n(t')|i\hbar\partial_{t'} - H(t')|\phi_n(t')\rangle dt'.$$

Lewis-Riesenfeld invariants were first used in a direct manner to solve the time dependent Schrödinger equation. This approach is reversed in Shortcuts to Adiabaticity and instead we combine the Lewis-Riesenfeld invariants with inverse engineering to achieve fast and robust manipulations of quantum systems.

2.1.3 Invariant based inverse engineering

Instead of the direct approach of using the Lewis-Riesenfeld invariants to solve the time dependent Schrödinger equation here we do the process in reverse. To underline the differences between this method and adiabatic control methods consider the following two scenarios:

(a) Adiabatic evolution

- We vary some paramaters in a given Hamiltonian $H(t)$ such that the state at initial time follows the instantaneous eigenstates of $H(t)$ until some final time where the population is in the corresponding eigenstate of final the Hamiltonian $H(t_f)$.

(b) Inverse engineering

- We also vary some paramaters in a given Hamiltonian $H(t)$. Here the key difference is we don't seek to follow the instantaneous eigenstates of $H(t)$. Instead we follow instantaneous eigenstates of $I(t)$ and this allows for transitions between eigenstates of the Hamiltonian $H(t)$ during evolution but with the condition that we arrive in the desired eigenstate of $H(t_f)$ at final time.

This method corresponds to engineering the time evolution operator to be

$$U = \sum_n e^{i\alpha_n(t)} |\phi_n(t)\rangle\langle\phi_n(0)|. \tag{2.11}$$

where the $|\phi_n\rangle$ are eigenstates of the invariant $I(t)$. From this expression we can derive the Hamiltonian $\partial_t U = \frac{1}{i\hbar} H(t)U(t)$. By applying $U^\dagger$ from the right we obtain $H(t) = i\hbar \dot{U} U^\dagger$. We want to ensure we start and end in eigenstates of $H(t)$ so must ensure that the eigenstates of the invariant $I(t)$ coincide with those of the Hamiltonian $H(t)$ at initial and final times i.e. they commute at initial and final times.

$$[H(t_f), I(t_f)] = [H(0), I(0)] = 0. \tag{2.12}$$

Explicitly we consider a system with Hamiltonian $H(t)$ that we can tune through some control functions (*e.g. this could be the frequency of a harmonic trap or centre of a trap*). We start in some state of the Hamiltonian $H(0)$ and want to finish in a desired state of the Hamiltonian $H(t_f)$, we derive the invariant $I(t)$ from Eq. (2.8) and finally we derive the boundary conditions on the control functions of $H(t)$ from the commutation relations in Eq.(2.12).

Lewis and Riesenfeld in their seminal paper [15] paid particular attention to the time dependent harmonic oscillator. Later Lewis and Leach [16] along with Dhara and Lawande [17] considered more general quadratic in momentum invariants of the form

$$H = \frac{p^2}{2m} + V(q,t). \tag{2.13}$$

They showed that if a potential $V(q,t)$ has form

$$V(q,t) = -F(t)q + \frac{1}{2}m\omega(t)^2 q^2 + \frac{1}{\rho(t)^2} U\left[\frac{q - q_c(t)}{\rho(t)}\right] \tag{2.14}$$

then the Hamiltonian admits an invariant of the form

$$I(t) = \frac{1}{2m}[\rho(p - m\dot{q}_c) - m\dot{\rho}(q - q_c)]^2 + \frac{1}{2}m\omega_0^2\left(\frac{q - q_c}{\rho}\right)^2 + U\left(\frac{q - q_c}{\rho}\right). \quad (2.15)$$

The ω_0 is a constant and q_c, ω, F and ρ are arbitrary functions of time that must satisfy the auxiliary equations

$$\ddot{\rho} + \omega^2(t)\rho = \frac{\omega_0^2}{\rho^3}, \quad (2.16)$$

$$\ddot{q} + \omega^2(t)q_c = \frac{F(t)}{m}. \quad (2.17)$$

Let us consider two simple examples in detail to demonstrate how this inverse-engineering works.

2.1.4 Example: STA for the expansion of a harmonic trap

First consider a particle in the ground state of a harmonic trap, at initial time $t = 0$ we have the particle trapped state with frequency ω_0 and at final time we want to expand the trap to frequency ω_f. We want to transition from the ground state of the trap with harmonic frequency ω_0 to the ground state with harmonic frequency ω_f, this problem is considered in [18]. The Hamiltonian of such a system is given by

$$H(t) = \frac{\hat{p}^2}{2m} + \frac{1}{2}m\omega(t)^2\hat{x}^2. \quad (2.18)$$

The Hamiltonian of this system is in the class of Hamiltonians with potentials described by Eq. (2.14). The Hamiltonian in Eq. (2.18) has corresponding invariant $I(t)$ as in Eq. (2.15) given by

$$I(t) = \frac{1}{2m}(\rho\hat{p} - m\dot{\rho}\hat{x})^2 + \frac{1}{2}m\omega_0^2\left(\frac{x}{\rho}\right)^2. \quad (2.19)$$

Looking at the Ermakov Eqns. (2.16)(2.17) we can set $q_c = F = 0$ as there's no linear dependence on $\hat{x}$ and we only need to consider

$$\ddot{\rho} + \omega^2(t)\rho = \frac{\omega_0^2}{\rho^3}. \tag{2.20}$$

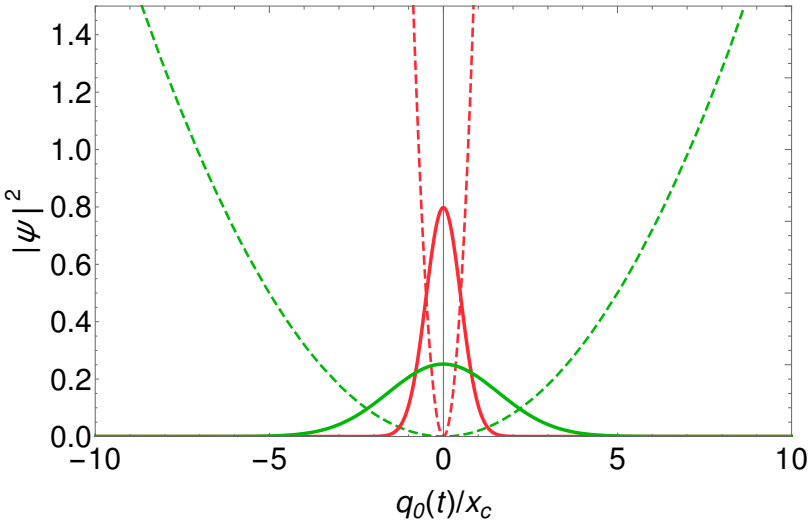

FIGURE 2.1: Expansion of a harmonic trap, initial and final trap and wave function: The dashed lines represent the trapping potential $V(t)$, the dashed red line is the trap at $t = 0$ and the green is at $t = t_f$. The solid lines are the corresponding ground states of the trap at initial and final times, the red is at time $t = 0$ and the green at time $t = t_f$.

A schematic of the initial and final trap and the relevant wave functions at initial and final times is given in Fig. 2.1 in terms of the characteristic length for a harmonic oscillator $x_c = \sqrt{\hbar/m\omega_0}$. To achieve the desired state change from ground state of the trap with frequency ω_0 to ground state of the trap with frequency ω_f we must ensure that the invariant and Hamiltonian commute at initial and final times, see Eq. (2.12). Let us derive the boundary conditions

using Eqs. (2.18) and (2.19), first we will evaluate the commutator,

$$\begin{aligned}
[H(t), I(t)] &= \left[\frac{\hat{p}^2}{2m} + \frac{1}{2}m\omega^2\hat{x}^2, \frac{1}{2m}(\rho\hat{p} - m\dot{\rho}\hat{x})^2 + \frac{1}{2}m\omega_0^2\left(\frac{x}{\rho}\right)^2\right] \\
&= \frac{1}{2m}\left(\left[\hat{p}^2, \frac{1}{2m}(\rho\hat{p} - m\dot{\rho}\hat{x})^2\right] + \left[\hat{p}^2, \frac{1}{2}m\omega_0^2\left(\frac{\hat{x}}{\rho}\right)^2\right]\right) \\
&+ \left(\left[\hat{x}^2, \frac{1}{2m}(\rho\hat{p} - m\dot{\rho}\hat{x})^2\right] + \left[\hat{x}^2, \frac{1}{2}m\omega_0^2\left(\frac{\hat{x}}{\rho}\right)^2\right]\right) \\
&= \frac{1}{4}\left[\hat{p}^2, \hat{x}^2\right]\left\{m\dot{\rho}^2 + \frac{1}{\rho^2}\omega_0^2 - \omega^2\rho^2\right\} + \frac{m}{2}\rho\dot{\rho}\left\{\frac{1}{m}([\hat{p}^2, \hat{x}\hat{p}] \right. \\
&+ \left.\left[\hat{p}^2, \hat{p}\hat{x}\right]) + m\omega^2(\left[\hat{x}^2, \hat{x}\hat{p}\right] + \left[\hat{x}^2, \hat{p}\hat{x}\right])\right\}. \qquad (2.21)
\end{aligned}$$

We first calculate the different commutators

$$\left[\hat{p}^2, \hat{x}^2\right] = -2i\hbar(\hat{x}\hat{p} + \hat{p}\hat{x}), \qquad (2.22)$$

$$\left[\hat{p}^2, \hat{x}\hat{p}\right] = \left[\hat{p}^2, \hat{p}\hat{x}\right] = -2i\hbar\hat{p}^2, \qquad (2.23)$$

$$\left[\hat{x}^2, \hat{x}\hat{p}\right] = \left[\hat{x}^2, \hat{p}\hat{x}\right] = 2i\hbar\hat{x}. \qquad (2.24)$$

So plugging these results into Eq. (2.21) we get the expression

$$\begin{aligned}
[H(t), I(t)] = \frac{1}{2}i\hbar(\hat{x}\hat{p} + \hat{p}\hat{x})\left\{\dot{\rho}^2 + \frac{1}{\rho^2}\omega_0^2 - \omega^2\rho^2\right\} \\
+2i\hbar m\rho\dot{\rho}\left\{\frac{\hat{p}^2}{m} + m\omega^2\hat{x}^2\right\}. \qquad (2.25)
\end{aligned}$$

Now we impose the condition in Eq. (2.12) *i.e. to achieve the desired expansion from the ground state of* $H(0)$ *to the ground state of* $H(t_f)$ from which the following boundary conditions are derived

$$\rho(0) = 1, \qquad \rho(t_f) = \sqrt{\frac{\omega_0}{\omega_f}},$$
$$\dot{\rho}(0) = 0, \qquad \dot{\rho}(t_f) = 0.$$

From Eq. (2.20) we can set $\omega(0) = \omega_0$, $\omega(t_f) = \omega_f$ and we have $\ddot{\rho}(0) = 0$ and

$\ddot{\rho}(t_f) = 0$. Now we pick a $\rho(t)$ that satisfies these boundary conditions, here we choose a polynomial function

$$\rho(t) = 6(t/t_f)^5 \left(\sqrt{\frac{\omega_0}{\omega_f}} - 1\right) - 15(t/t_f)^4 \left(\sqrt{\frac{\omega_0}{\omega_f}} - 1\right) + 10(t/t_f)^3 \left(\sqrt{\frac{\omega_0}{\omega_f}} - 1\right) + 1. \tag{2.26}$$

We can solve for $\omega(t)$

$$\omega^2(t) = \frac{\omega_0^2}{\rho^4} - \frac{\ddot{\rho}}{\rho}. \tag{2.27}$$

Now by substituting the chosen $\rho(t)$ from Eq. (2.26) into Eq. (2.27) we can find $\omega(t)$. In principle the t_f can be arbitrarily small, however there is experimental considerations to take account of: for very short time scales the transient energy excitation may be too large making the scheme impossible to implement (particle leaving the trap), further for short time scales we may get imaginary values of ω which will make the harmonic trap a repeller which again may pose experimental difficulties requiring very quick and precise control of trap frequency. Plotted in Fig. 2.2 are the functions $(\omega(t/t_f)/\omega_0)^2$ for $t_f = 1/\omega_0, 2/\omega_0, 5/\omega_0$. We see for $t_f = 1/\omega_0$ and $t_f = 2\omega_0$ that for a duration of time the harmonic trap becomes a harmonic repeller.

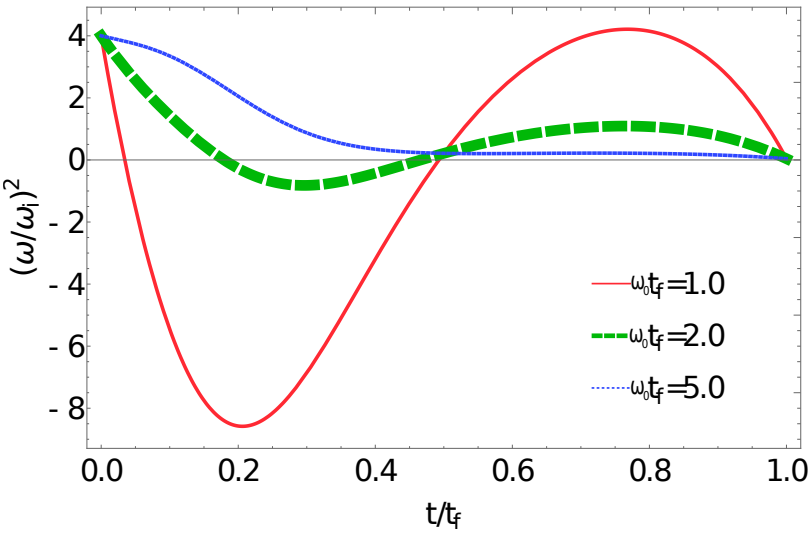

FIGURE 2.2: Expansion of a harmonic trap, different control functions $\omega(t)$ for different final t_f values.

Now to investigate how well the control protocol works we need to consider the fidelity of the process, which we define as

$$\mathcal{F} = \left| \langle \psi(t_f) | \phi_{\text{ideal}} \rangle \right|^2. \tag{2.28}$$

Here the $|\psi(t)\rangle$ is the wave function after expansion and the $|\phi_{\text{ideal}}\rangle$ is the target ground state of the Hamiltonian $H(t_f)$. In Fig. 2.3 the fidelity $\mathcal{F}$ versus the final time $t_f\omega_0$ is plotted for both the adiabatic and shortcut protocols. For the comparative adiabatic scheme we used the function

$$\omega(t) = (\omega_f - \omega_0) \sin\left(\frac{t\pi}{2t_f}\right)^2 + \omega_0. \tag{2.29}$$

As expected we see the shortcut scheme achieves perfect fidelities even for very short final times $t_f\omega_0$. This is in contrast to the adiabatic scheme in Eq. (2.29)) which takes until $\omega_0 t_f \geq 12$ before it achieves fidelities of $\mathcal{F} \geq 0.95$. Both approaches work for transferring any eigenstate of the initial Hamiltonian $H(0)$ to the corresponding eigenstate of the final Hamiltonian $H(t_f)$, however the STA approach achieves the desired fidelities much faster.

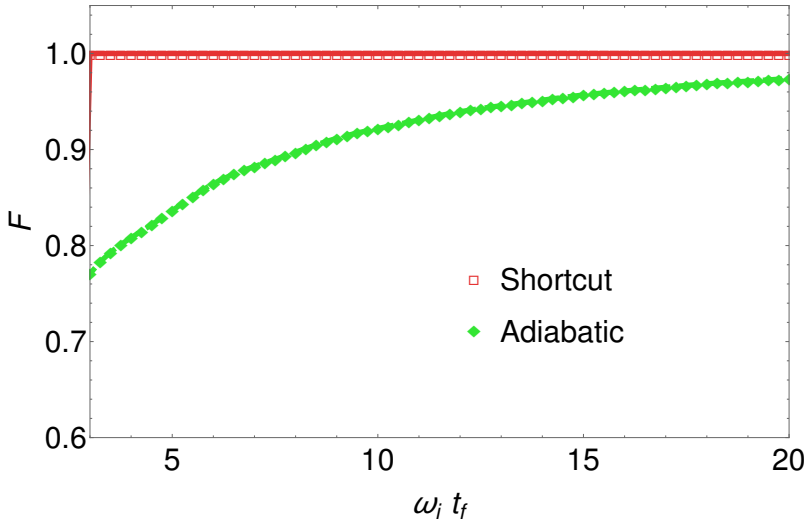

FIGURE 2.3: Expansion of a harmonic trap, fidelity $\mathcal{F}$ versus final time $t_f\omega_0$: The red squares are the shortcut scheme given by Eq. (2.27) and the green diamonds are the adiabatic scheme given by Eq. (2.29).

2.1.5 Example: Transport of a harmonic trap

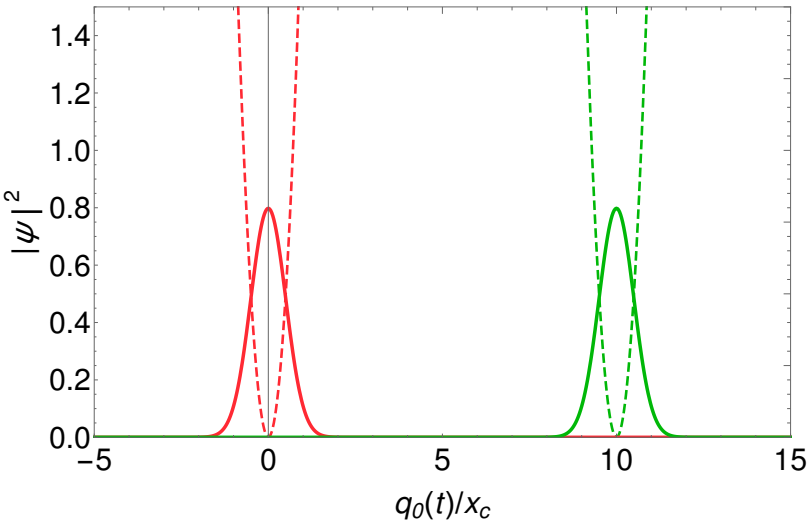

FIGURE 2.4: Transport of a harmonic trap, initial and final trap and wavefunction: The dashed lines represent the trapping potential $V(t)$, the dashed red line is the trap at $t = 0$ and the green is at $t = t_f$. The solid lines are the corresponding ground states of the trap at initial and final times, the red is at time $t = 0$ and the green at time $t = t_f$ wavefunction.

Here again consider a particle in a harmonic trap, a schematic of the system is seen in Fig. 2.4 using the length unit $x_c = \sqrt{\hbar/m\omega}$. The goal now is to move the harmonic trap from some initial point $q_0(0)$ at time $t = 0$ to $q_0(t_f)$ at final time $t = t_f$ while remaining in the ground state of the trap. This system is considered in more detail in [19]. The Hamiltonian of this system is

$$H(t) = \frac{\hat{p}^2}{2m} + \frac{1}{2}m\omega^2(x - q_0(t))^2, \tag{2.30}$$

which is again a special case of the Hamiltonian in Eq. (2.13) with $F(t)/m = \omega^2 q_0$. Looking at the auxiliary Eqns. (2.16) and (2.17) we can set $\rho(t) = 1$ so we only have to consider one of the equations

$$\ddot{q}_c(t) + \omega(q_c(t) - q_0(t)) = 0. \tag{2.31}$$

The derivation of the boundary conditions on the auxiliary function $q_c(t)$ and its derivatives are determined in a similar manner to the boundary conditions derivation in section 2.1.4 i.e. imposing $[I(0), H(0)] = [I(t_f), H(t_f)] = 0$. This gives us the conditions $q_c(0) = q_0(0), q_c(t_f) = q_0(t_f)$ along with $\dot{q}_c(0) = \ddot{q}_c(0) = \dot{q}_c(t_f) = \ddot{q}_c(t_f) = 0$. We now pick a $q_c(t)$ such that it fits these boundary conditions, here we will choose a polynomial of minimal degree

$$\begin{aligned} q_c(t) = q_0(0) - \quad & 6(t/t_f)^5(q_0(0) - q_0(t_f)) + 15(t/t_f)^4(q_0(0) - q_0(t_f)) \\ & -10(t/t_f)^3(q_0(0) - q_0(t_f)). \end{aligned} \tag{2.32}$$

We now rewrite the above Eq. (2.31) to get an explicit expression for $q_0(t)$

$$q_0(t) = \frac{\ddot{q}_c(t)}{\omega} + q_c(t). \tag{2.33}$$

In Fig. 2.5 we have plotted the different $q_0(t)$ functions for different values of t_f. We see for shorter values of t_f the trap has to move outside of the interval $[q_0(0), q_0(t_f)]$ which may not be desirable. However these will still obtain perfect fidelities.

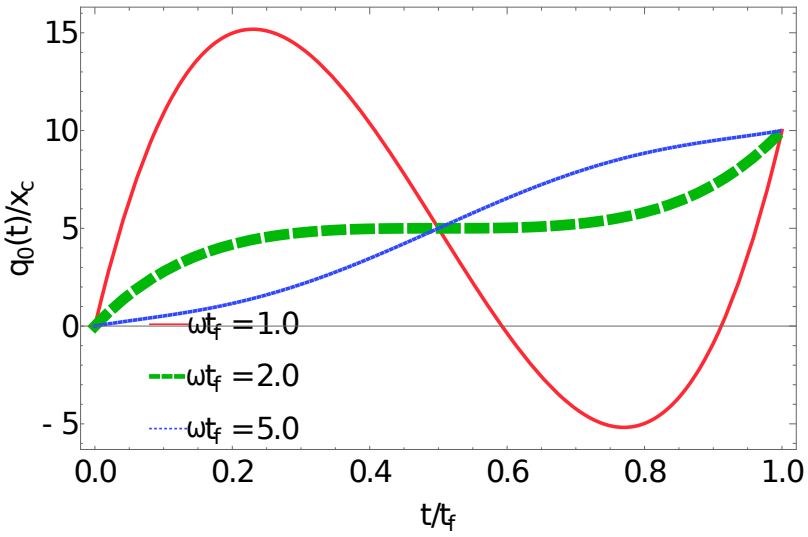

FIGURE 2.5: Transport of a harmonic trap, different $q_0(t)$ schemes for different final t_f values.

Here we have used a simple trigonometric function for the adiabatic protocol. We vary the position by

$$q_0(t) = (q_0(tf) - q_0(0)) \sin\left(\frac{t\pi}{2t_f}\right)^2 + q_0(0). \tag{2.34}$$

We define the fidelity $\mathcal{F}$ the same as in the previous section. In Fig 2.6 we have plotted the fidelity $\mathcal{F}$ versus final time $t_f\omega$. Again we see that for arbitrarily short times the shortcut scheme achieves perfect fidelity. This is in contrast to the adiabatic scheme which takes until about $\omega t \geq 12$ to achieve a fidelity of $\mathcal{F} \geq 0.95$ for all longer t_f. We are able to achieve better fidelities with STA than the adiabatic case for short time scales.

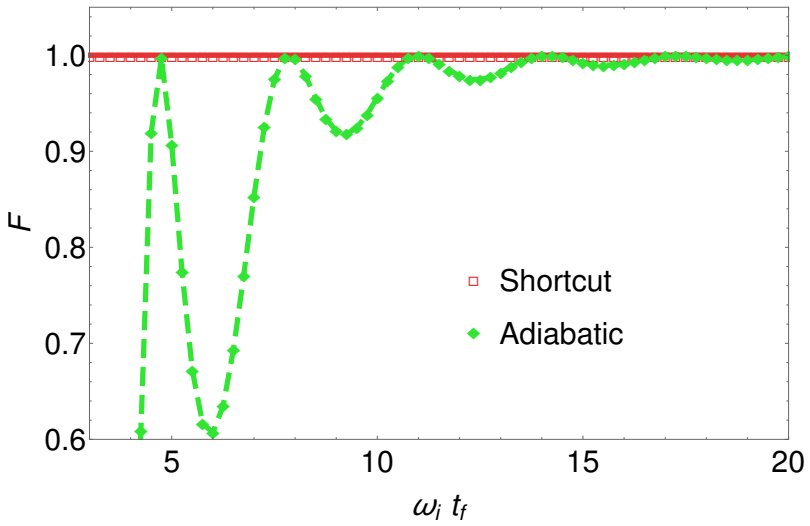

FIGURE 2.6: Transport of a harmonic trap, fidelity $\mathcal{F}$ v t_f: The red squares are the shortcut scheme given by Eq. (2.33) and the green diamonds are the adiabatic scheme given by Eq. (2.34).

2.2 Many Particle Physics

In this section we will now discuss the physics of many particle systems. We will discuss identical particles, Bosons and Fermions along with their statistics.

2.2.1 Identical Particles

Here we will follow the discussion in [20]. It is useful to first consider the differences between identical particles in classical and quantum mechanics

(a) Classical identical particles

In classical physics two identical particles can be distinguished by their past trajectories. That is to say for example, if you have two identical classical objects then they have well defined trajectories. Through tracking these trajectories we can distinguish between two identical classical objects.

(b) Quantum identical particles

However in quantum mechanics we do not have this same ability to tell which identical particle is which, because particles in quantum mechanics do not have a well defined "trajectory" that we can track to distinguish particles from one another.

Now consider two indistinguishable particles, we perform some experiment where we measure the positions of the particles in some state specified by quantum numbers n_1 and the other particle in state n_2. Due to the fact that the two particles are indistinguishable we can not say that particle 1 is in state n_1 and particle 2 in state n_2 or vice versa. Instead we have the constraint that

$$|\psi(n_1, n_2)\rangle = \alpha|\psi(n_2, n_1)\rangle \tag{2.35}$$

where α is any complex number. We obtain this constraint from the fact that the two states must be physically equivalent, and this is only possible if they differ by a global phase as when being measured $|\psi(n_1, n_2)|^2 = |\psi(n_2, n_1)|^2$.

As such imposing the condition in Eq. (2.35) we see that if we take the vector

$$|\psi(n_1, n_2)\rangle = \gamma|n_1 n_2\rangle + \lambda|n_2 n_1\rangle$$

where the ket $|n_i n_j\rangle$ represents particle 1 in state i and particle 2 in state j, then from Eq. (2.35) we obtain

$$\gamma|n_1 n_2\rangle + \lambda|n_2 n_1\rangle = \alpha\left(\gamma|n_2 n_1\rangle + \lambda|n_1 n_2\rangle\right). \tag{2.36}$$

Now if we equate the coefficients of $|n_1 n_2\rangle$ and $|n_2 n_1\rangle$ we get the relations

$$\gamma = \alpha\lambda \quad , \quad \lambda = \alpha\gamma$$

$$\alpha = \pm 1, \tag{2.37}$$

$$\lambda = \frac{1}{\sqrt{2}}. \tag{2.38}$$

From this result we can see that there exists two different possible states

$$|\psi(n_1 n_2)\rangle = \frac{1}{\sqrt{2}}(|n_1 n_2\rangle + |n_2 n_1\rangle) \qquad \text{(Symmetric)} \tag{2.39}$$

and

$$|\psi(n_1 n_2)\rangle = \frac{1}{\sqrt{2}}(|n_1 n_2\rangle - |n_2 n_1\rangle). \qquad \text{(Anti-symmetric)} \tag{2.40}$$

We call the state in Eq. (2.39) the symmetric states and the state in Eq. (**??**) the anti-symmetric states because under exchange of the quantum numbers n_1 and n_2 the symmetric state stays the same but the anti-symmetric state is changed by a factor of -1. We make the following assertion: **A given particle species must be either symmetric or anti-symmetric.** Consider if this statement was not true. Then the Hilbert space would have linear combinations of symmetric and anti-symmetric states which are then neither symmetric or

anti-symmetric. The particles with symmetric states are referred to as **Bosons** and the ones with anti-symmetric states are called **Fermions**.

Properties

- Particles with integer spin are bosons.
- Particles with half integer spin are fermions [21].

From Eq.(2.40) we can derive a fundamental property of fermions. We have some state specified by quantum numbers n_1 and n_2

$$|\Psi_F\rangle = \frac{1}{\sqrt{2}}\left(|n_1 n_2\rangle - |n_2 n_1\rangle\right)$$

where for example n could refer to energy level in a given system, if we set $n_1 = n_2$ then we obtain

$$|\Psi_F\rangle = \frac{1}{2}\left(|n_1 n_1\rangle - |n_1 n_1\rangle\right) = 0.$$

The above results it the *Pauli exclusion principle*, it tells us that two fermions cannot occupy the exact same quantum state. This result will be used to speed up manipulations of many particle fermion systems in Chapter 3. The same is not true of Bosons, for Bosons the above scenario of identical particles becomes

$$|\Psi_B\rangle = \frac{1}{2}\left(|n_1 n_1\rangle + |n_1 n_1\rangle\right) = |n_1 n_1\rangle.$$

At low temperatures these differences become particularly prominent, the fermionic particles don't share identical states and the Bosons condense into a single state. Next we will discuss the differences in statistics of these two particle types.

Particle-Statistics

Consider an ideal gas of non interacting fermionic or bosonic particles specified by occupation numbers $N_1, N_2, \ldots, N_i, \ldots$ of single particle states with corresponding energies $\epsilon_1 \leq \epsilon_2 \leq \ldots$. The number of particles N is given by $\sum_i N_i$ and the gas has energy $E = \sum_i N_i \epsilon_i$. The grand partition function of the system is given by

$$\begin{aligned} Z = \sum_{N_i} e^{\beta(\mu N - E)} &= \underbrace{\left\{ \sum_{N_1} e^{\beta(\mu-\epsilon_1)N_1} \right\}}_{Z_1} \underbrace{\left\{ \sum_{N_2} e^{\beta(\mu-\epsilon_2)N_2} \right\}}_{Z_2} \ldots \\ &= \prod_{i=1}^{\infty} Z_i \end{aligned} \tag{2.41}$$

For bosons we have no restriction on how many particles can occupy a given state and so each occupation number N_i is summed from 0 to ∞, the same is not true of fermions. As discussed earlier fermions obey the Pauli exclusion principle and as such the occupation number N_i must be either 0 or 1. The Gibbs distribution gives the probability of finding N_1 particles in the single particle state 1, N_2 particles in state 2, etc,

$$p_N = p(N_1, N_2, \ldots) = \frac{\exp\{\beta\Big(\mu(\sum_i N_i) - \sum_i N_i \epsilon_i\Big)\}}{Z} = \frac{\prod_{i=1}^{\infty} e^{\beta(\mu-\epsilon_i)N_i}}{\prod_{i=1}^{\infty} Z_i}.$$

$$p(N_1, N_2, \ldots) = \prod_{i=1}^{\infty} p_i(N_i) \tag{2.42}$$

where the $p_i(N_i)$ are given by

$$p_i(N_i) = \frac{e^{\beta(\mu-\epsilon_i)N_i}}{Z_i}. \tag{2.43}$$

Here we can see the differences between fermions and bosons. Consider a single particle state, for Fermi-Dirac statistics ($N_i = 0, 1$) we have

$$Z_i = 1 + e^{\beta(\mu-\epsilon_i)}. \tag{2.44}$$

For Bose-Einstein statistics the partition function in Eq. (2.41) is a geometric series that converges for $\mu < \epsilon_i$ and this inequality must hold for all energy states. Provided this condition is satisfied the Z_i converges to

$$Z_i = \frac{1}{1 - e^{\beta(\mu-\epsilon_i)}}. \tag{2.45}$$

The differences between these two particles and their statistics is most noticeable at low temperatures. Bosons tend to all condense into a single ground state at very low temperatures; this is called Bose-Einstein condensation. This characteristic is not found in systems of fermions where at low temperatures fermions tend to occupy all the lower energy states up to the fermi-level.
From Eqs. (2.41) and (2.42) we can calculate the mean occupation number of the i^{th} single particle state

$$\bar{N}_i = \sum_{N_i} N_i p_i(N_i) = \frac{1}{\beta}\left(\frac{\partial \ln Z_i}{\partial \mu}\right)_{T,V} = \frac{1}{e^{\beta(\epsilon_i-\mu)} \pm 1}, \tag{2.46}$$

where the plus is for the Fermi-Dirac distribution and the minus for the Bose-Einstein distribution. Summing over all these states we obtain the total mean number of particles in the system

$$N = \sum_{i=1}^{\infty} \bar{N}_i = \sum_{i=1}^{\infty} \frac{1}{e^{\beta(\epsilon_i-\mu)} \pm 1}. \tag{2.47}$$

2.2.2 Bose-Einstein Condensation

In this subsection we will discuss Bose-Einstein condensation and derive the conditions required for Bose-Einstein condensation, for more detail see [22]. Consider a gas of massive spinless Bosons in a box of volume V, the total number of particles is given by Eq. (2.47)

$$N = \sum_i \frac{1}{e^{\beta(\varepsilon_i - \mu)} - 1}. \tag{2.48}$$

For Bose gasses where the lowest lying energy level corresponds to $\epsilon = 0$ we have the dispersion relation $E = p^2/2m$ where $p = \hbar k$. The chemical potential μ must be negative $\mu < 0$ as otherwise the energy level $E = 0$ would have to be infinite or negative occupation. When approximating the sum in Eq. (2.48) by an integral we must take care to include the first $\epsilon = 0$ term. If we do not the $\epsilon = 0$ state will have no weighting (*i.e.* $f(0) = 0$ *in Eq. 2.50*) in the integral.

$$N = \underbrace{\frac{1}{e^{-\beta\mu} - 1}}_{N_0} + \underbrace{\int_0^\infty \frac{f(\varepsilon)d\varepsilon}{e^{\beta(\varepsilon-\mu)} - 1}}_{N_{\epsilon>0}}, \tag{2.49}$$

where N_0 is the population of the ground $\epsilon_0 = 0$ state, and $N_{\epsilon>0}$ is the population of all the remaining states with $\varepsilon > 0$. The $f(\varepsilon)d\varepsilon$ here is the energy density of states and is given by

$$f(\varepsilon)d\varepsilon = \frac{V(2m)^{3/2}}{(2\pi)^2\hbar^3}\sqrt{\varepsilon}d\varepsilon. \tag{2.50}$$

We can plug this into the $N_{\epsilon>0}$ term and calculating the integral we obtain

$$N_{\epsilon>0} = \frac{V}{2\pi^2}\left(\frac{m}{2\beta\hbar^2\pi}\right)^{3/2} Li_{3/2}(e^{\beta\mu}), \tag{2.51}$$

$$\frac{N_{\varepsilon>0}}{V}\left(\frac{2\beta\hbar^2\pi}{m}\right)^{3/2} = Li_{3/2}(e^{\beta\mu}), \tag{2.52}$$

where $Li_a(b)$ is the polylogarithmic function. Now consider holding the particle density N/V constant. Then as T is lowered $|\mu|$ must increase ($\mu < 0$), otherwise

for low values of T the ground state N_0 would not be heavily occupied. This equation then defines a minimum temperature for which $\mu \to 0$

$$T_c = \frac{2\pi\hbar^2}{mk_B}\left(\frac{N}{\zeta(3/2)V}\right)^{2/3}. \tag{2.53}$$

Below temperature T_c the number of particles in the $\epsilon > 0$ states is given by

$$N_{\epsilon>0} = \frac{V2\hbar^2\pi\zeta(3/2)}{k_b T m} \tag{2.54}$$

and the total particle number is given by

$$N = \frac{V2\hbar^2\pi\zeta(3/2)}{k_b T_c m}. \tag{2.55}$$

So we can write the fraction of the particles in the ground state as

$$\frac{N_0}{N} = \frac{N - N_0}{N} = 1 - \left(\frac{T}{T_c}\right)^{3/2}. \tag{2.56}$$

We see in Eq. (2.56) that as the temperature T continues to be cooled further and further below T_c that the population of of the ground state grows. This occupation of the ground state is called **Bose-Einstein condensation**, this effect comes purely from the symmetry properties of Bosons discussed in section 2.2.1. Bose-Einstein condensation was first predicted in 1925 by Albert Einstein building upon the work of Satyendra Nath Bose. The first condensation of bosons was achieved seventy years later in 1995 at the University of Colorado Boulder by Eric Cornell and Carl Wieman new cooling techniques developed such as laser and evaporative cooling, early experiments achieved condensation of dilute gases of rubidium, lithium and sodium [23, 24, 25] and culminated in Nobel prizes for E. Cornell, C. Wieman and W. Ketterle [2]. Bose-Einstein condensates have been loaded onto optical lattices generated by two detuned counter-propagating lasers, allowing the simulation and study of many body

systems with applications in condensed matter physics. Typically the gases used to make a Bose-Einstein condensate are dilute and they have to be cooled to exceptionally low temperatures to observe the quantum effects this is, in contrast to denser systems such as solids and liquids. Of particular interest is how to achieve cooling to such low temperatures, which we will discuss now.

Evaporative cooling

Here we will mostly follow the discussion in [26]. The idea behind evaporative cooling is simple, a trapped gas has its trap depth decreased allowing the higher energy particles to escape the rest of the sample is then allowed to thermalise reducing the temperature of the gas. These higher energy particles carry away a significant amount of kinetic energy from the sample leaving the remaining trapped sample cooled. This is not dissimilar to cooling a liquid by blowing on it. First developed for use producing condensates it allows for otherwise unachievable low temperatures to be reached [27]. This is typically achieved by reducing the depth of the trapping potential, higher energy particles are then capable of escaping the trapping potential while lower energy ones remain trapped. Following an example in [26] consider a trapped atomic gas with average total atomic energy given by ε. We take the average energy of any given evaporated particle to be $(1+\beta)\varepsilon$ and then the change this induces in the average energy of the gas may be obtained from the conservation of the total energy of all the particles. Then the change in energy from some number of evaporated particles is given by

$$(1+\beta)\varepsilon dN, \tag{2.57}$$

where $dN < 0$ is the change in number of particles in the gas. Through the energy conservation the total energy of the gas remaining in the trap is $E + (1+\beta)\varepsilon dN$ where the number of particles remaining in the trap is $N + dN$ (for

evaporation dN is negative). The average energy of the gas in the trap after evaporation is given by

$$\varepsilon + d\varepsilon = \frac{E + (1+\beta)\varepsilon dN}{N + dN}. \tag{2.58}$$

If β is independent of N then we can solve this differential equation with solution

$$\frac{\varepsilon}{\varepsilon(0)} = \left(\frac{N}{N(0)}\right)^{\beta}, \tag{2.59}$$

where $\varepsilon(0)$ and $N(0)$ are the initial average energy and particle number in the trapped gas. This is a simple model that doesn't discuss the relationship between the average energy of the sample and its temperature.

Gross-Piteavskii Equation

In this thesis we will be discussing Bose-Einstein condensates that can be modelled by the Gross-Piteavskii equation (GP-Eqn) [28, 29]. The GP-Eqn describes the condensed part of a bosonic gas close to zero temperature which has a scattering length a is less than the average spacing between particles in the gas. It is derived assuming that all the interactions between particles in the condensate can be modelled by an average interaction term with interaction strength g. The GP-Eqn requires that interactions between the particles in the gas are either rare, as in dilute condensates or alternatively that the interaction strength between particles in the gas itself is weak. This equation is valid for many experiments where particle density at the centre of the gas is about $10^{13} - 10^{15}$ cm^{-3}, much less dense than air at room temperature on earth [26]. To derive it we assume that the many particle wave function Ψ can be written as a product of single particle wave functions ϕ, that is

$$\Psi(\mathbf{x_1}, \ldots, \mathbf{x_n}) = \prod_{\mathbf{i=1}}^{\mathbf{N}} \phi(\mathbf{x_i}) \tag{2.60}$$

where the single particle wave functions are normalised in the regular way $\int d\mathbf{x}|\phi(\mathbf{x})|^{\mathbf{2}} = \mathbf{1}$. This $\Psi(\mathbf{x_1}, \ldots, \mathbf{x_N})$ does not account for any interaction in the system, and these interaction terms will be taken care of by an effective interaction term $g\delta(\mathbf{x} - \mathbf{x}')$. The Hamiltonian of such a system is given by

$$H = \sum_{i=1}^{N} \left(\frac{\mathbf{p_i}}{2m} + V(\mathbf{x_i}) \right) + g \sum_{i<j} \delta(\mathbf{x_i} - \mathbf{x_j}). \tag{2.61}$$

The corresponding energy expectation value of the above Hamiltonian is

$$E = N \int d\mathbf{x} \left(\frac{\hbar^2}{2m} |\nabla\phi(\mathbf{x})|^2 + V(\mathbf{x})|\phi(\mathbf{x})|^2 + \frac{N-1}{2} g|\phi(\mathbf{x})|^4 \right) \tag{2.62}$$

and assuming that N is sufficiently large we can approximate this last term simply as $\frac{1}{2}Ng \int d\mathbf{x}|\phi(\mathbf{x})|^{\mathbf{4}}$, now for simplicity in notation let us introduce a wave function $\psi(\mathbf{x})$ of the condensate defined as

$$\psi(\mathbf{x}) = \sqrt{N}\phi(\mathbf{x}), \tag{2.63}$$

then we can rewrite the equation Eq. (2.62) as

$$E = \int d\mathbf{x} \left(\frac{\hbar^2}{2m} |\nabla\psi(\mathbf{x})|^2 + V(\mathbf{x})|\psi(\mathbf{x})|^2 + \frac{1}{2} g|\psi(\mathbf{x})|^4 \right). \tag{2.64}$$

Now using standard methods from the calculus of variations [30] we minimise the functional E in Eq. (2.64) with respect to $\psi(\mathbf{x})$ and its conjugate $\psi^\star(\mathbf{x})$ preserving the particle number

$$N = \int dx|\psi(\mathbf{x})|^{\mathbf{2}}. \tag{2.65}$$

After variation we obtain the time-independent Gross Piteavskii equation

$$\left(\frac{\hat{\mathbf{p}}^2}{2m} + V(\mathbf{x}) + g|\psi(\mathbf{x})|^2 \right) \psi(\mathbf{x}) = \mu\psi(\mathbf{x}) \tag{2.66}$$

We can immediately see that Eq. (2.66)has the form of the Schrödinger equation, except with non-linear term $g|\psi(x)|^2$ that accounts of the inter-particle interaction within the gas of bosons. Another difference from the Schrödinger equation is that here the eigenvalue is the chemical potential as opposed to the energy in the usual Schrödinger equation. When considering dynamical problems we use the corresponding time dependent Gross-Piteavksii equation given by,

$$i\hbar\partial_t\psi(\mathbf{x},t) = \left(\frac{\hat{\mathbf{p}}^2}{2m} + V(\mathbf{x},t) + g|\psi(\mathbf{x},t)|^2\right)\psi(\mathbf{x},t). \tag{2.67}$$

Eq. (2.67) can be derived by a similar process using the calculus of variations, and it is used to study the dynamics of condensates.

2.3 Computational Methods

To achieve accurate simulations of many particle quantum systems we needed a variety of different computational methods. This collection of numerical techniques allows for the simulation of such systems. In this section the different techniques used in this thesis to obtain the numerical results will be discussed.

2.3.1 Split Operator method

We consider the time-dependent Schrödinger equation,

$$i\hbar\partial_t|\psi(t)\rangle = H(t)|\psi(t)\rangle = (T + V(t))\,|\psi(t)\rangle, \tag{2.68}$$

where $T = \frac{p^2}{2m} = -\frac{\hbar^2}{2m}\nabla^2$ in the position basis. If we first consider the time-independent case where $V(t) = V$ then we can formally write the solution to Eq. (2.68) with

$$|\psi(t)\rangle = \exp\left\{-\frac{iHt}{\hbar}\right\}|\psi(0)\rangle. \tag{2.69}$$

If we take some small time interval denoted by Δt and expand the exponential term we obtain

$$\begin{aligned}\exp\left\{-\frac{iH\Delta t}{\hbar}\right\} &= 1 - i\frac{\Delta t(T+V)}{\hbar} - \frac{\Delta t^2(T+V)^2}{2\hbar^2} + \mathcal{O}(\Delta t^3) \\ &= 1 + 2\left(\frac{i\Delta t}{2\hbar}V - \frac{\Delta t^2}{4\hbar^2}V^2\right) - \left(\frac{i\Delta t}{\hbar}T - \frac{\Delta t^2}{2\hbar^2}T^2\right) \\ &\quad - \frac{\Delta t^2}{2\hbar^2}(VT+TV) + \mathcal{O}(\Delta t^3) \\ &= \exp\left\{-\frac{iV\Delta t}{2\hbar}\right\}\exp\left\{-\frac{iT\Delta t}{\hbar}\right\}\exp\left\{-\frac{iV\Delta t}{2\hbar}\right\} \\ &\quad + \mathcal{O}(\Delta t^3). \end{aligned} \tag{2.70}$$

This splitting in Eq. (2.70) has an error of order Δt^3 and for sufficiently small time steps any terms of order higher than Δt^2 are negligible. It is also interesting to note this splitting is advantageous over a more "naive"

$$\exp\left\{-\frac{iH\Delta t}{\hbar}\right\} = \exp\{iT\Delta t/\hbar\}\exp\{iV\Delta t/\hbar\} + \mathcal{O}(\Delta t^2). \tag{2.71}$$

We can immediately see why this splitting in Eq. (2.70) is useful for numerical calculations. The operators T and V have simple representations (they just act as multiplications) in the momentum and position bases respectively. Using fast fourier transforms (FFT) we can take advantage of the simplicity of the T and V operators in their respective bases.

We would like to extend this approach to the case of time-dependent Hamiltonians so that we can simulate a much larger class of systems. Inspired by the time independent case we approximate the time evolution operator in a similar manner. Over a time interval Δt we approximate the time evolution operator

by

$$\mathcal{T}\exp\left\{-\frac{i}{\hbar}\int_{t_0}^{t_0+\Delta t}H(s)ds\right\}\approx \exp\left\{-\frac{iV_l\Delta t}{2\hbar}\right\}\exp\left\{-\frac{iT\Delta t}{\hbar}\right\}\exp\left\{-\frac{iV_l\Delta t}{2\hbar}\right\}+\mathcal{O}(\Delta t^3) \tag{2.72}$$

where

$$V_l=\frac{V(t_0+\Delta t)+V(t_0)}{2} \tag{2.73}$$

is an average value across the time interval Δt of the potential. The actual time evolution operator is given by the Dyson series

$$\mathcal{T}\exp\left\{-\frac{i}{\hbar}\int_{t_0}^{t+\Delta t}(T+V(t))\,ds\right\}=1-\frac{i}{\hbar}\int_{t_0}^{t_0+\Delta t}(T+V(t_1))\,dt_1 -\frac{1}{\hbar^2}\int_{t_0}^{t_0+\Delta t}\int_{t_0}^{t_1}(T+V(t_1))\,(T+V(t_2))\,dt_2dt_1 +\mathcal{O}(\Delta t^3). \tag{2.74}$$

Provided the chosen Δt is small enough we can approximate these integrals using the trapezoidal rule (i.e. $\int_a^b f(x)dx=\frac{1}{2}f(a)+f(b)(b-a)$). Apply the trapezoidal rule to the integrals in Eq. (2.74)

$$\int_{t_0}^{t_0+\Delta t}V(t_1)dt_1=V_l\Delta t+\mathcal{O}(\Delta t^3) \tag{2.75}$$

and

$$\int_{t_0}^{t_0+\Delta t}\int_{t_0}^{t_1}TV(t_2)dt_2dt_1= \frac{1}{2}\int_{t_0}^{t_0+\Delta t}T\{V(t_1)+V(t_0)\}(t_1-t_0)dt_1+\mathcal{O}(\Delta t^3) =\frac{\Delta t^2}{2}TV_l+\mathcal{O}(\Delta t^3) \tag{2.76}$$

and

$$\int_{t_0}^{t_0+\Delta t}\int_{t_0}^{t_1}V(t_1)Tdt_2dt_1\approx\frac{\Delta t^2}{2}V(\Delta t+t_0)T+\mathcal{O}(\delta t^3) \tag{2.77}$$

and

$$\int_{t_0}^{t_0+\Delta t}\int_{t_0}^{t_1} V(t_1)V(t_2)dt_2dt_1 \approx \int_{t_0}^{t_0+\Delta t} V(t_1)\left\{\frac{V(t_1)+V(t_0)}{2}\right\}(t_1-t_0)dt_1 \\ +\mathcal{O}(\Delta t^3) \\ = \frac{\Delta t^2}{4}\left\{V(t_0+\Delta t)^2 + V(t_0+\Delta t)V(t_0)\right\} + \mathcal{O}(\Delta t^3). \tag{2.78}$$

Putting all these integrals together we can rewrite the Dyson series in Eq. (2.74) as

$$\mathcal{T}\exp\left\{-\frac{i}{\hbar}\int_{t_0}^{t+\Delta t} H(s)ds\right\} \approx 1 - \frac{i\Delta t}{\hbar}(T+V_l) - \frac{\Delta t^2}{2}\Bigg(T^2 + \frac{1}{2}V(t_0+\Delta t)^2 \\ +V(t_0+\Delta t)T + TV_l + \frac{1}{2}V(t_0+\Delta t)V(t_0)\Bigg) + \mathcal{O}(\Delta t)^3, \\ = 1 - i\frac{\Delta t}{\hbar}(T+V_l) - \frac{\Delta t^2}{2\hbar^2}\left(T^2 + V_l^2 + TV_l + V_lT\right) + \mathcal{O}(\Delta t^3), \tag{2.79}$$

Now we can compare this expression with the one in Eq. (2.74) expanding the exponential terms,

$$\begin{aligned}\exp\left\{-\frac{iV_l\Delta t}{2\hbar}\right\}\exp\left\{-\frac{iT\Delta t}{\hbar}\right\}\exp\left\{-\frac{iV_l\Delta t}{2\hbar}\right\} \\ \approx\ & 1 - i\frac{\Delta t(T+V_l)}{\hbar} - \frac{\Delta t^2(T+V_l)^2}{2\hbar^2} + \mathcal{O}(\Delta t^3) \\ =\ & 1 - i\frac{\Delta t}{\hbar}(T+V_l) - \frac{\Delta t^2}{2\hbar^2}\left(T^2 + V_l^2 + TV_l + V_lT\right) \\ +\ & \mathcal{O}(\Delta t^3).\end{aligned} \tag{2.80}$$

Through comparison of Eqs. (2.79) and (2.80) we can see that the error between them is of order Δt^3. Provided we have a small enough Δt this should be negligible as the terms proportional to Δt^3 can be neglected. As discussed earlier the particular strength of this method lies in the fact that in momentum and position space the T and V operators respectively are simple multiplications.

2.3.2 Quantum Trajectories

In this section we will discuss a method for numerically solving master equations called the Quantum Trajectories approach which will be used in Chapter 4. First we can write the master equation describing the time evolution of an open quantum system as

$$\frac{\partial}{\partial t}\rho(t) = \mathcal{L}(\rho(t)) \tag{2.81}$$

where $\mathcal{L}$ here is a linear super operator that maps operators to operators. Now we split $\mathcal{L}$ into a time dependent $\mathcal{J}(t)$ part and a time independent part $\mathcal{L}_0$

$$\frac{\partial}{\partial t}\rho(t) = (\mathcal{L}_0 + \lambda\mathcal{J}(t))\rho(t). \tag{2.82}$$

We assume that $\rho(t)$ is of the form

$$\rho(t) = e^{\mathcal{L}_0 t}\tilde{\rho}(t), \tag{2.83}$$

and plugging this into Eq. (2.82) we obtain

$$\frac{\partial}{\partial t}\rho(t) = \mathcal{L}_0\rho(t) + e^{\mathcal{L}_0 t}\frac{\partial}{\partial t}\tilde{\rho}(t) = (\mathcal{L}_0 + \lambda\mathcal{J}(t))\rho(t). \tag{2.84}$$

Looking at the time dependent part of the equation we can see

$$\frac{\partial}{\partial t}\rho(t) = \lambda e^{-\mathcal{L}_0 t}\mathcal{J}e^{\mathcal{L}_0 t}\rho(t). \tag{2.85}$$

From here the process is very similar to deriving Dyson series in quantum mechanics, we integrate Eq. (2.85) and multiply by $e^{\mathcal{L}_0 t}$ to obtain

$$\rho(t) = e^{\mathcal{L}_0 t}\rho(0) + \lambda\int_0^t e^{\mathcal{L}(t-t_1)}\mathcal{J}(t_1)\rho(t_1)dt_1. \tag{2.86}$$

We now repeat the same steps iteratively for $\rho(t_i)$ $i = 1 \ldots \infty$

$$\rho(t) = \sum_{i=0}^{\infty} \lambda^i \int_0^t dt_i \ldots \int_0^{t_{i-1}} dt_1 \Big\{ e^{\mathcal{L}_0(t-t_i)} \mathcal{J}(t_i) e^{\mathcal{L}_0(t_i - t_{i-1})} \ldots \mathcal{J}(t_1) e^{\mathcal{L}_0 t_1} \Big\} \rho(0). \tag{2.87}$$

Letting

$$\rho_{\mathcal{T}}(t_1, \ldots, t_i) = \left\{ e^{\mathcal{L}_0(t-t_i)} \mathcal{J}(t_i) e^{\mathcal{L}_0(t_i - t_{i-1})} \ldots \mathcal{J}(t_1) e^{\mathcal{L}_0 t_1} \right\} \rho(0). \tag{2.88}$$

We can write Eq. (2.88) in a simpler looking form

$$\rho(t) = \sum_{i=0}^{\infty} \lambda^i \int_0^t dt_1 \ldots \int_0^{t_{i-1}} dt_i \rho_{\mathcal{T}}(t). \tag{2.89}$$

The $\rho_{\mathcal{T}}(t)$ are like the trajectories of the system and the $\mathcal{J}(t_i)$ are like "jumps" occurring at times t_i, these for example could be spontaneous emission. Let's now turn our attention to the system in Chapter 5, which is described by the master equation

$$\begin{aligned} \frac{\partial}{\partial t}\rho(t) &= -\frac{i}{\hbar}\left[\hat{H}_{3L}(t), \rho(t)\right] - \frac{\gamma}{2}\left\{\rho(t)|3\rangle\langle 3| + |3\rangle\langle 3|\rho(t)\right\} \\ &+ \gamma|2\rangle\langle 3|\rho(t)|3\rangle\langle 2|. \end{aligned} \tag{2.90}$$

Using the method developed above we can set $\lambda = 1$ and so

$$\mathcal{L}_0\rho(t) = -\frac{i}{\hbar}\left[H_{3L}, \rho(t)\right] - \frac{\gamma}{2}\left\{\rho(t)|3\rangle\langle 3| + |3\rangle\langle 3|\rho(t)\right\}, \tag{2.91}$$

$$\mathcal{J}\rho(t) = \gamma|2\rangle\langle 3|\rho(t)|3\rangle\langle 2|. \tag{2.92}$$

We can see now why the $\mathcal{J}$ is referred to as a jump as it describes a jump from state $|3\rangle$ to $|2\rangle$. For the system in Chapter 5 we assume that we start in some pure state $\rho(0) = |\psi(0)\rangle\langle\psi(0)|$ and before the first jump it stays in some pure

state then we can write

$$\begin{aligned}\frac{\partial}{\partial t}\rho(t) &= \mathcal{L}_0\rho(t) = -\frac{i}{\hbar}\left[H_{3L},\rho(t)\right] - \frac{\gamma}{2}(\rho(t)|3\rangle\langle 3| + |3\rangle\langle 3|\rho(t)) \\ &= \left(-\frac{i}{\hbar}H_{3L} - \frac{\gamma}{2}|3\rangle\langle 3|\right)\rho(t) + \rho(t)\left(\frac{i}{\hbar}H_{3L} - \frac{\gamma}{2}|3\rangle\langle 3|\right) \end{aligned} \quad (2.93)$$

$$\begin{aligned}\frac{\partial}{\partial t}\left(|\psi(t)\rangle\langle\psi(t)|\right) = &\left(-\frac{i}{\hbar}H_{3L} - \frac{\gamma}{2}|3\rangle\langle 3|\right)|\psi(t)\rangle\langle\psi(t)| \\ &+|\psi(t)\rangle\langle\psi(t)|\left(\frac{i}{\hbar}H_{3L} - \frac{\gamma}{2}|3\rangle\langle 3|\right)\end{aligned} \quad (2.94)$$

Since the state of the system remains pure then we can equivalently solve the corresponding Schrödinger-like equation

$$i\hbar\frac{\partial}{\partial t}|\psi(t)\rangle = \underbrace{\left(H_{3L} - \frac{i\gamma\hbar}{2}|3\rangle\langle 3|\right)}_{\tilde{H}}|\psi(t)\rangle, \quad (2.95)$$

with solution

$$|\psi(t)\rangle = e^{-it\tilde{H}/\hbar}|\psi(0)\rangle. \quad (2.96)$$

it is important to note here that $\tilde{H}$ is non-hermitian and so the time-evolution is non unitary and the norm is not preserved. Rather, it decays. Now lets turn our attention to the "jump" in the equation.

$$\mathcal{J}\rho(t) = \gamma|2\rangle\langle 3|\rho(t)|3\rangle\langle 2| = \gamma|2\rangle\langle 3|\psi(t)\rangle\langle\psi(t)|3\rangle\langle 2| = \mathcal{J}_{3\to 2}|\psi\rangle\langle\psi|\mathcal{J}_{3\to 2}^{\dagger} \quad (2.97)$$

We can see from above that the "jump" operator keeps ρ in a pure state. Here $\mathcal{J}_{3\to 2}$ is given by

$$\mathcal{J}_{3\to 2} = \sqrt{\gamma}|2\rangle\langle 3|$$

We can now write the $\rho(t)$ operator as follows

$$\rho(t) = \sum_{i=0}^{\infty} \lambda^i \quad \int_0^t dt_i \dots \int_0^{t_{i-1}} dt_1 \Big\{ e^{-i\tilde{H}(t-t_i)/\hbar} \mathcal{J}_{1/2} e^{-i\tilde{H}(t_i-t_{i-1})/\hbar} \dots \mathcal{J}_{1/2} e^{-i\tilde{H}t_1/\hbar} |\psi(0)\rangle \Big\}$$
$$\Big\{ \langle\psi(0)| e^{-i\tilde{H}t_1/\hbar} \mathcal{J}_{1/2}^\dagger e^{-i\tilde{H}(t_2-t_3)/\hbar} \dots \mathcal{J}_{1/2}^\dagger e^{-i\tilde{H}(t-t_i)/\hbar} \Big\}. \tag{2.98}$$

We now have to average about all the trajectories of the system using the following algorithm discussed in [31]

Quantum Trajectories Algorithm

1. Firstly initialise some state at $t = 0$, $|\psi(0)\rangle$ normalised appropriately $||\psi(0)\rangle||^2 = 1$.

2. A random number is then chosen from the interval $r \in [0, 1]$.

3. $|\psi(t)\rangle$ is time evolved according to the Schrödinger-like equation

$$i\hbar \frac{\partial}{\partial t} |\psi(t)\rangle = \underbrace{(H_{3L} - \frac{i\gamma\hbar}{2} |3\rangle\langle 3|)}_{\tilde{H}} |\psi(t)\rangle, \tag{2.99}$$

   until time t_1 which is given by

$$1 - ||\psi(t_1)||^2 = \int_0^{t_1} \langle\psi(s)| J_{3\to 2}^\dagger J_{3\to 2} \psi(s)\rangle ds = r \tag{2.100}$$

   where the $\int_{t_0}^{t_1} \langle\psi(s)| J_{1/2}^\dagger J_{1/2} \psi(s)\rangle ds$ is the probability of a jump occurring during the time interval $t = t_0$ to t_1.

4. The system after the jump is in state $|2\rangle$ and the wave function is renormalised and the time evolution then continues with the new post jump Hamiltonian.

5. We then repeat the same process starting from step 2 of picking a new random number r except this time we replace t_0 with t_1

6. After sufficiently many iterations we will reach $t = t_f$ and we then renormalise the state a final time.

7. Finally we sum over a large N of the final states, as an approximate solution to Eq. (2.98)

$$\rho(t) \approx \frac{1}{N} \sum_{i=1}^{N} |\psi_i(t_f)\rangle\langle\psi_i(t_f)|. \tag{2.101}$$

2.3.3 Imaginary Time Evolution

Here we turn our attention towards a numerical technique for finding the ground states of an arbitrary stationary Hamiltonian H. This is particularly useful for dealing many particle interacting systems. Explicitly we assume we have some Hamiltonian H and we introduce some trial wave function that we will write as

$$|\psi_{trial}(0)\rangle = \sum_{n=0}^{\infty} c_n |\phi_n\rangle \tag{2.102}$$

where the $|\phi_n\rangle$ are the unknown energy eigenstates of H with unknown ordered energy levels $E_0 < E_1 < \dots$. Evolving these in time gives

$$|\psi_{trial}(t)\rangle = e^{-iHt/\hbar}|\psi_{trial}(0)\rangle \tag{2.103}$$

$$= \sum_{n=0}^{\infty} c_n e^{-iE_n t/\hbar}|\phi_n\rangle. \tag{2.104}$$

Now consider the variable transformation $\tau = it$, $\tau \in \mathbb{R}$, switching the time to imaginary so we can write

$$|\psi_{trial}(\tau)\rangle = \sum_{n=0}^{\infty} c_n e^{-E_n \tau/\hbar}|\phi_n\rangle. \tag{2.105}$$

Immediately we can see from Eq. (2.105) that during time propagation all the bound states of the Hamiltonian H decay at a rate proportional to their energy.

To see this more clearly we can re-write Eq. (2.105) as Eq. (2.106)

$$|\psi_{trial}(t)\rangle = c_0 e^{-E_0\tau}\left(|\phi_0\rangle + \sum_{n=1}^{\infty}\frac{c_n}{c_0}e^{-\tau(E_n-E_0)}|\phi_n\rangle\right). \tag{2.106}$$

This process of course doesn't preserve the norm of the wavefunction and so to ensure that we obtain the ground state $|\phi_0\rangle$ after enough iterations we must ensure that we renormalise the wavefunction after each time step. This method ensures that we obtain the ground state of the Hamiltonian H so long as we started with a trial wavefunction that had some overlap with the ground state.

Chapter 3

Fast and robust quantum control based on Pauli blocking

3.1 Abstract

Coherent quantum control over many-particle quantum systems requires high fidelity dynamics. One way of achieving this is to use adiabatic schemes where the system follows an instantaneous eigenstate of the Hamiltonian over timescales that do not allow transitions to other states. This, however, makes control dynamics very slow. Here we introduce another concept that takes advantage of preventing unwanted transitions in fermionic systems by using Pauli blocking: excitations from a protected ground state to higher-lying states are avoided by adding a layer of *buffer* fermions, such that the *protected* fermions cannot make a transition to higher lying excited states because these are already occupied. This allows to speed-up adiabatic evolutions of the system. We do a thorough investigation of the technique, and demonstrate its power by applying it to high fidelity transport, trap expansion and splitting in ultracold atoms systems in anharmonic traps. Close analysis of these processes also leads to insights into the structure of the orthogonality catastrophe phenomenon.

This chapter is based on the following publication:

Tom Dowdall, Albert Benseny, Thomas Busch and Andreas Ruschhaupt,

Fast and robust quantum control based on Pauli blocking,

Phys. Rev. A **96**, 043601 (2017)

I derived the expressions for fidelity of the process along with performing the calculations of the fidelities for the different manipulations considered. Albert Benseny and Thomas Busch contributed in the discussion, in particular of the orthogonality catastrophe. Albert Benseny produced the initial program for simulating the system dynamics, these were then altered and re-written by both myself and Andreas Ruschhaupt. All authors contributed to the writing of the manuscript.

3.2 Introduction

Preparation of and coherent control over many-particle quantum states requires quantum engineering techniques that lead to high fidelities. Adiabatic processes, where the system follows an eigenstate of the time-dependent Hamiltonian, are known to allow for this; however they require that the Hamiltonian is varied sufficiently slowly in order to avoid transitions to other eigenstates [32]. This leads to long process times and leaves the system vulnerable to decoherence, reducing also the possible repetition rates of the process.

How quickly or slowly an eigenstate can be followed depends roughly on the distance to the next closest-lying eigenstate [32]. Therefore, one strategy for expediting adiabatic processes is to adjust the instantaneous speed of the process with respect to the size of the instantaneous level gap such that the transition probability to unwanted eigenstates remains small during the whole process [33, 34, 35]. This, however, requires the knowledge of the energy eigenspectrum during the whole process.

In recent years, a number of techniques to speed up adiabatic processes have been developed under the name "shortcuts to adiabaticity" [8, 36]. One example of these techniques relies on the implementation of an additional counter-diabatic Hamiltonian, which is designed to compensate for any excitations that appear during the finite time evolution process, such that the system does not leave the eigenstates of the original Hamiltonian [37, 38, 39]. However, this additional Hamiltonian can be very complicated and thus be demanding to implement experimentally. Other shortcut techniques are based on Lewis–Riesenfeld invariant inverse engineering [18], which allow for a fast transfer of all initial eigenstates simultaneously to all final eigenstates (up to a phase).

Generalizing these techniques to many particle systems is not a straightforward task, as the number of degrees of freedom increases exponentially with larger particle numbers. The effects of this are well known and can be seen immediately when considering one of the most simple systems possible, namely an ideal, spin-polarized, one-dimensional Fermi gas at low temperatures: even in the presence of almost perfect single-particle process fidelities, the overlap between two many-particle wavefunctions scales with $N^{-\alpha}$, where α depends on the specific nature of the change between the initial and final Hamiltonian [40]. This is the so-called orthogonality catastrophe (OC) [41, 42], which has recently been examined for systems of ultracold fermions [43, 44]

Here, however, we show that this behavior does not necessarily limit the engineering of many-particle states, as the OC does not affect all states inside a Fermi sea in the same way. In fact, one can always find a kernel of particles that is essentially unperturbed, and whose size scales with the overall number of particles. This is due to the fact that transitions inside the Fermi sea are forbidden by the Pauli exclusion principle and lead to the so-called Pauli blocking, which has recently been examined to engineer cold atomic systems [45, 46, 47, 48, 49].

In this work we will consider a system of trapped, ultracold, spin-polarized

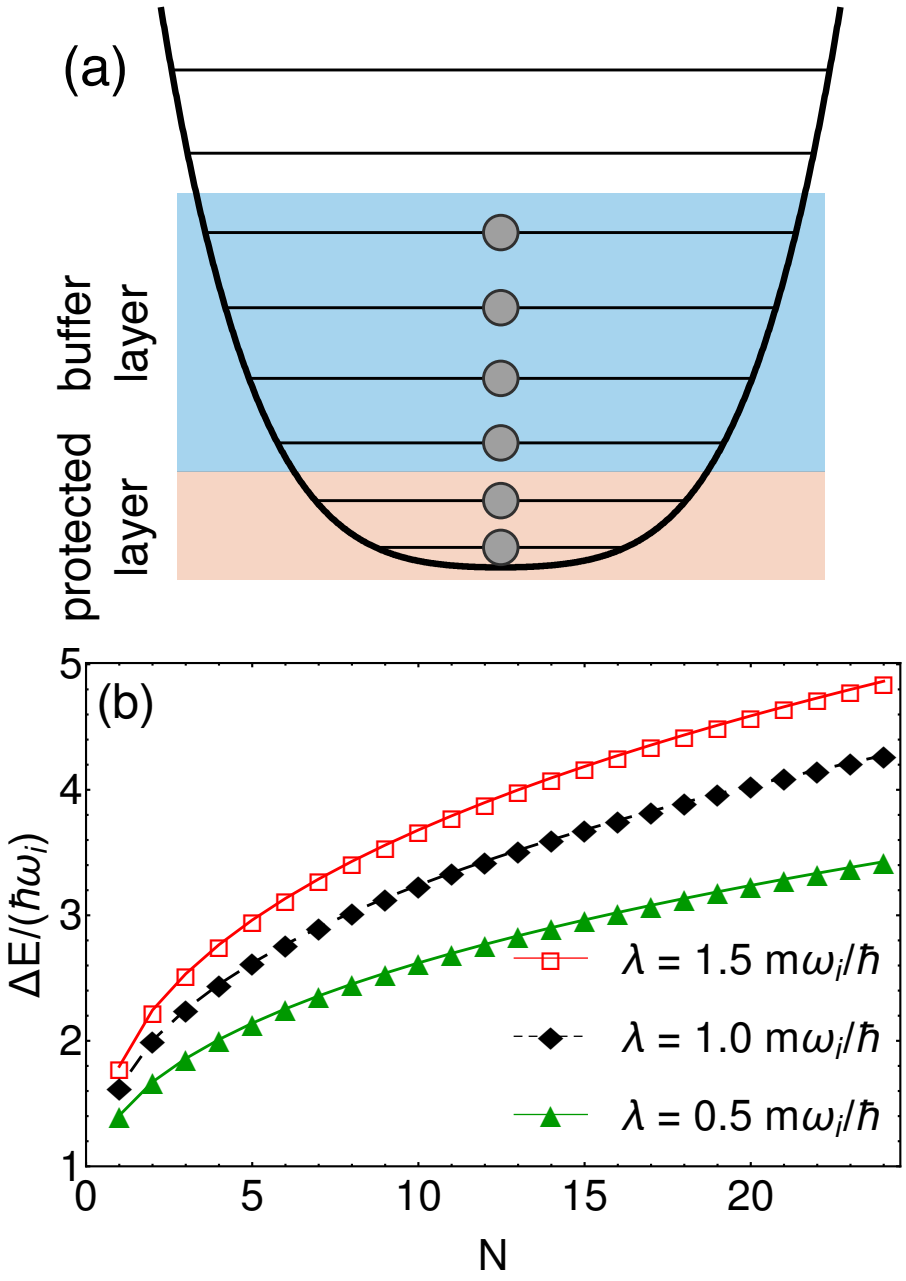

FIGURE 3.1: (a) Schematic of the key idea: In order for the particles in the protected zone to remain in the lower energy eigenstates during a time-dependent change of the external control parameters, a buffer zone is added. The Pauli principle then prevents the protected atoms from accessing any level in the buffer zone and to access an unoccupied level above the Fermi edge requires a large amount of energy. (b) Fermi gap $\Delta E = E_{N+1} - E_N$ versus total particle number N for the anharmonic trap $V(x) = m\omega_i^2(x^2 + \lambda x^4)/2$ for different anharmonicities λ.

fermionic atoms, and explore the idea of using Pauli blocking for speeding up adiabatic evolutions. In addition to the ground state layer of particles that should be protected from making transitions we are also adding a buffer layer of particles, see Fig. 3.1(a). The basic idea now is that only the fermions close to the Fermi edge can make transitions, whereas all atoms inside the Fermi sea need significantly more energy to get excited. Since we are only interested in the protected particles, this will allow to carry out *adiabatic* processes much faster, as long as the energies introduced by the dynamics do not allow for particles in the protected layer to make transitions. Once the evolution is finished, the *buffer fermions* can be discarded by, for example, lowering the trap walls [50], weakening and squeezing the trap [51, 52] or inducing spin-flips as in similar techniques for the evaporative cooling of bosons [53].

As this technique can most easily protect ground states, it is particularly well suited to prepare initial states in potentials where direct ground-state cooling is either challenging or done at a different stage than the processing. Ultracold, spin-polarised fermi gases, which are to first order non-interacting, are usually cooled to temperatures below the Fermi temperature through sympathetic cooling with a second atomic component (either bosonic or fermionic) [54]. The second component is then removed and the experiment on the degenerate gas is carried out. Since no further sympathetic cooling is possible once the second component is removed, buffer fermions would allow to protect the ground state.

The idea we present relies on the specific form of the energy spectrum around the Fermi edge. If the Fermi edge is close to the continuum states in a finite height potential, it is not guaranteed that the process we investigate will work. However, if the spectrum becomes increasingly sparse beyond the Fermi edge (for example in anharmonic trapping potentials, see Fig. 3.1(b)), significant speedups can be obtained. In fact, in this limit the idea of Hilbert space engineering through quantum statistics is largely independent of the potential shape, i.e. the exact form of the Hamiltonian.

Since the technique we discuss below will protect the lower motional energy states, and since the protection is done by the presence of a Fermi sea, it requires fermionic samples that are deep within the quantum degenerate regime. For neutral atoms these can be produced routinely in laboratories worldwide these days [55, 56, 57] and since the removal of the higher energy particles from a trap can also be done using standard techniques, we will concentrate in this paper on the control process itself.

In the following we will first introduce the system we investigate and define and discuss the process fidelity as our figure of merit. We will then apply the method in detail to three specific control tasks in Sec. 3.4, and conclude in Sec. 3.5.

3.3 System and fidelity

We consider a gas of spin-polarized fermions that formally consists of N_p particles whose state we want to protect and N_b particles that form a buffer layer (see Fig. 3.1(a)), so that the overall number of particles is $N = N_p + N_b$. Since at ultracold temperatures the dominant scattering interaction is of symmetric s-wave form, such gases can be efficiently described as non-interacting and they therefore form a perfect Fermi sea at zero temperature [58]. This also means that the time evolution of the many-particle wave function, $|\Psi(t)\rangle$, can be obtained by solving the single-particle Schrödinger equations for each state within the Fermi sea

$$i\hbar\frac{\partial}{\partial t}|\psi_i(t)\rangle = \left[-\frac{\hbar^2}{2m}\frac{\partial^2}{\partial x^2} + V(x,t)\right]|\psi_i(t)\rangle, \tag{3.1}$$

where the shape and time-dependence of the potential, $V(x,t)$, depends on the particular task that is to be implemented. The many particle wavefunction then

follows from calculating the Slater determinant as

$$|\Psi(t)\rangle = \frac{1}{\sqrt{N}} \sum_{\sigma\in\Pi[N]} \mathrm{sgn}(\sigma) \prod_{i=1}^{N} |\psi_{\sigma(i)}(t)\rangle_i, \tag{3.2}$$

where $\Pi[N]$ consists of all the permutations of the set $\{1,\ldots,N\}$.

3.3.1 Process fidelity

In the following we will consider processes where the N_p lowest eigenstates of an initial Hamiltonian are occupied by N_p relevant particles and we aim at having this subset of the Fermi sea to be undisturbed during the evolution towards the final Hamiltonian. In order to quantify how well the process works we calculate the overlap between the evolved state at the final time T, $|\Psi\rangle \equiv |\Psi(T)\rangle$, and the lowest lying eigenstates $|\phi_i\rangle (i = 1,\ldots,N_p)$ of the Hamiltonian at the end of the process. In detail, we define the fidelity of the process as

$$\mathcal{F} = \langle\Psi|\hat{\mathscr{M}}\Psi\rangle, \tag{3.3}$$

where $|\Psi\rangle$ is an element of the fermionic subspace $\mathcal{H}_F^N$ of the N-particle Hilbert space $\mathcal{H}^N$ and the measurement operator $\hat{\mathscr{M}}$ is defined as

$$\hat{\mathscr{M}} = \frac{1}{N_b!} \sum_{\tau\in\Pi[N]} \hat{M}^{(\tau(1))} \otimes \ldots \otimes \hat{M}^{(\tau(N))}, \tag{3.4}$$

$$\hat{M}^{(i)} = \begin{cases} |\phi_i\rangle\langle\phi_i| & \text{if} \quad i = 1,\ldots,N_p, \\ \mathbb{1} & \text{if} \quad i = N_p+1,\ldots,N. \end{cases} \tag{3.5}$$

The operator $\hat{M}^{(i)}$ checks the occupation probability of the i-th eigenstate of the Hamiltonian, provided that $i \leq N_p$, and, as we are not interested in the population of levels above N_p, $\hat{M}^{(i)}$ acts as the identity for $i > N_p$.

Let $\hat{P}_F$ be the projector on the fermionic subspace $\mathcal{H}_F^N$. For $|\Psi\rangle \in \mathcal{H}_F^N$, we have $\mathcal{F} = \langle\Psi|\hat{\mathscr{M}}\Psi\rangle = \langle\Psi|\hat{\mathscr{M}}_F\Psi\rangle$ where $\hat{\mathscr{M}}_F := \hat{P}_F\hat{\mathscr{M}}\hat{P}_F$. One can show by

using the fermionic number basis states $|\Phi_{\vec{n}}\rangle$ that

$$\hat{\mathscr{M}}_F = \sum_{\vec{n}} |\Phi_{\vec{n}}\rangle\langle\Phi_{\vec{n}}|, \tag{3.6}$$

where the sum is over all vectors $\vec{n}$ fulfilling $n_j = 1$ for $j = 1, \ldots, N_p$ and $\sum_{j=N_p+1}^{\infty} n_j = N_b$. From its structure it is clear that the operator $\hat{\mathscr{M}}_F$ is a projector. This proves that always $0 \leq \mathcal{F} \leq 1$ as it should be for a meaningful fidelity definition.

The fidelity (3.3) can then be rewritten as (see Appendix for details)

$$\mathcal{F} = \sum_{U} \left| \sum_{\sigma \in \Pi[N_p]} \mathrm{sgn}(\sigma) \prod_{i=1}^{N_p} \langle \psi_{U(\sigma(i))}(T) | \phi_i \rangle \right|^2, \tag{3.7}$$

where the first sum U is over all mappings $U : \{1, \ldots, N_p\} \to \{1, \ldots, N\}$ with $U(i) < U(i+1)$ for $i = 1, \ldots, N_p - 1$ (which can be also viewed as all subsets of cardinality N_p of the set $\{1, \ldots, N\}$). As mentioned above, the states $|\psi_j(T)\rangle$ can be obtained from the single-particle Schrödinger equation (3.1).

From Eq. (3.7), it also follows that $\mathcal{F}^{(N_b+1)} \geq \mathcal{F}^{(N_b)}$, i.e. that $\mathcal{F}$ increases monotonically with the number of buffer particles N_b. This can be seen because

$$\begin{aligned} \Delta\mathcal{F} &= \mathcal{F}^{(N_b+1)} - \mathcal{F}^{(N_b)} \\ &= \sum_{U \setminus \tilde{U}} \left| \sum_{\sigma \in \Pi[N_p]} \mathrm{sgn}(\sigma) \prod_{i=1}^{N_p} \langle \psi_{U(\sigma(i))}(T) | \phi_i \rangle \right|^2 \geq 0 \end{aligned} \tag{3.8}$$

where U are all a subset of cardinality N_p of the set $\{1, \ldots, N+1\}$ and $\tilde{U}$ are all a subset of cardinality N_p of the set $\{1, \ldots, N\}$. Note that from this property and the fact that $\mathcal{F}$ is bounded by 1, we know that the limit $\lim_{N_b \to \infty} \mathcal{F}^{(N_b)}$ must exist, but it is not necessarily 1.

3.3.2 Adiabaticity and shortcuts

Let us first look at schemes which work perfectly in the adiabatic limit, i.e., for $T \to \infty$. In this limit one gets $|\psi_j(T)\rangle + e^{i\zeta_j(t)}|\phi_j(T)\rangle$ where the ζ_j are phases. It immediately follows from Eq. (3.7) that $\mathcal{F} = 1$. To be more general, if T is large but finite, we get that $|\psi_i(T)\rangle = e^{i\zeta_i(t)}|\phi_i(T)\rangle + \frac{1}{T}|\chi_i^{(1)}(T)\rangle + \frac{1}{T^2}|\chi_i^{(2)}(T)\rangle + \ldots$ where the phase of $|\phi_i(t)\rangle$ can be chosen in such a way that $\langle\phi_i(T)|\chi_i^{(1)}(T)\rangle = 0$. Based on this, we can make a series expansion of the fidelity in the small parameter $1/T$ as

$$\mathcal{F} \simeq 1 + \frac{1}{T^2}\left[\alpha^{(0)} + \sum_{\mu=1}^{N_p}\sum_{\lambda=1}^{N_b}\left|\langle\chi_{N_p+\lambda}^{(1)}(T)|\phi_\mu(T)\rangle\right|^2\right], \tag{3.9}$$

where $\alpha^{(0)}$ is an expression independent of N_b. However, it can be seen that all terms which depend on N_b are always positive and therefore improve the fidelity. This coincides with the general monotonicity of the fidelity in N_b shown above.

Another special case are settings where shortcuts to adiabaticity techniques can be applied exactly, like for example the expansion of a harmonic trap [18] or the transport in a harmonic trap [19]. One can see from the above equation that one would obtain $\mathcal{F} = 1$ exactly for arbitrary numbers of particles on arbitrary timescales. In the following, we will therefore concentrate on settings where a shortcut to adiabaticity cannot be found easily, in particular anharmonic settings.

3.3.3 Temperature effects

To extend this approach to the case of a finite temperature τ, the initial state is of canonical form and the probability for a specific occupation m at initial time is given by

$$p_m = \frac{1}{Z}\exp\left[-\frac{1}{k_B\tau}\sum_{j=1}^{N}(E_{m(j)} - E_j)\right]. \tag{3.10}$$

Here $Z = \sum_m \exp\left[-\sum_{j=1}^{N}(E_{m(j)} - E_j)/k_{\mathrm{B}}\tau\right]$ is the partition function and k_{B} is the Boltzmann constant. The sum is over all functions $m : \{1, ...N\} \to \mathbb{N}$ with $m(i) < m(i+1)$, i.e. $(m(1), \ldots, m(N))$ are the numbers of the energy eigenstates occupied by the N fermions and the E_j are the ordered eigenenergies of the Hamiltonian at the initial time. The finite-temperature fidelity will then be the average over the fidelities of the different possible permutations of the particles

$$\mathcal{F} = \sum_m p_m \mathcal{F}_m, \tag{3.11}$$

where $\mathcal{F}_m$ is the fidelity defined similar to the one above with just the states in $(m(1), \ldots, m(N))$ initially occupied instead of $(1, \ldots, N)$:

$$\mathcal{F}_m = \sum_U \left| \sum_{\sigma \in \Pi[N_p]} \mathrm{sgn}(\sigma) \prod_{i=1}^{N_p} \langle \psi_{m(U(\sigma(i)))}(T) | \phi_i \rangle \right|^2. \tag{3.12}$$

Note that while this sum is in principle infinite, we will truncate it for its numerical evaluation at a maximal energy level chosen such that the result is practically independent from the exact level of truncation.

3.4 Control tasks

In this section we focus on particles trapped in potentials with significant anharmonicities, such that these cannot be treated as perturbations, and discuss three manipulation examples: expansion, transport, and splitting of the trap. For small (or zero) trap anharmonicity shortcuts for expansion and transport have been derived [8, 19, 59, 60, 61] and shortcuts related to the splitting can be found, for example, in [62, 63].

This broad variety of tasks will show that, in contrast to other shortcut-to-adiabaticity protocols, the idea presented here is insensitive to the details of how the trap parameters are varied in time and does not require any specific time-dependence parameter functions which might be very complex and hard to

implement experimentally. The only parameter is the number of buffer particles, N_b, and we will show below how the fidelity depends on the size of the buffer for each of the three processes.

3.4.1 Trap expansion

We first consider the expansion of the trapping potential, which we choose to be of the form

$$V(x,t) = \frac{m}{2}\omega(t)^2\left(x^2 + \lambda x^4\right), \tag{3.13}$$

and in which the anharmonicity is quantified by the parameter λ. We set $\lambda = m\omega_i/\hbar$ such that the anharmonicity is significant and far from being just a small perturbation. For the control task the trapping frequency $\omega(t)$ is changed from ω_i at $t = 0$ to ω_f at $t = T$ and we consider two different forms of the time-dependence, linear and sinusoidal, respectively given by

$$\omega_{\text{lin}}(t) = \omega_i + (\omega_f - \omega_i)\frac{t}{T}, \tag{3.14}$$

$$\omega_{\text{sin}}(t) = \omega_i + (\omega_f - \omega_i)\sin^2\left(\frac{\pi t}{2T}\right). \tag{3.15}$$

The resulting fidelities $\mathcal{F}$ for both schemes are shown in Fig. 3.2(a) for $N_p = 2$. One can clearly see that adding just a small number of buffer particles leads to significantly larger $\mathcal{F}$, even at total times for which the fidelity without buffer particles was very low. We also see that this is independent of the control scheme, underlining the fact that our method does not depend on the precise time-dependence of the control parameters. Nonetheless, it can be seen that the sinusoidal scheme generally results in larger $\mathcal{F}$ than the linear scheme for fixed T and N_b. Since both schemes yield roughly similar results we will in the following focus on the sinusoidal scheme only.

The dependence of the fidelity on the number of buffer particles for different numbers of protected particles N_p is shown in Fig. 3.2(b) for a fixed process

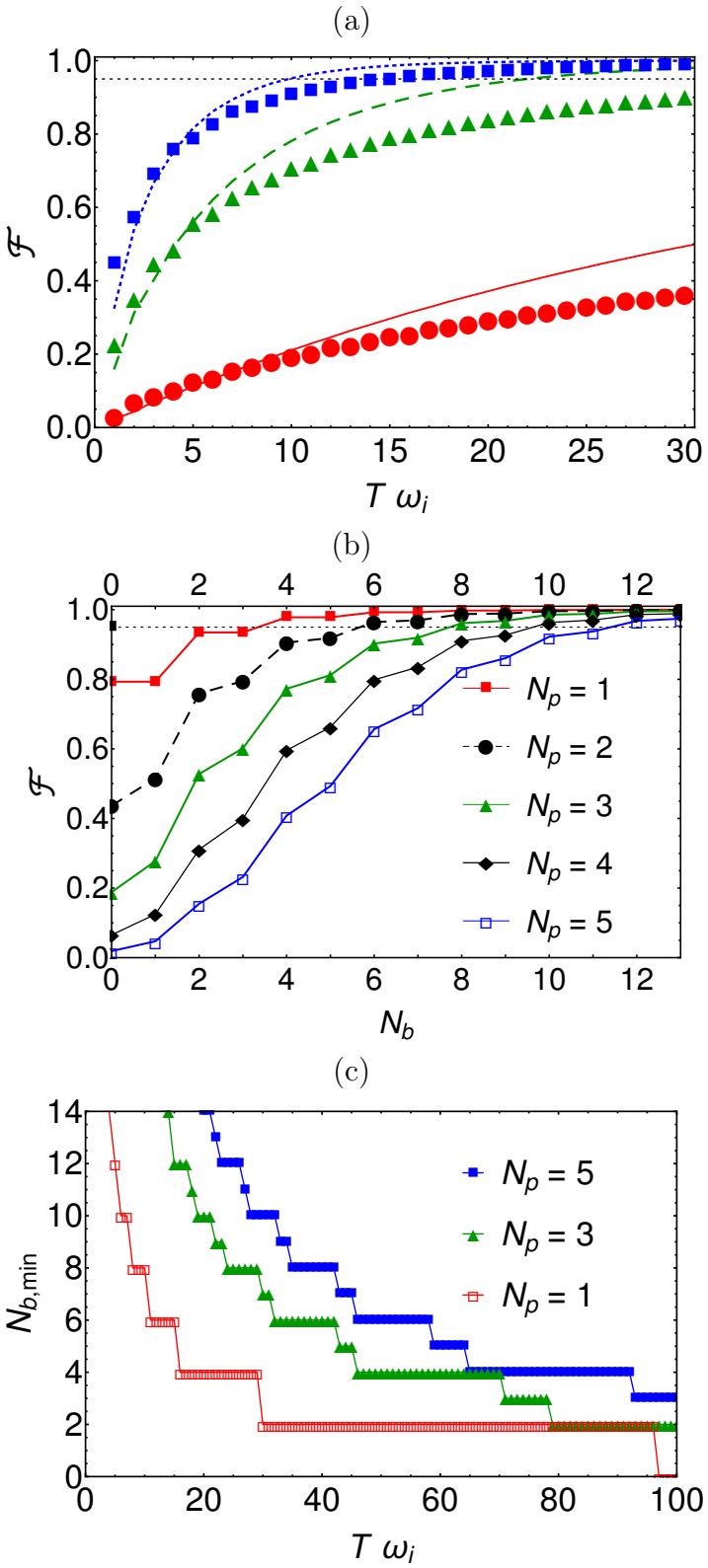

FIGURE 3.2: Trap expansion with $\omega_f/\omega_i = 0.01$ at a temperature $\tau = 0$. (a) $\mathcal{F}$ versus $T\ \omega_i$ for $N_p = 2$; lines indicate the sinusoidal scheme and the markers indicate the linear scheme. $N_b = 0$ (red solid line/circles), $N_b = 6$ (green dashed line/triangles), $N_b = 12$ (blue dotted line/squares). The horizontal black dotted line in (a) and (b) indicates $\mathcal{F} = 0.95$. (b) $\mathcal{F}$ versus N_b for $T = 25/\omega_i$ with the sinusoidal scheme for different N_p. (c) Minimal number of buffer particles required to achieve $\mathcal{F} \geq 0.95$ versus $T\ \omega_i$ for different N_p.

time of $T = 25/\omega_i$. The fidelity increases monotonically with increasing N_b (for fixed N_p), agreeing with the general property of the fidelity derived in Sec. 3.3. In addition, it is interesting to note that adding an even number of particles is more effective than adding an odd number. This can be understood by first considering the extreme case of $N_p = 1$ (red line in Fig. 3.2(b)), where it can be seen that, if one add a single buffer particle to an even number of buffer particles, the process fidelity does not change. The reason for this is that expansion is a symmetric operation with respect to the center of the trap, i.e. the Hamiltonian commutes with the parity operator. Therefore states of different parity do not couple and for $N_p = 1$ the subspace of buffer particles in odd eigenstates completely decouples from the subspace of the single, protected particle (as the ground state is even) and also from the buffer particles in even eigenstates. The fidelity then depends only on the *even* subspace and adding an additional *odd* buffer particle has no effect. For larger N_p, both subspaces are involved in the fidelity, making the situation more complex and the effect less prominent.

Fig. 3.2(b) also illustrates the effect of the OC, as one can see that fidelities decrease dramatically with larger system sizes (larger N_p). However, it is also worth pointing out that in our situation this is slightly surprising, as due to the trap anharmonicity, the Fermi gap is bigger for larger N_p, see Fig. 3.1(b), and one could therefore expect the OC to be suppressed for larger systems at fixed T. Nevertheless, Fig. 3.2(b) clearly shows that adding more particles to the system increases the fidelity of the relevant, lower lying many-body state, and therefore allows to *beat* the OC. In all cases a fidelities $\mathcal{F} \geq 0.95$ can be achieved by adding a large enough number of buffer particles and Fig. 3.2(c) shows the relation between the process time T and the minimal number of buffer particles $N_{b,\min}$ needed for achieving $\mathcal{F} \geq 0.95$ for all process times larger than T. It can clearly be seen that smaller T must be combined with a larger number of buffer particles, N_b, to result in the desired threshold fidelity.

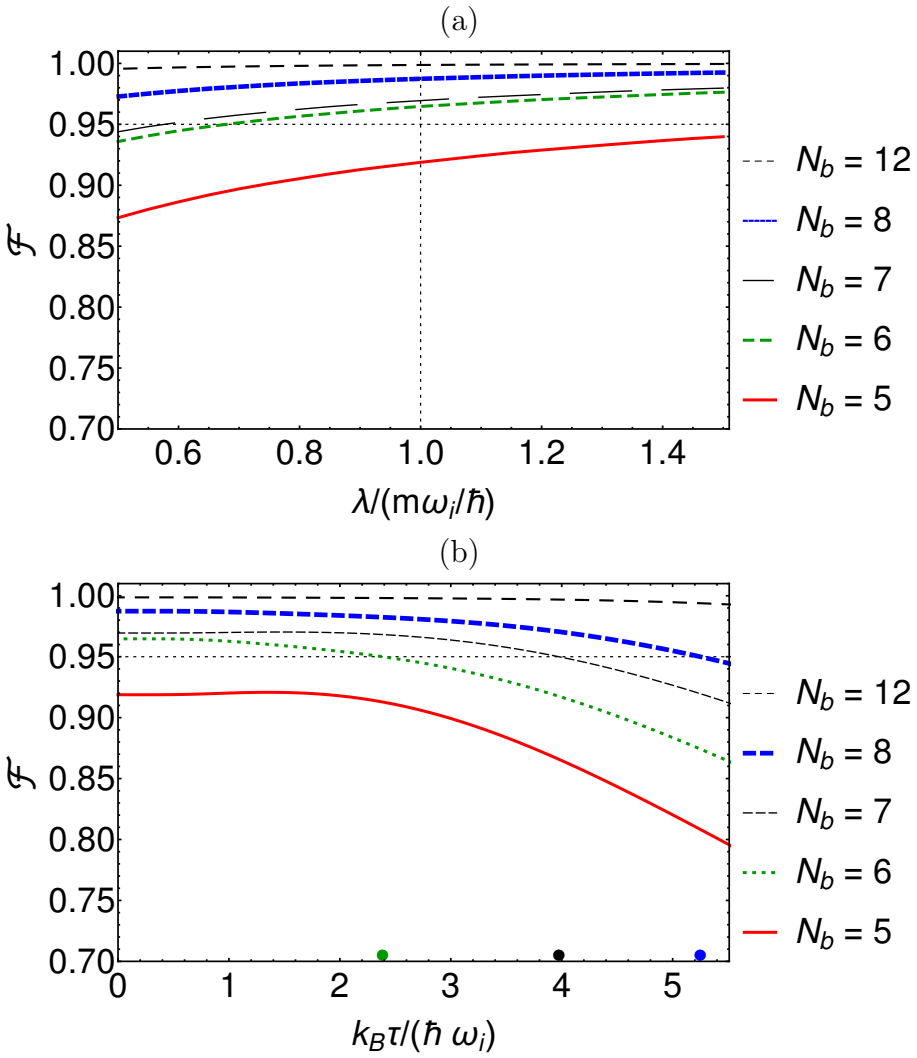

FIGURE 3.3: Trap expansion with a sinusoidal scheme for different number of buffer particles N_b. (a) Fidelity $\mathcal{F}$ versus anharmonicity λ at temperature $\tau = 0$; the vertical line indicates $\lambda = m\omega_i/\hbar$, to allow easy comparison to Fig. 3.2. (b) Fidelity $\mathcal{F}$ versus temperature τ, $\lambda = m\omega_i/\hbar$. In both figures: $\omega_f/\omega_i = 0.01$, $N_p = 2$ with $T = 25/\omega_i$; the horizontal line indicates a fidelity of $\mathcal{F} = 0.95$; in (b) the dots on the horizontal axis indicate when the corresponding line crosses this threshold fidelity.

Next, we study the effects of the potential shape and the temperature on our scheme and start by considering the dependence on $\mathcal{F}$ for different (relevant, non-perturbative) anharmonicities λ. The results shown in Fig. 3.3(a) confirm that this method does not require a detailed knowledge of the trapping potential, as for $N_b \geq 8$ the fidelity stays always above the threshold fidelity of 0.95 for the whole range of λ values shown. In fact, we note that the fidelity increases

with λ as our scheme takes advantage of the increased energy gap at the Fermi energy for larger λ (see again Fig. 3.1(b)).

Finite temperature results are shown in Fig. 3.3(b) for different numbers of buffer particles N_b (with fixed $T = 25/\omega_i, N_p = 2, \lambda = m\omega_i/\hbar$). and it can be seen that the scheme is quite stable under temperature perturbations. Increasing temperatures can be compensated by increasing the number of buffer particles to achieve the same target fidelity: N_b should be increased by one to compensate for an increase in temperature of the order of $\hbar\omega_i/k_B$ (see the dots in Fig. 3.3(b)). This is also what one would expect heuristically as the "width" of the edge in the Fermi–Dirac distribution is of the order of $k_B\tau$ and the energy gap is of the order $\hbar\omega_i$. As one might expect, the increase of the fidelity is again monotonic with increasing N_b with finite temperature for the shown parameter range.

3.4.2 Transport

The second dynamical scheme we examine is the spatial translation of the trapping potential described by

$$V(x,t) = \frac{1}{2}m\omega^2\left((x - x_0(t))^2 + \lambda(x - x_0(t))^4\right), \tag{3.16}$$

and we choose the movement of the trap center $x_0(t)$ between $x_i = x_0(0)$ and $x_f = x_0(T)$ to be of the form

$$x_0(t) = x_i + (x_f - x_i)\sin^2\left(\frac{\pi t}{2T}\right). \tag{3.17}$$

Let $d = \sqrt{\hbar/m\omega}$, and we set $\lambda = 1/d^2$. The resulting fidelities $\mathcal{F}$ are shown in Fig. 3.4(a) for $N_p = 2$ and one can see that, similarly to the expansion scheme, fidelities of $\mathcal{F} \geq 0.95$ can be achieved by increasing the number of buffer particles N_b instead of increasing the total time T. In this case, however, the fidelities

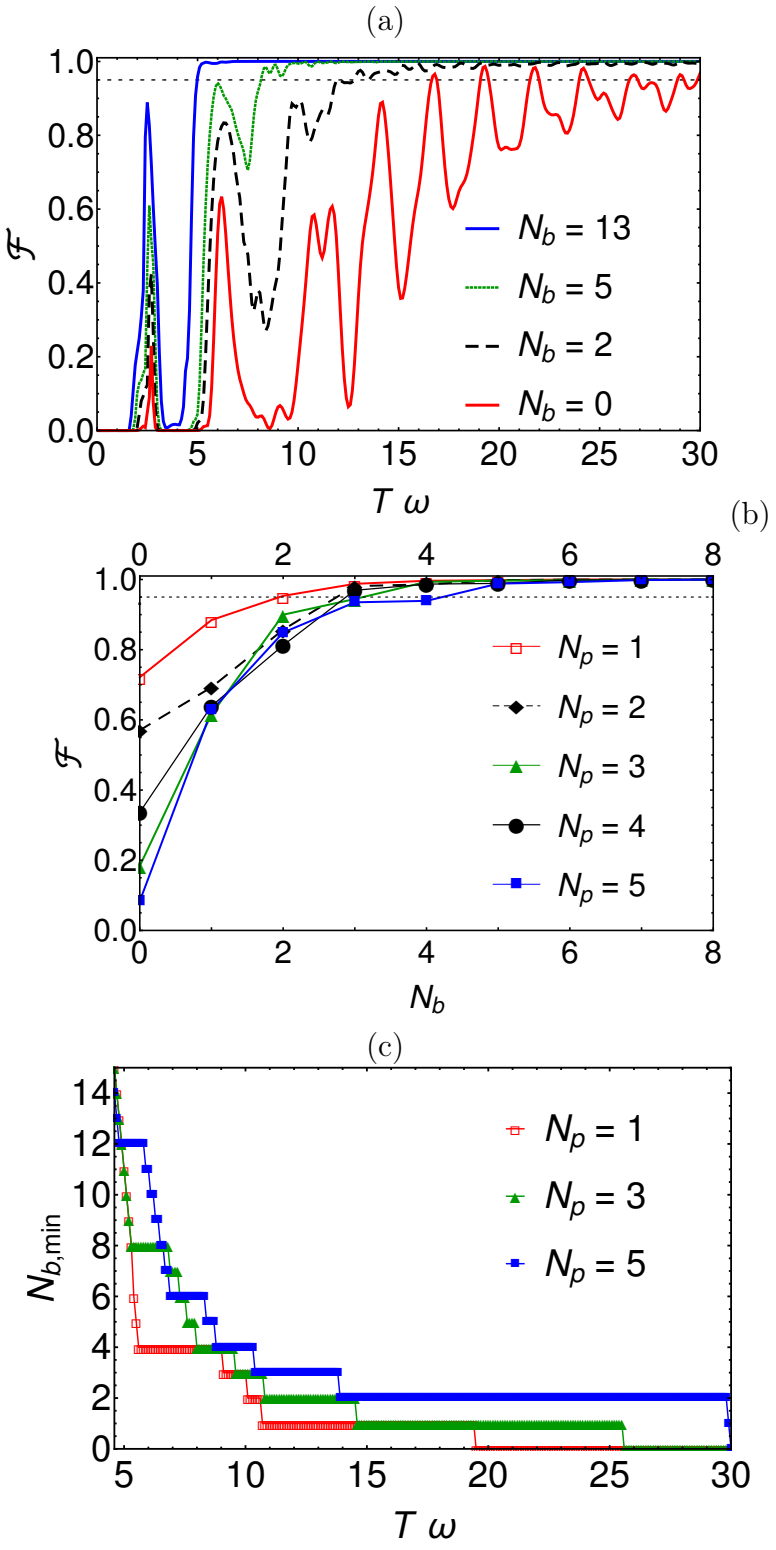

FIGURE 3.4: Trap transport with the sinusoidal scheme from $x_{0i} = 0$ to $x_{0f} = 90d$ at temperature $\tau = 0$. (a) Fidelity $\mathcal{F}$ versus process time T for different N_b with $N_p = 2$. (b) Fidelity versus N_b for different N_p, $T = 11.5/\omega$. (c) Minimal buffer particles $N_{b,\min}$ versus process time T for different N_p. The horizontal black dotted lines in (a) and (b) indicate a fidelity of $\mathcal{F} = 0.95$.

exhibit oscillations for shorter T, giving high fidelities for some specific final times. This is directly related to the single particle behavior where magic times exist, for which the transport of the wavepacket becomes optimal [64, 65].

In Fig. 3.4(b) we examine how the fidelity depends on the number of buffer particles for different numbers of protected particles N_p (for a fixed process time $T = 11.5/\omega$). As expected, adding buffer particles N_b always increases the fidelity (see again also Sec. 3.3). However, it is worth pointing out certain differences compared to the expansion scheme (see Fig. 3.2(a)). First, adding a single buffer particle always has a significant effect and second, the fidelity is now not monotonic in N_p (for fixed N_b and T, compare to Fig. 3.2(b)): all fidelity lines for the different N_p cross the threshold line of $\mathcal{F} = 0.95$ given enough N_b.

Figure 3.4(c) shows the relation between the process time T and the minimal number of buffer particles $N_{b,\mathrm{min}}$ required to reach $\mathcal{F} \geq 0.95$ for all process times larger than or equal to T. Similar to the expansion scheme, $N_{b,\mathrm{min}}$ goes to 0 for large enough T and the required buffer is increasing for shorter process times T. In addition, $N_{b,\mathrm{min}}$ does not have a strong dependence on N_p in the transport case.

The relation between $\mathcal{F}$ and temperature τ, for different values of N_b (with fixed $T = 11.5/\omega$, $N_p = 2$), is shown in Fig. 3.5(a). One can see that the scheme is again stable against temperature perturbation, however, for increasing temperature the number of buffer particles N_b has to be increased to still achieve a fidelity $\mathcal{F} \geq 0.95$. Again, from the dots on the horizontal axis it can be seen that N_b has to be increased by one if the temperature increases by an order of $\hbar\omega_i/k_B$. Again, we note that for the temperatures shown there is still the monotonic increase of the fidelity with increasing N_b.

It is also interesting to note that the fidelity in general does not always decrease monotonically with increasing temperature. This can be seen in Fig. 3.5(b), where a linear transport scheme is considered (with fixed $T = 23/\omega$, $N_p = 2$).

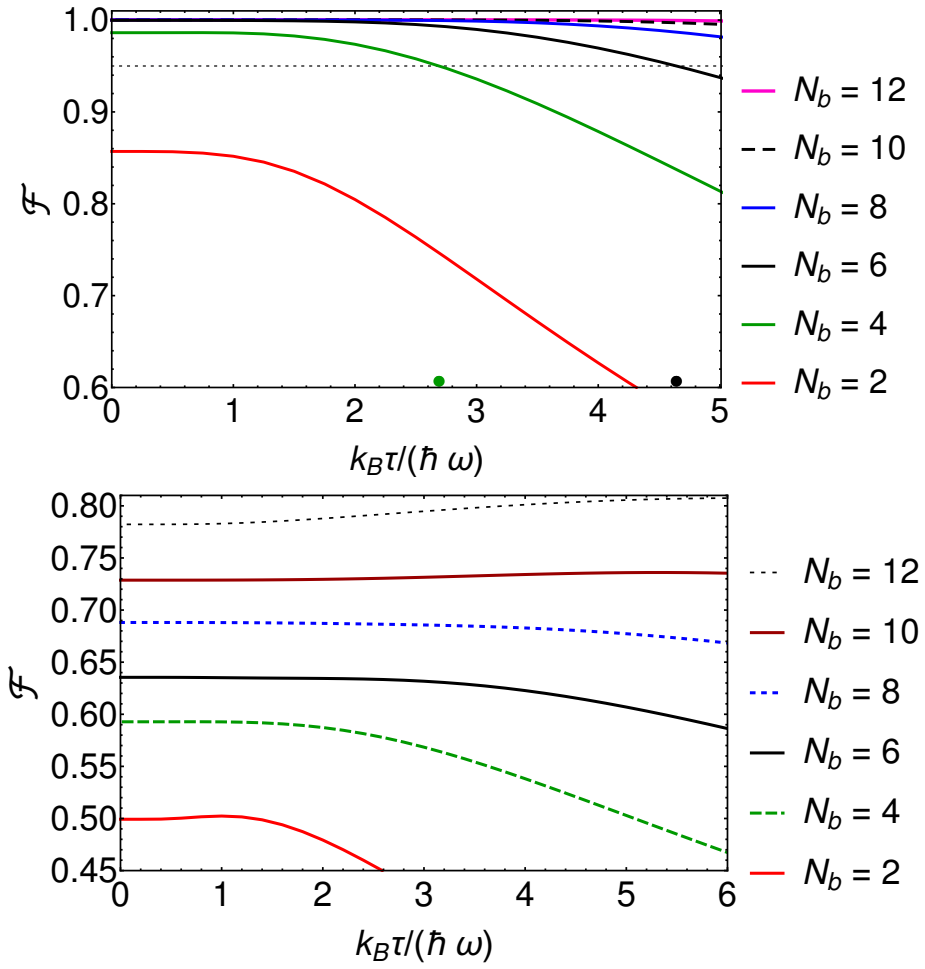

FIGURE 3.5: Trap transport from $x_{0i} = 0$ to $x_{0f} = 90d$, fidelity $\mathcal{F}$ versus temperature τ for different N_b, $N_p = 2$:(a) Sinusoidal scheme; $T\omega = 11.5$ (b) Linear scheme $x_0(t) = x_{0f}t/T$; $T\omega = 23$; the horizontal line indicates $\mathcal{F} = 0.95$, and the dots on the horizontal axis indicate when the corresponding line crosses this threshold fidelity.

The fidelity increases for finite temperatures in some cases, but decreases again for higher temperatures. The reason for this is a complex interplay between the energy spectrum of the system and the softening of the Fermi edge at finite temperatures.

3.4.3 Splitting

In our final example we will discuss the process where raising a Gaussian barrier at the center of a harmonic trap leads to a splitting of the atomic cloud. For

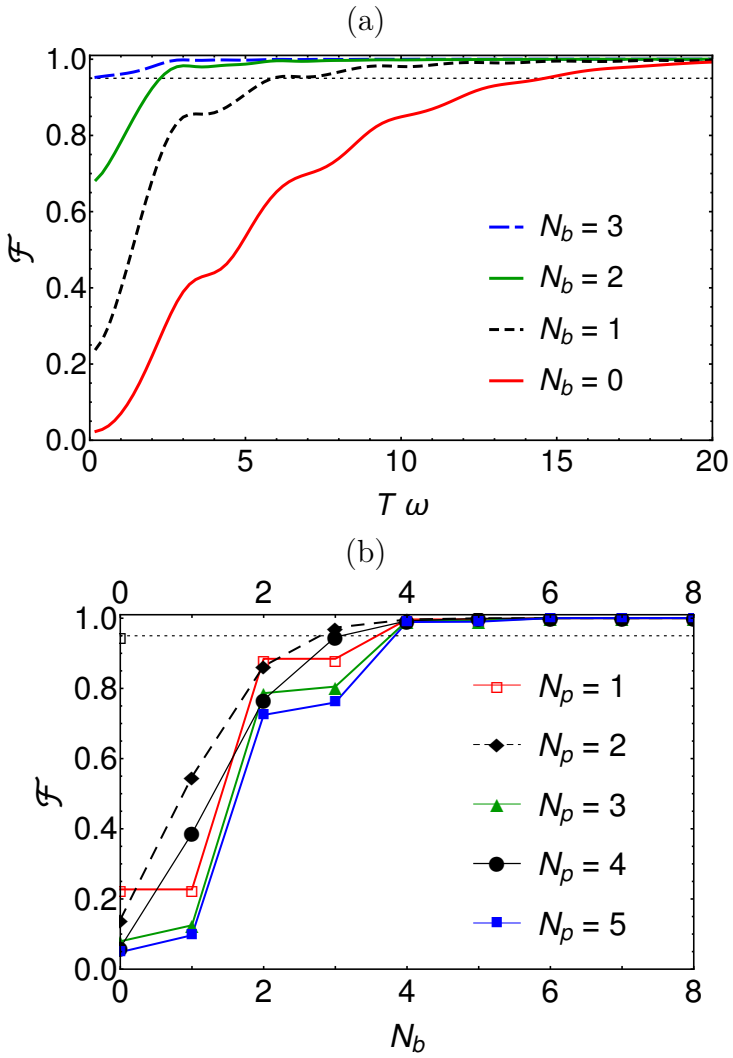

FIGURE 3.6: Splitting of a trap from height $h_i = 0$ to $h_f = 20\hbar\omega$, sinusoidal scheme, temperature $\tau = 0$. (a) Fidelity $\mathcal{F}$ versus process time T for different N_b, $N_p = 2$. (b) Fidelity $\mathcal{F}$ versus N_b for different N_p, $T = 2/\omega$.

this we choose

$$V(x,t) = \frac{1}{2}m\omega^2 x^2 + h(t)e^{-x^2/d^2}, \tag{3.18}$$

where again $d = \sqrt{\hbar/m\omega}$. The time dependence of the barrier height chosen as

$$h(t) = h_i + (h_f - h_i)\sin^2\left(\frac{\pi t}{2T}\right), \tag{3.19}$$

where h_i is the initial height of the barrier at $x = 0$ before the splitting and

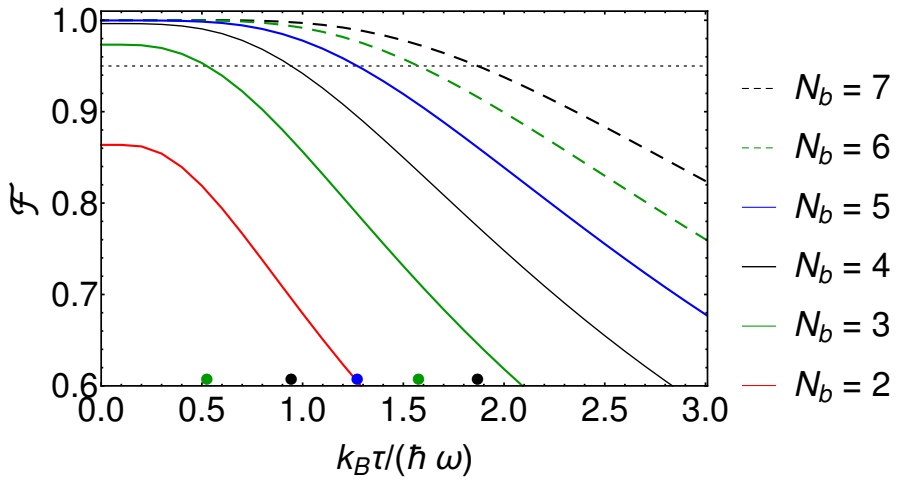

FIGURE 3.7: Splitting of a trap from height $h_i = 0$ to $h_f = 20\hbar\omega$, sinusoidal scheme, temperature $\tau = 0$: Fidelity $\mathcal{F}$ versus temperature τ for different N_b, $T = 2/\omega$, $N_p = 2$. In all figures, the horizontal black dotted line indicates a fidelity of $\mathcal{F} = 0.95$.

h_f after the process. Similarly to the case of expansion, splitting is a symmetric operation , i.e. the Hamiltonian is commuting with the parity operator. As such it is expected that even numbers of additional particles are more effective than are odd numbers. Splitting is also quite distinct from the other manipulations in that it affects higher energy states in the trap less, whereas transport or expansion affect the whole spectrum of states in the trap. In the following, we set $h_i = 0$ and $h_f = 20\hbar\omega$, which lead to a final separation in two wells for approximately the 18 lowest energy eigenstates.

In Fig. 3.6(a) one can see that, as expected, increasing N_b gives higher fidelities $\mathcal{F}$ on shorter timescales and $\mathcal{F}$ increases monotonically with T. In fact, the process is very robust and already for $N_b = 3$ a fidelity of $\mathcal{F} \geq 0.95$ can be achieved for almost instant timescales. The dependence of the fidelity on N_b is shown for different N_p in Fig. 3.6(b). For odd numbers of particle N_p one can see an effect similar to the one observed in the expansion process, where an even number of buffer particles N_b is needed to see an increase in fidelity. This can again be understood by considering the symmetric nature of the splitting dynamics. However, while one would naively expect the same for states with

even numbers of particles N_p, it is absent in this case. The reason for this can be found in the specific structure of the eigenspectrum of the split trap, where for our parameters successive even and odd eigenstates are effectively energetically degenerate. An even number of particles in the system therefore has two particles with energies close to the Fermi edge and adding any number of buffer particles will lead to an increase in fidelity as one possible transition is blocked.

Finally, from Fig. 3.7(c), one can see that the splitting is slightly more sensitive to temperature than the previous two operations. The dots on the horizontal axis show heuristically that an additional buffer particle is required for every increase in temperature of about $0.25k_B/\hbar\omega$, while in the previous two schemes this was about $k_B/\hbar\omega$.

3.5 Conclusion

In this work we have explored the idea of using Pauli blocking for speeding up adiabatic evolution by using an additional layer of buffer particles to protect the lowest-energy fermions when the system parameters are dynamically changed. We have presented a thorough investigation, both analytical and numerical, showing that the presence of this additional layer allows the speed-up of adiabatic manipulations without exciting unwanted transitions. By discussing three different examples, we have demonstrated that this method is robust and applicable to a wide range of scenarios.

The proposed technique is particularly well suited to protect ground states during changes of the external potential, resulting in a speed-up of ground state preparation in potentials for which these states cannot easily be prepared directly with high fidelity. The method does not require precise knowledge of the shape of the trap or the energy spectrum of the system. It is also insensitive to the details of how the trap parameters are varied in time and no specific

time-dependence of the parameter functions is necessary, which might be very complex and hard to implement experimentally. All this makes it a very robust and readily applicable technique.

In this work we have discussed an ideal fermion system without interactions. In fact, this is a good approximation for spin polarized, ultracold Fermi gases where the short-range s-wave interaction between two atoms has to be absent due to the Pauli exclusion principle, and where higher order scattering terms are known to be small. Our work is therefore directly applicable to current experimental settings. Nevertheless, as the Pauli principle is general, the main idea of our work also applies to fermionic gases in the presence of interactions. However, the initial and the final states of the many-particle system are no longer just anti-symmetrized product-states, see Eq. (3.2), and consequently the fidelity expression given in Eq. (3.3) would need to be adapted. In addition, the numerical simulations of the time-evolution would become significantly more demanding, as the full many-body problem needs to be solved. Of course, for stronger attractive interactions, the relevant Hamiltonian describes pairing of fermions into Cooper pairs and BCS superfluidity, whereas for positive interactions the BEC limit is realized where the fermions form composite bosons. The ground state is then a Bose–Einstein condensate of atom pairs. Our idea is not applicable to either of these limits.

Finally, we would like to stress again that our study gives a deep insight into the phenomenon of the orthogonality catastrophe. We have shown that the fidelity of a subsystem can be much larger than the one of the full many-body system and in particular, that the particles close to the Fermi edge play a much stronger role in the effect of the many-body state becoming orthogonal.

3.6 Appendix for chapter 3

We calculate the fidelity of the final state, $\mathcal{F} = \langle\Psi|\hat{\mathscr{M}}\Psi\rangle$, with the measurement operator defined by Eq. (3.4), where $|\Psi\rangle$ is the state of our N-fermion wave function after some unitary time evolution. We want to calculate $\mathcal{F}$ as a function of the single-particle states $|\psi_i\rangle$, cf. Eq. (3.2). Expanding the definitions of $\hat{\mathscr{M}}$ and $|\Psi\rangle$, we get

$$\begin{aligned}\mathcal{F} &= \frac{1}{N!N_b!}\sum_{\sigma}\sum_{p,q}\operatorname{sgn}(p)\operatorname{sgn}(q)\prod_{i=1}^{N_p}\langle\psi_{p(i)}|\phi_{\sigma(i)}\rangle\langle\phi_{\sigma(i)}|\psi_{q(i)}\rangle\prod_{j=N_p+1}^{N}\langle\psi_{p(j)}|\psi_{q(j)}\rangle \\ &= \frac{1}{N!N_b!}\sum_{\sigma}\sum_{p,q}\operatorname{sgn}(p)\operatorname{sgn}(q)\prod_{i=1}^{N_p}\langle\psi_{p(\sigma^{-1}(i))}|\phi_i\rangle\langle\phi_i|\psi_{q(\sigma^{-1}(i))}\rangle \\ &\qquad\prod_{j=N_p+1}^{N}\langle\psi_{p(\sigma^{-1}(j))}|\psi_{q(\sigma^{-1}(j))}\rangle.\end{aligned}$$

Since the $|\psi_i\rangle$ are orthogonal before manipulation (as eigenstates of the Hamiltonian), they remain orthogonal after the unitary evolution. Let us also define $P = p\circ\sigma^{-1}$ and $Q = q\circ\sigma^{-1}$, so that

$$\mathcal{F} = \frac{1}{N_b!}\sum_{P,Q}\operatorname{sgn}(P)\operatorname{sgn}(Q)\prod_{i=1}^{N_p}\langle\psi_{P(i)}|\phi_i\rangle\langle\phi_i|\psi_{Q(i)}\rangle\prod_{j=N_p+1}^{N}\delta_{P(j)Q(j)}.$$

We see that only the permutations that fulfill $P(j) = Q(j)$ for $j = N_p + 1,\ldots,N$ contribute to the sum. This allows us to rewrite the contributing permutations as $P = \mu\circ\pi_P$ and $Q = \mu\circ\pi_Q$. μ should be a permutation $\mu : \{1,\ldots,N\}\to\{1,\ldots,N\}$ with $\mu(i) = P(i) = Q(i)$ for $i > N_p$ and $\mu(i) < \mu(i{+}1)$ for $i = 1,\ldots,N_p - 1$. $\pi_P = \mu^{-1}\circ P$ and $\pi_Q = \mu^{-1}\circ Q$ are then permutations on $\{1,\ldots,N\}$ such that they permute $\{1,\ldots,N_p\}$ but act as the identity on $\{N_p+1,\ldots,N\}$. Note that there is a one-to-one correspondence between P

and the pair μ, π_P. Then we get

$$\mathcal{F} = \frac{1}{N_b!} \sum_{\mu} \sum_{\pi_P, \pi_Q} \operatorname{sgn}(\pi_P) \operatorname{sgn}(\pi_Q) \prod_{i=1}^{N_p} \langle \psi_{\mu(\pi_P(i))} | \phi_i \rangle \langle \phi_i | \psi_{\mu(\pi_Q(i))} \rangle.$$

This fidelity is independent of $\mu(N_p + 1), ...\mu(N)$. Therefore, for each μ we can define a mapping $U : \{1, \ldots, N_p\} \to \{1, \ldots, N\}$ by $U(i) = \mu(i)$ for $i = 1..N_p$ such that $U(i) < U(i + 1)$ for $i = 1..N_p - 1$. Note that each U can also be viewed as a subsets of cardinality N_p of the set $\{1, \ldots, N\}$. As $N_b!$ different μ result in the same U, this allows us to write the fidelity as

$$\begin{aligned} \mathcal{F} &= \sum_{U} \sum_{\pi_P} \sum_{\pi_Q} \operatorname{sgn}(\pi_P) \operatorname{sgn}(\pi_Q) \prod_{i=1}^{N_p} \langle \psi_{U(\pi_P(i))} | \phi_i \rangle \langle \phi_i | \psi_{U(\pi_Q(i))} \rangle \\ &= \sum_{U} \left| \sum_{\pi_P} \operatorname{sgn}(\pi_P) \prod_{i=1}^{N_p} \langle \psi_{U(\pi_P(i))} | \phi_i \rangle \right|^2, \end{aligned}$$

which corresponds to Eq. (3.7).

Chapter 4

Trapping and cooling particles using a moving atom diode and an atomic mirror

4.1 Abstract

We propose a theoretical scheme for atomic cooling, i.e. the compression of both velocity and position distribution of particles in motion. This is achieved by collisions of the particles with a combination of a moving atomic mirror and a moving atom diode. An atom diode is a unidirectional barrier, i.e. an optical device through which an atom can pass in one direction only. We show that the efficiency of the scheme depends on the trajectory of the diode and the mirror. We examine both the classical and quantum mechanical descriptions of the scheme, along with the numerical simulations to show the efficiency in each case.

This chapter is based on the following publication:

T. Dowdall and A. Ruschhaupt,

Trapping and cooling particles using a moving atom diode and an atomic mirror,

Phys. Rev. A **97**, 013412 (2018)

4.2 Introduction

One standard cooling technique for neutral atoms is using magneto-optical traps [66]. Evaporative cooling of bosons is used for achieving condensates [53] and ultracold, spin-polarised Fermi gases are usually cooled to temperatures below the Fermi temperature through sympathetic cooling [54].

Recently another method has been introduced, called single photon cooling [67, 68, 69], which allows one to cool atoms and molecules which cannot be handled in a standard way. The method is based on an atom diode or one-way barrier [70, 71]. An atom diode is a device which allows the atom to pass through it only in one direction whereas the atom is reflected if coming from the opposite direction. Such a device has been studied theoretically [68, 72, 73, 74, 75] and also experimentally implemented as a realisation of a Maxwell demon [76, 77].

A way of changing or reducing the velocity of particles (which does not necessarily correspond to cooling) is letting particles collide with a moving mirror. An early example is the production of an ultracold beam of neutrons colliding with a moving Ni-surface [78]. Atomic mirrors can be built using reflection by an evanescent light field [79, 80]. Moving such an mirrors for cold atom waves has been also implemented with a time-modulated, blue-detuned evanescent light wave propagating along the surface of a glass prism [81, 82, 83]. More recently, the diffraction of a Bose-Einstein condensate on a vibrating mirror potential created by a blue-detuned evanescent light field was studied [84] and the reflection of an atomic cloud from an optical barrier of a blue-detuned beam was used to study first-order and second-order catastrophes in the cloud density [85]. Even Rb atoms which fall on a magnetic mirror have been examined [86] and Rb atoms have even been stopped using a moving magnetic mirror [87]. Furthermore solid atomic mirrors have been used for focusing neutral atomic and molecular beams [88, 89, 90]. Si-crystals on a spinning rotor have been

used as a solid atomic mirrors to slow down beams of Helium atoms [91, 92].

A stream of particles can be slowed by collision with a moving mirror travelling in the same direction as the particles. One limitation of standard settings at present is that for a fixed mirror velocity only pulses of particles with a specific and well defined initial velocity are stopped. In [93], it was shown that by designing a particular trajectory for the mirror it is even possible to stop a pulse in which the initial velocities are broadly distributed or possibly unknown. But slowing an ensemble of atoms solely with one mirror of course does not result in phase-space compression. In order to achieve this, we introduce a required irreversible step.

In this work we develop a scheme to cool (*i.e* compress in phase space) a travelling cloud of particles. This is done by combining the idea of a moving mirror with an irreversible atom diode also in motion.

In the next section, we present and investigate our cooling method, first in an idealised classical setting, i.e. assuming a point-particle with classical motion. In Section 4.4, we discuss a quantum-mechanical implementation of our cooling scheme. The paper ends with a conclusion.

4.3 Cooling classical particles with diode and mirror

First we shall investigate a classical scheme for achieving our goals before moving on to a full quantum treatment of the problem. We assume classical point particles and restrict the scenario to a one-dimension motion. The setting consists of two main objects: a moving atomic mirror potential and an atom diode. The particles move freely between the collisions with these two objects. Let us start by reviewing properties of a single moving atomic mirror potential.

4.3.1 Elastic collision stopping a single particle with moving mirror

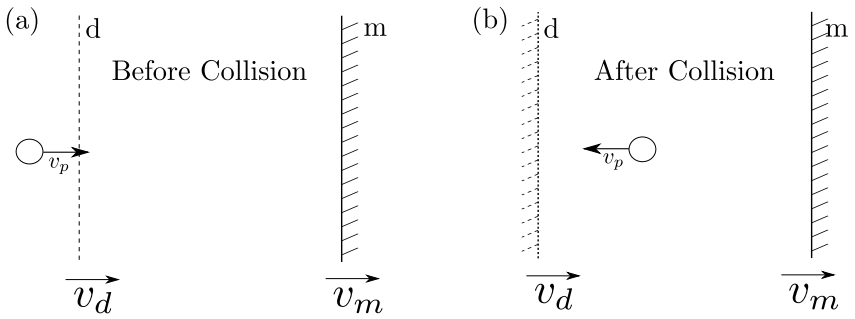

FIGURE 4.1: (a) and (b) Diode-mirror setting: A particle approaches the moving diode-mirror system; it can enter one way through the diode in (a) but in (b) from the other direction the diode behaves as another mirror travelling at a different velocity.

A collision between a number bodies is called elastic if there is no loss of mechanical energy during the collision. With this in mind consider the collision of a particle (moving with velocity v_0) with a moving mirror (with velocity v_m). The velocity of the particle after the elastic collision is given by

$$v_f = 2v_m - v_0. \tag{4.1}$$

It is immediately apparent that if we let $v_m = \frac{v_0}{2}$ the particle is stopped instantly by the collision. We can see that in particular, if a particle has trajectory $x(t) = v_0 t$, the trajectory of the mirror is $x_m(t)$ and the collision occurs at time t_c then we have

$$\left.\frac{dx_m}{dt}\right|_{t_c} = \frac{v_0}{2} = \frac{x_m(t_c)}{2t_c}. \tag{4.2}$$

We require that the same mirror trajectory should stop all particles independent of their velocity $v_0 > 0$, i.e. the previous equation should be fulfilled for all $t_c > 0$. This ordinary differential equation (with t_c replaced by t) has then a solution $x_m(t) = \alpha\sqrt{t}$ with $\alpha > 0$. This trap trajectory has been explored in

[93], where it stops particles of arbitrary velocity. Unfortunately, these particles can be completely delocalised in space and thus no real cooling (i.e. phase space compression) is achieved with just a single atomic mirror.

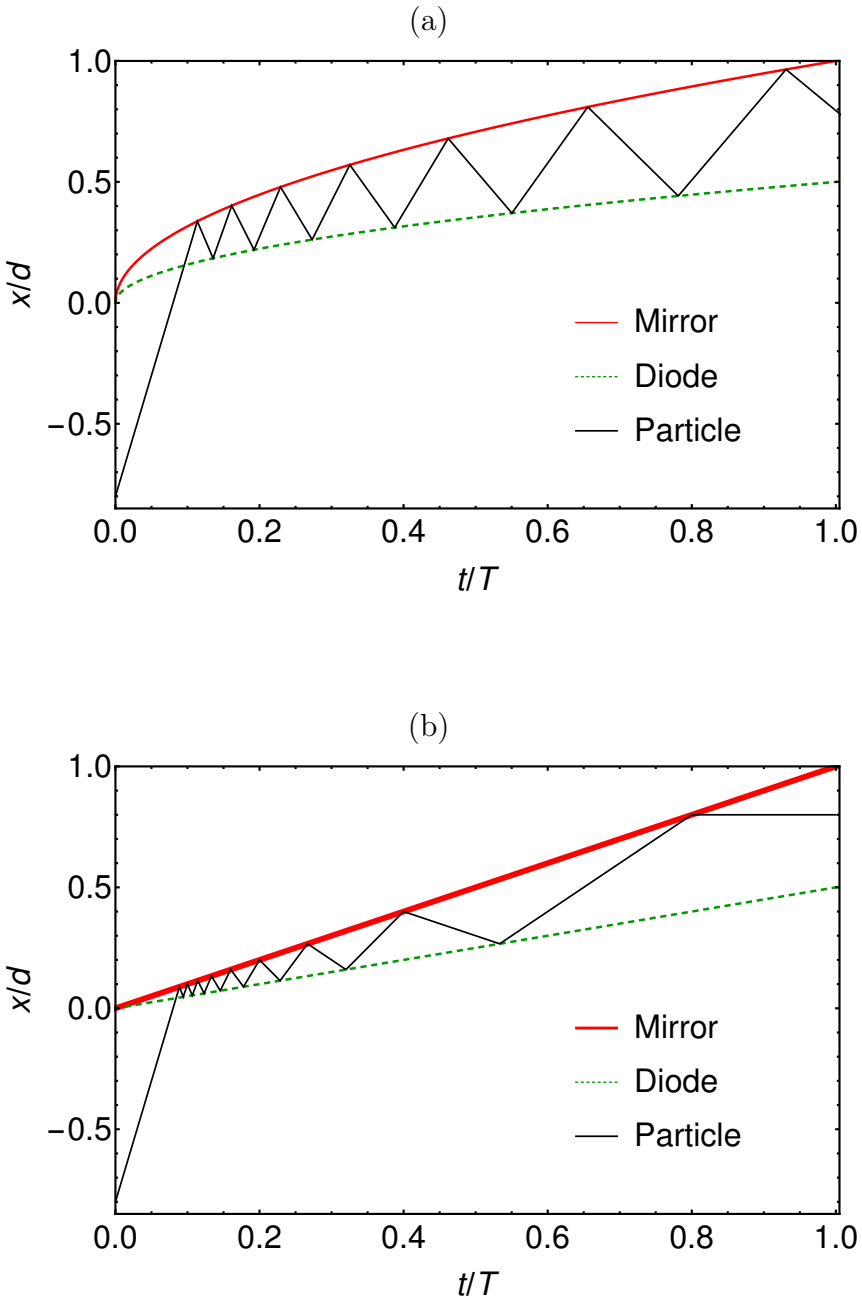

FIGURE 4.2: (a) and (b) Motion of the atom diode and the mirror with trajectories (a) $\sim \sqrt{t}$ and (b) $\sim t$.

4.3.2 Cooling with atom diode and atomic mirror

In this paper we propose a slightly different approach. Instead of attempting to stop the particles we demonstrate a method for cooling them.

A schematic of our setting is seen in Fig. 4.1 (a) and (b): it consists of an atom diode (d) shown here on the left and a mirror potential (m) on the right, moving with velocities v_d and v_m. Let us consider a single particle incident on the diode from one direction (here from the left to the right) which passes through (Fig. 4.1) (a). The particle is then reflected by the mirror as a result its absolute velocity is reduced. However in the next collision the particle is reflected by the diode which now acts as an atomic mirror (Fig. 4.1) (b).

In Fig. 4.2 (c) and (d) this idea demonstrated again; the particle incident from the below can pass through the barrier but this particle, when it is then travelling downwards, is reflected by the diode. This traps the particle in between the two objects. According to Eq. (4.1) every time the particle collides with the mirror it experiences a reduction in velocity and every time the particle is reflected by the diode, its velocity is increased. Since the mirrors is travelling at a faster velocity than the diode, there is an overall reduction in velocity after two collisions. The absolute velocities the particle continue to slow down until the particle is not travelling fast enough to collide with the mirror. Because the setting confines the particle and the collisions between the particle and the moving diode/mirror slow down the particle, through continued collisions inside the diode-mirror trap a cooling can be achieved.

This idea was first proposed in [94] where both diode and mirror travel with the same velocity $\sim 1/\sqrt{t}$ but they are displaced by a constant distance. With these trajectories a slight compression in velocity has been achieved.

In this work, we show that the efficiency depends strongly on the trajectories of diode and mirror. By considering different trajectories, we show that significant phase space compression can be achieved. Motivated by the Section

4.3.1, we first consider a square-root scheme where the trajectories of diode (d) and mirror (m) are

$$x_d(t) = \alpha_d\sqrt{t}, \qquad x_m(t) = \alpha_m\sqrt{t}, \tag{4.3}$$

with $\alpha_m > \alpha_d$, see also Fig. 4.2 (c).

Alternatively, we consider a linear scheme where the trajectories of diode (d) and mirror (m) are

$$x_d(t) = v_d t, \qquad x_m(t) = v_m t, \tag{4.4}$$

with $v_m > v_d$, see also Fig. 4.2 (d). As it will turn out later that the linear scheme is more advantageous than the square root scheme, we derive some general formulas and properties for the linear scheme first.

4.3.3 Properties of the linear scheme

In the linear case, there is an explicit formula for the velocity of the classical particle after the n^{th} collisions, namely

$$v_n = \begin{cases} n(v_d - v_m) + v_0 & n \text{ even} \\ (n-1)(v_m - v_d) + 2v_m - v_0 & n \text{ odd} \end{cases} \tag{4.5}$$

where even n corresponds to the velocity after a diode collision and odd n corresponds to the velocity after a mirror collision. We can also write down an expression for the corresponding time t_n for which the n^{th} collision happens

$$t_n = \frac{x_i}{v_m - v_0}\left(\prod_{k\geq 2 \text{ even}}^{n-1} \frac{v_k - v_d}{v_k - v_m}\right)\left(\prod_{l \text{ odd}}^{n-1} \frac{v_l - v_m}{v_l - v_d}\right). \tag{4.6}$$

We can use Eq. (4.5) to calculate the maximum number of collisions (if there is no further time restriction): After the last collision ($n = n_{max}$), we have

$v_d \leq v_{n_{max}} \leq v_m$. From this, it follows:

$$\begin{aligned} v_d \leq \; & v_0 - n_{max}\Delta v_{md} \; \leq v_m, \\ \frac{v_0 - v_m}{\Delta v_{md}} \leq \; & n_{max} \; \leq \frac{v_0 - v_d}{\Delta v_{md}}, \\ r - 1 \leq \; & n_{max} \; \leq r \end{aligned} \tag{4.7}$$

where $\Delta v_{md} = v_m - v_d > 0$ and $r = \dfrac{v_0 - v_d}{\Delta v_{md}}$. For an even n, with $1 < n \leq n_{max}$, it follows therefore that $n \leq r$ and therefore

$$\begin{aligned} v_0 - n\Delta v_{md} \; & \geq \; (n-2)\Delta v_{md} + 2v_m - v_0, \\ v_n \; & \geq \; v_{n-1}. \end{aligned} \tag{4.8}$$

From Eq. (4.5), it also follows immediately that

$$v_n - v_{n-2} = \begin{cases} -2\Delta v_{md} < 0 & n \text{ even} \\ 2\Delta v_{md} > 0 & n \text{ odd} \end{cases}. \tag{4.9}$$

We want to recall that v_n is an algebraic value here, not the absolute value of the velocity. In the case of n odd (after a collision with the mirror), v_n and v_{n-2} are almost always negative, therefore from the statement $v_n - v_{n-2} > 0$ it follows that almost always $|v_n| < |v_{n-2}|$.

4.3.4 Comparison of the square-root and linear schemes for a single particle

Let $v_m = d/T$ where d is the final position of the mirror and T is the total time, v_m is also the velocity of the mirror in the linear scheme. For comparison, we chose $\alpha_{d/m} = v_{d/m}\sqrt{T}$ in the square-root scheme in such a way that the initial and final position of diode and mirror is the same in both schemes.

In Fig. 4.3, the velocity of the particle v_n after a collision is shown versus

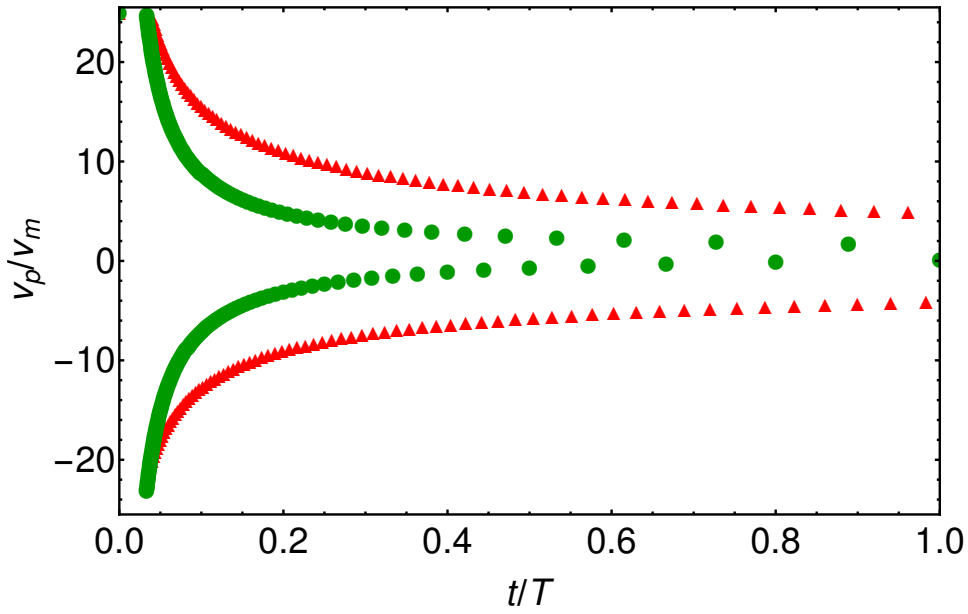

FIGURE 4.3: Classical setting: graph of the velocity of the particle as a function of time, each symbol indicates the velocity of the particle after a collision; parameters for linear scheme (green dots): $v_m = d/T$, $v_d = 0.9v_m$; parameters for square root scheme (red triangles): $\alpha_m = v_m\sqrt{T}$, $\alpha_d = v_d\sqrt{T}$.

time, for the square-root scheme as well as for the linear scheme. We see the velocity of the particle in the trap tends towards $v_d \leq v_p(t) \leq v_m$ for larger t; furthermore the particle is localised $x_d(t) \leq x_p(t) \leq x_m(t)$. We see this behaviour in the linear case and in the case of the square root; however we do not see the same level of velocity reduction in Fig. 4.3 in the square-root case as in the linear case: the reducing of the velocity occurs in the linear trap on a much shorter timescale than that of the square root trap (it takes much longer to achieve the same reduction in velocity for the square-root trap).

If we consider again the linear case in Fig. 4.3, then we will also see all the general properties of Eq. (4.9): the upper branch (corresponds to n even, i.e. velocities after diode collisions) is decreasing with increasing time (which correspond to increasing number of collisions), the lower branch (corresponds to n odd, i.e. velocities after mirror collisions) is increasing with increasing time (which correspond to increasing number of collisions) and the upper branch is always above the lower branch.

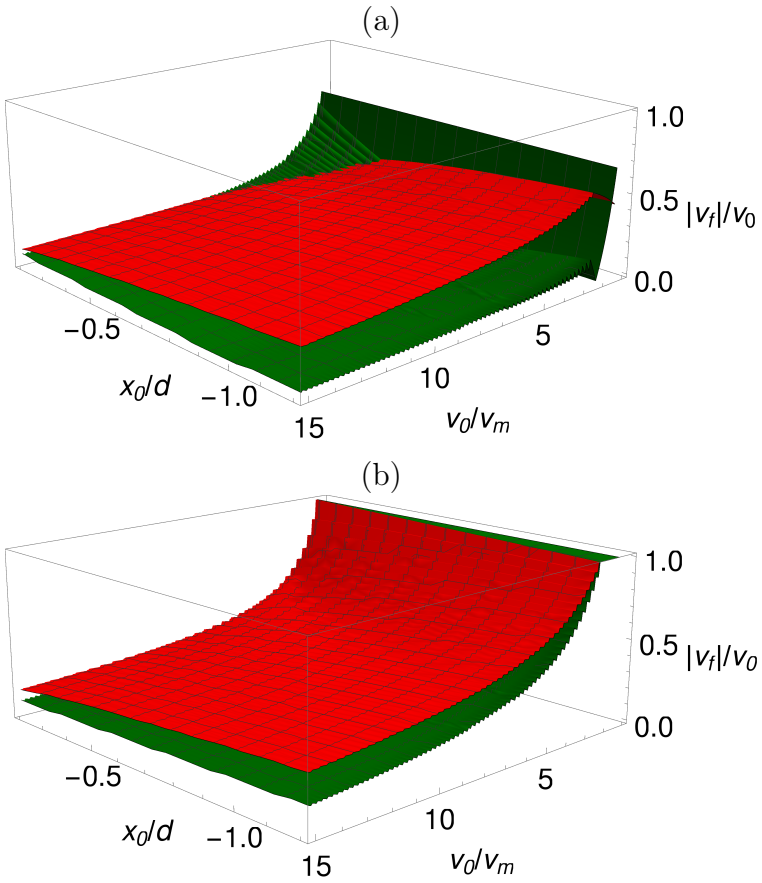

FIGURE 4.4: Classical setting: plot of $\frac{|v_f|}{v_0}$ versus initial particle velocity v_0 and initial particle position x_0: (a) velocity v_f after the last collision with the mirror, (b) velocity v_f after the last collision with the diode. Linear scheme (green, lower planes) and square root scheme (red, higher planes), other parameters are the same as in Fig. 4.3.

The ratio between final particle velocity after the last mirror resp. diode collision and the initial particle velocity is shown in Fig. 4.4. We see from $|v_f|/v_0 < 1$ that we have achieved a reduction in velocity. We can compare this relative performance of the square root and linear schemes. We see the linear scheme is much more successful for reducing final velocity ($\frac{|v_f|}{v_0}$ displayed) than the square root scheme. The surfaces begin to approach each other when the particle that is travelling slowly and starts close to the diode-mirror system. This is because a slow travelling particle is less likely to collide with the the diode-mirror system and so is less likely to have achieved any velocity reduction.

From Fig. 4.4 we expect that by sending in a particle or an ensemble with a

probability distribution of velocity and position, we achieve the cooling desired, this is examined in the following.

4.3.5 Compression in classical phase space

We now discuss the more general case where we have a cloud of non-interacting particles characterised by some probability density $\rho(t, x, v)$. In particular we look at a Gaussian initial distribution given by

$$\rho(0, x, v) = \frac{1}{2\pi\Delta v\Delta x} e^{-\left[\left(\frac{x-x_0}{2\Delta x}\right)^2+\left(\frac{v-v_0}{2\Delta v}\right)^2\right]}. \tag{4.10}$$

We calculate the final probability distribution at time $t = T$, $\rho(T, x, v)$ for the linear and square root schemes and compare the ability in each case to cool the cloud. In Fig. 4.5 this comparison between the initial and final velocity distributions ($\rho(t, v) = \int dx\rho(t, x, v)$ for $t = 0, T$) is shown and we see that both schemes achieve a reduction in velocity. The linear scheme however achieves a greater reduction in velocity than the square root one similar to the single particle case shown in Fig. 4.3 and Fig. 4.4. It is interesting that the final velocity distribution is independent of the initial average velocity v_0 for the linear scheme. The dots in Fig. 4.5 correspond to the final velocities after the mirror collision resp. diode collision which are achieved if we consider a single particle in the diode-mirror system with v_0 and x_0 being the average velocity and position of the ensemble.

We find that the positions of the peaks correspond approximately to these velocities. To underline the compression in phase space, the initial and final distribution $\rho(0, x, v)$ resp. $\rho(T, x, v)$ is shown in Fig. 4.6 for the linear scheme. For clarification, both distributions are shown scaled such that their maximum is one and the initial distribution is also shifted. It can be clearly seen that the cooling resp. compression in phase space is achieved.

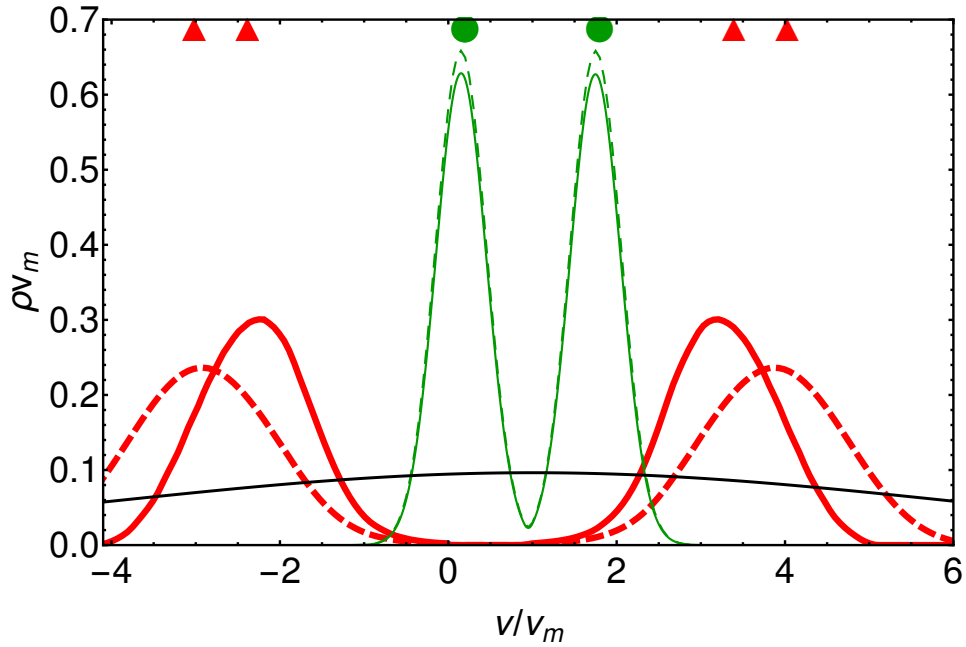

FIGURE 4.5: Classical setting: comparison between velocity distribution using the linear and square root schemes: initial velocity distribution for both schemes (shifted, black, lowest broad distribution), final velocity distribution: for the square-root scheme: $v_0 = 10v_m$ (red, thick, solid line), $v_0 = 15v_m$ (red, thick, dashed line); for the linear scheme: $v_0 = 10v_m$ (green, thin, solid line), $v_0 = 15v_m$ (green, thin, dashed line). The dots above the plots correspond to a single particle simulation with initial velocity v_0 and initial position x_0; other parameters: $x_0 = -0.8d, \Delta x = 0.1d, \Delta v = 5v_m$; other parameters are the same as in Fig. 4.3.

We have shown that the efficiency depends strongly on the trajectories of atom diode and atomic mirror. It turns out that the linear scheme is much more efficient that the square-root scheme in the classical setting. Therefore, we will consider now solely the linear scheme in a quantum setting.

4.4 Quantum Catcher

Inspired by the preliminary and promising classical results, we would like to consider if such a similar cooling is possible using a quantum mechanical treatment. We again consider a single quantum particle moving in one dimension. We want the quantum diode-mirror system to operate similarly to the classical

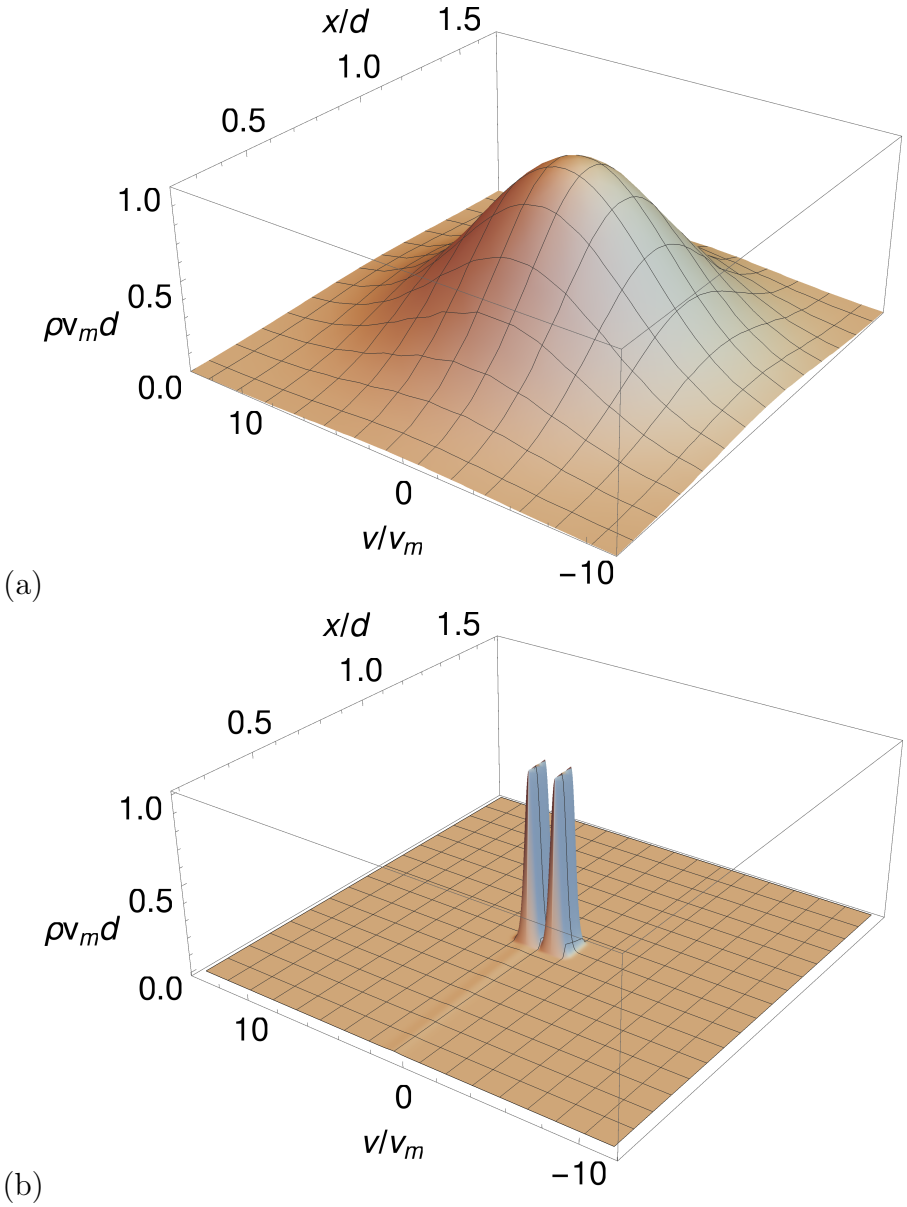

FIGURE 4.6: Classical setting: (a) shifted initial distribution $\rho(0, x, v)$ and (b) final distribution $\rho(T, x, v)$. Both distributions are scaled such that their maximum is one. Linear scheme, $v_0 = 10v_m$, other parameters as in Fig. 4.5.

case; we expect however differences as there will be quantum effects and the dependence on mass in the Schrödinger equation.

4.4.1 Implementing a quantum atom diode and mirror

While the reflection mirror can be realised for example in experiments by an optical potential, the implementation of an atom diode is less straightforward.

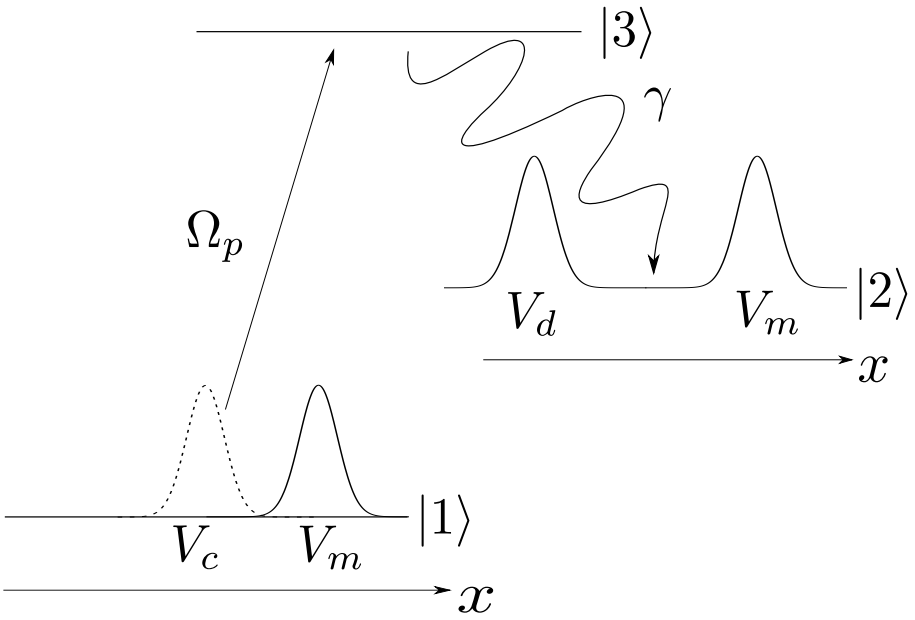

FIGURE 4.7: Quantum atom diode and atomic mirror scheme.

A theoretical proposal for such a diode is found for example in [75] and a similar one (see Fig. 4.7) we use throughout the remaining paper.

We assume a three-level atom where the three levels are represented by $|1\rangle$, $|2\rangle$ and $|3\rangle$, see Fig. 4.7; the states $|1\rangle$ and $|2\rangle$ are (meta-)stable and there is spontaneous emission from state $|3\rangle$ to state $|2\rangle$. We start with the mirror potential $V_m(x)$ which acts on the atom independent of whether it's in state $|1\rangle$ or $|2\rangle$. For implementation of the atom diode, we assume a coupling between levels $|1\rangle$ and $|3\rangle$ with a Rabi frequency $\Omega_p(x)$. State $|3\rangle$ decays quickly with decay constant γ to the stable state $|2\rangle$. Finally there is a state selective potential $V_d(x)$ (placed on the left hand side of $\Omega_p(x)$ and $V_m(x)$) which effects the atom only if it is in state $|2\rangle$. Assume the particle is now incident from the left in state $|1\rangle$ it is then pumped to state $|3\rangle$ where it decays to state $|2\rangle$ in such a way that it is then located and therefore trapped between the the two potentials $V_d(x)$ and $V_m(x)$.

The master equation for the three level diode-mirror system described above (neglecting recoil) is

$$\frac{\partial}{\partial t}\rho(t) = -\frac{i}{\hbar}\left[\hat{H}_{3L}, \rho(t)\right]_- - \frac{\gamma}{2}\{\rho(t)|3\rangle\langle 3| + |3\rangle\langle 3|\rho(t)\} + \gamma|2\rangle\langle 3|\rho(t)|3\rangle\langle 2|. \tag{4.11}$$

The Hamiltonian is

$$\hat{H}_{3L} = -\frac{\hbar^2}{2m}\frac{\partial^2}{\partial x^2} + \begin{pmatrix} V_m(x,t) & 0 & \hbar\Omega_p(x,t)/2 \\ 0 & V_d(x,t)+V_m(x,t) & 0 \\ \hbar\Omega_p(x,t)/2 & 0 & 0 \end{pmatrix}. \tag{4.12}$$

The situation is quite different from the classical case because here the probability density depends on the mass m of the particle chosen.

At initial time $t = 0$, we start in a pure state and the initial wavefunction of the particle is a Gaussian (not necessarily a minimum-uncertainty product one)

$$\psi_0(x) = A\times \exp\left\{-\frac{1}{1+ic}\left(\frac{m^2\Delta v^2}{\hbar^2}(x-x_0)^2 + i\frac{mv_0}{\hbar}(x-x_0)\right)\right\} \tag{4.13}$$

where $c = \sqrt{\frac{\Delta x^2 m^2 \Delta v^2}{\hbar^2} - \frac{1}{4}}$ and A is a normalisation constant. Note that $c \geq 0$ due to the Heisenberg uncertainty relation.

We use the quantum jump/trajectory approach [95, 96, 97, 98] to solve the above 1D master equation (4.11) numerically. In the quantum-jump approach, the master equation (4.11) is solved by averaging over "trajectories" with time intervals in which the wave function evolves with the conditional Hamiltonian interrupted by random jumps (decay events). In the dynamics before the first

spontaneous photon emission, we assume that the quenching laser Ω_p and the decay can be approximated by an effective complex potential $-iV_c(x-x_c(t)) = -i\frac{\hbar\Omega_p(x-x_c(t))^2}{2\gamma}$. To be more explicit, before the jump we model our effective Hamiltonian by

$$\hat{H}_A = -\frac{\hbar^2}{2m}\frac{\partial^2}{\partial x^2} + V_m(x-x_m(t)) - iV_c(x-x_c(t)) \tag{4.14}$$

and after the jump we model our Hamiltonian by

$$\hat{H}_B = -\frac{\hbar^2}{2m}\frac{\partial^2}{\partial x^2} + V_m(x-x_m(t)) + V_d(x-x_d(t)) \tag{4.15}$$

where

$$V_{d/m}(x) = V_{0,d/m}e^{\frac{-x^2}{2\sigma_{d/m}}},\ V_c(x) = V_{0,c}e^{\frac{-x^2}{\sigma_c}}. \tag{4.16}$$

This means that atomic mirror and the reflecting potential of the atom diode are both implemented with Gaussian potentials $V_{d/m}(x)$. To avoid having the diode, mirror and imaginary potential all starting in the same point, we assume that all potentials are at rest until a given time t_{rest} and only then begin moving linearly, i.e. their trajectory is

$$x_{d/m/c} = \begin{cases} v_{d/m/c}t_{rest} & 0 \geq t \geq t_{rest} \\ v_{d/m/c}t & t > t_{rest} \end{cases}. \tag{4.17}$$

At final time the velocity-probability distribution is given by $\rho(T,v) = \langle v|\rho(T)|v\rangle$, and the position-probability distribution is given by $\rho(T,x) = \langle x|\rho(T)|x\rangle$.

4.4.2 Results

In the following, we choose the parameters shown in the caption of Fig. 4.8. The classical results are independent of the particle mass (as only free motion

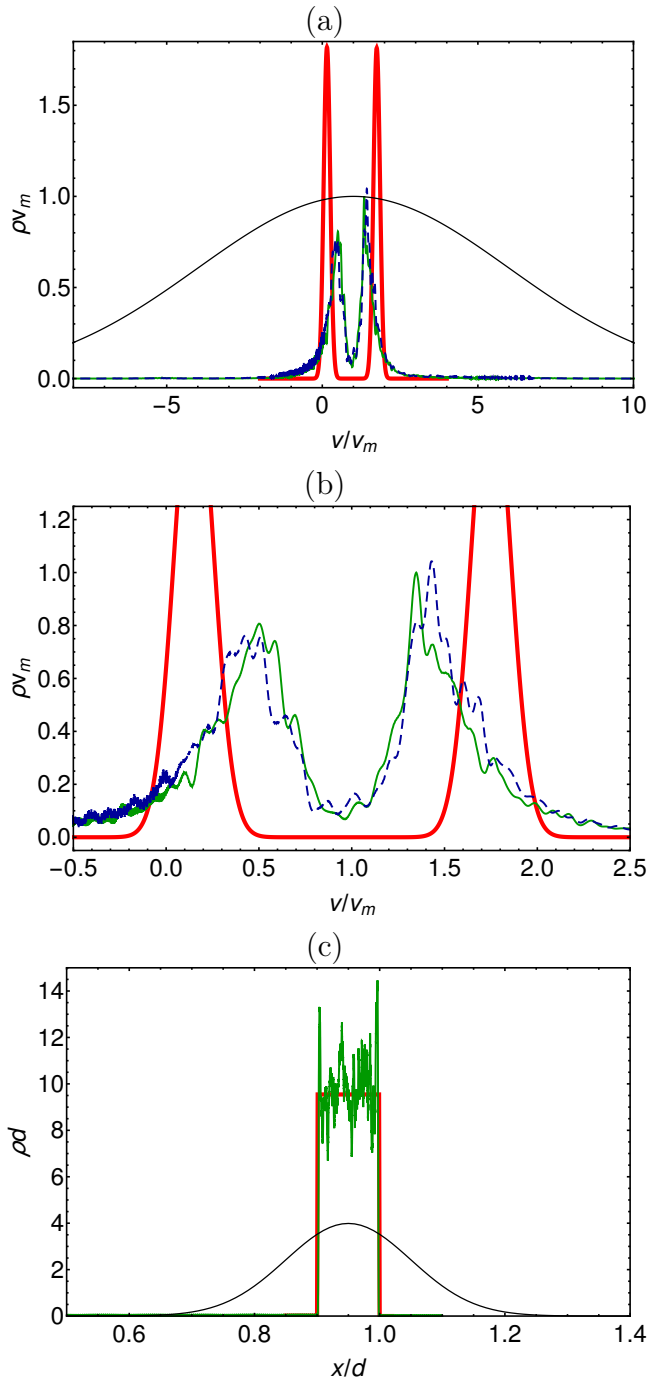

FIGURE 4.8: Probability distributions: initial distribution (shifted, black, solid lines), final distributions for the classical setting (red, thick line), quantum setting with $v_0 = 10v_m$ (green, thin line) and quantum setting with $v_0 = 8v_m$ (blue, dashed line); (a) velocity space, (b) velocity space zoomed in (c) position space. Common parameters: $v_d = 0.9v_m$, $\Delta v = 5v_m$, $x_0 = -0.8d$, $\Delta x = 0.1d$. Additional parameters in the quantum setting: $V_{0,d/m} = 5 \times 10^6 \hbar/T$, $V_{0,c} = 4 \times 10^4 \hbar/T$, $v_c = 0.98v_m$, $\sigma_c = 0.0006d, \sigma_d = \sigma_m = 0.0001d$, $m = 1000T\hbar/d^2$.

and ideal, elastic collisions with ideal walls are considered). The quantum-mechanical result depends on the mass. First, we set $m = 1000T\hbar/d^2$ and later we will examine different mass values.

In Fig. 4.8 the initial and final velocity distribution are shown and there is a good qualitative correlation between the classical and quantum distributions. In Fig. 4.8 (a) we see that in both the quantum and classical distributions are much compressed compared to the original very broad distribution. As expected the particles are confined between the two walls of the catcher (see Fig. 4.8 (c)). Therefore the position distribution is much narrower than the initial distribution, together with the compression in velocity distribution gives us the cooling we desired. The quantum scheme even retains another interesting property of the classical system; we see in Fig. 4.8 (b) that, similar to the classical version, the velocity at final time T is almost independent of the initial velocity.

In Fig. 4.8 (a) and (b) a difference between the two cases can be seen, the quantum distribution is significantly broader than the classical; further they are less smooth. This appears to be partly because of the quenching of the wave function when it has to transition from being in state $|1\rangle$ to state $|2\rangle$.

An interesting effect to note however is that the quantum system performs better than the classical. This effect appears to be due to the broadness of our potentials $V_{d/m}$; in the classical simulation we treat these walls as infinitely high while in the quantum case they have the form of Eq. (4.16).

Heuristically this cooling scheme works through repeated collisions with the mirror/diode and so the effect of the broad potential increases cooling as the particle is reflected far from the centre of the potential. Therefore, in Fig. 4.9, we examine the effect of reducing $\sigma_{d/m}$. We see that for smaller $\sigma_{d/m}$ we get closer agreement between quantum and classical schemes. This is because for smaller values of $\sigma_{d/m}$ our quantum potentials behave more and more like the infinite potential barriers in the classical case. As there are so many collisions

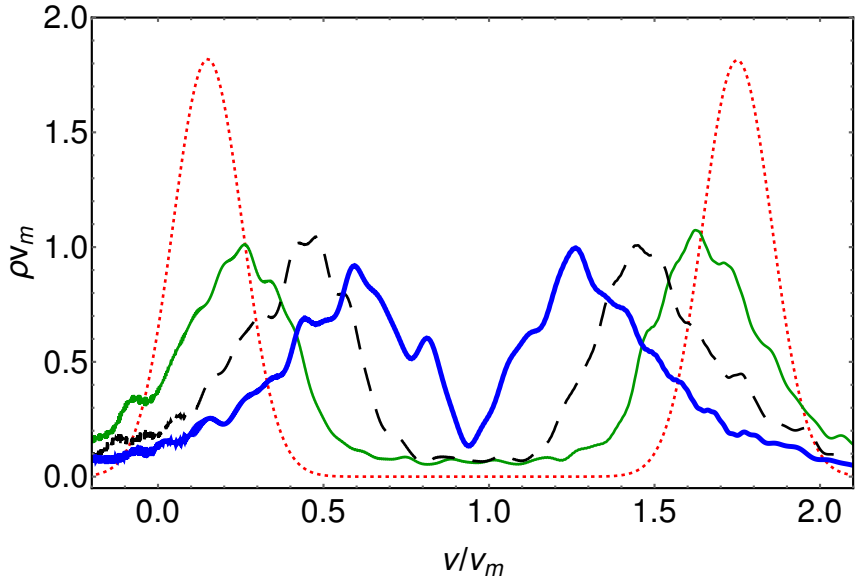

FIGURE 4.9: Final quantum velocity distribution with decreasing $\sigma_{d/m}$: $\sigma_{d/m} = 0.0008d$ (blue, thick, solid line), $\sigma_{d/m} = 0.0004d$ (black, dashed line), $\sigma_{d/m} = 0.0001d$ (green, thin, solid line) and classical distribution (red, dotted line). $V_{d/m} = 5 \times 10^5 \hbar/T$, other parameters are the same as in Fig. 4.8.

that take place in the diode-mirror system it is quite sensitive to tuning of the parameter $\sigma_{d/m}$, with broader potentials enabling better cooling in the trap.

To underline further the generality of this cooling method, we now consider different mass values in Fig. 4.10. We see that for all mass values examined, we get a similar compression of the velocity distribution. In all these cases, the position distribution is also located at the end between diode and mirror potential (similar to the case shown in Fig. 4.8(c)). Therefore, for all mass values examined, we get a similar compression of the velocity and position distribution, i.e. cooling of the quantum particle.

All the results are presented using dimensionless variables to underline the broad applicability of the cooling method. Therefore, the results can correspond to several, different physical settings. For example, the dimensionless parameters in Fig. 4.10 (red, dotted line) would in the case of the light alkali ^7Li and when we assume a $1/e^2$ beam waist of $1\mu m$, we get $\sigma_{d/m} = 0.5\,\mu m$ and $d = 500\,\mu m$ then correspond to $T \approx 13.8\,ms$ and $v_0 \approx 0.36\,ms^{-1}$.

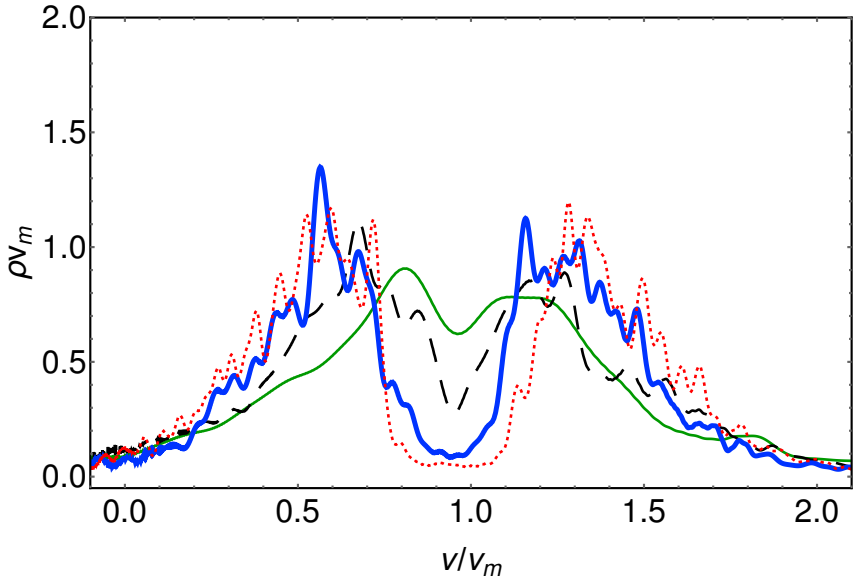

FIGURE 4.10: Final quantum velocity distribution with different masses: $m = 500T\hbar/d^2$ (green, thin, solid line), $m = 1000T\hbar/d^2$ (black, dashed line), $m = 1500T\hbar/d^2$ (blue, thick, solid line) and $m = 2000T\hbar/d^2$ (red, dotted line). $V_{d/m} = 5 \times 10^5\hbar/T$, $\sigma_{d/m/c} = 0.001d$, other parameters are the same as in Fig. 4.8.

4.5 Conclusion

In this paper we have presented a method for trapping and cooling particles using an atom diode-mirror system. We investigated different trajectories for the diode and the mirror. In particular we found a strong dependence of the efficiency on the trajectory: through classical numerical simulations of linear and square root trajectories we deduced the advantages of the linear scheme for cooling. We propose a way to implement the atom diode and mirror system quantum mechanically; we then applied it to the trapping and cooling of a quantum particle. Through further numerical simulations we demonstrated that we can achieve cooling also in this quantum setting. Especially, we examined several parameter setting to underline the the broad applicability of this cooling method.

Chapter 5

Fast and robust moving of atoms through an optical lattice

Abstract

Precise control of quantum particles is required for many interesting or novel experiments. Here we consider the task of moving atoms from one well of an optical lattice to another without motional excitations. To achieve this we apply techniques from Shorctuts to Adiabaticity (STA) enabling fast and robust state manipulation. The process is split up into three independent building blocks; first the atoms must be loaded into an additional external harmonic trap; this trap is then moved from one lattice site to another and finally is it unloaded back onto the lattice by decreasing the frequency of the external harmonic trap.

5.1 Introduction

Robust high fidelity control of quantum systems is essential for all quantum technologies. Of particular interest is the movement of particles without energy excitations. Optical tweezers have become a common approach to enable precise control of single atom experiments and in recent years have been used to atom-by-atom assemble arrays in two and three dimensions [99, 100]. A major

application of these optical tweezers has been as a means of transporting particles [101] and trying to achieve robust and lossless transport on shorter than adiabatic timescales [102].

Other applications of optical tweezers are used to assemble defect-free one-dimensional arrays of cold neutral atoms [103], motivated by a number of applications such as many qubit experiments or studying many-body physics in the Hubbard model such as antiferromagnetic spin chains in an optical lattice [104] or entangling neutral atoms using local spin exchange [105].

The ability to manipulate arrays of atoms on a lattice immediately has applications of realizing Maxwell's demon in a three-dimensional lattice [106]. Here the sorting of a lattice, such that every site is filled, leads to a lower entropy state. This has potential as a first step towards neutral atom quantum computers. There are also potential applications in the manipulation of Bose-Einstein condensates for mixing different species [107] for experiments in many body quantum physics such as Bose polarons created through impurities in condensates [108] . Both the transport and loading of atoms are important goals in all these experiments and applications.

The preparation and manipulation of many-particle systems e.g. Bose-Einstein condensates, requires fast and robust quantum engineering protocols. A typical approach to manipulate these quantum systems is through the use of an adiabatic Hamiltonian; however this Hamiltonian must be varied sufficiently slowly to avoid excitations [32]. Adiabatic processes have long process times and are vulnerable to decoherence, this makes them unsuitable for processes that need to be both fast and robust.

One set of techniques to achieve a more robust manipulation is Shortcuts to Adiabaticity [8]. This collection of techniques allows for high fidelity preparation and manipulation of quantum systems on short time-scales. Previous works have demonstrated the effectiveness of Shortcuts to Adiabatacity for transport of particles and have extended this treatment to Bose Einstein condensates [11]

and also to fast trap variations with condensates [12]. In this chapter we seek to transport atoms across an optical lattice using techniques from Shortcuts to Adiabaticity, suggesting a new approach to the transport of atoms across optical lattices. We examine a number of different strategies for achieving fast and robust transport of atoms or Bose-Einstein condensates over a lattice using invariant engineering based on the methods of STA.

5.2 Model and STA

We consider a potential consisting of harmonic trap and an optical lattice in one dimension, the potential $V(x,t)$ of such a system is given by,

$$V(x,t) = \frac{1}{2}m\omega(t)^2(\hat{x} - q_0(t))^2 + U_0 \sin^2\left(\frac{\hat{x}}{\sigma}\right). \tag{5.1}$$

Where the trap frequency $\omega(t)$ and the trap centre position $q_0(t)$ are time dependent. We now examine two different systems, first let us start by considering a single quantum particle governed by the one dimensional Schrödinger equation,

$$i\hbar\frac{\partial}{\partial t}|\psi(t)\rangle = \left[\frac{p^2}{2m} + V(x,t)\right]|\psi(t)\rangle. \tag{5.2}$$

Further we also discuss a Bose-Einstein condensate governed by the Gross-Pitaevskii equation (G-P Eq.),

$$i\hbar\frac{\partial}{\partial t}|\psi(t)\rangle = \left[\frac{p^2}{2m} + V(x,t) + g(t)|\psi(x,t)|^2\right]|\psi(t)\rangle. \tag{5.3}$$

The $g(t)$ here models the atom-atom interaction in the condensate.

Our goal is to move a particle or Bose-Einstein condensate from one lattice site to another using an external trap. To achieve this we split the moving process into a number of building blocks as follows:

- Loading particles initially on a lattice into a harmonic trap,
- Transport of particles confined in a harmonic trap across an optical lattice,
- Opening the harmonic trap and unloading the particles back onto the lattice.

A schematic of these three building blocks is seen in Fig. 5.1; in (a) there is a schematic of loading the particles or condensate into the external trapping potential, (b) shows the transport of the trap across a lattice site and (c) shows the unloading of the particle or condensate back onto the lattice. Through the concatenation of these steps we can move particles across many different lattice sites. We will apply STA techniques to perform each of these building blocks to achieve fast and robust movement across the lattice.

5.2.1 Single Particle System

We first make a harmonic approximation of the potential in Eq. (5.1) obtaining

$$V(x,t) = \frac{1}{2}m\tilde{\omega}(t)^2(\hat{x} - x_{min}(t))^2 + V(x_{min}), \tag{5.4}$$

where we have the frequency of the virtual harmonic trap $\tilde{\omega}(t)$ and trap centre position for the virtual trap $x_{\min}(t)$ related to the real trap frequency $\omega(t)$ and real trap centre position $q_0(t)$ by

$$\omega(t)^2 = \tilde{\omega}(t)^2 - \Omega^2 \cos\left(2x_{\min}(t)/\sigma\right), \tag{5.5}$$

$$q_0(t) = x_{min}(t) + \frac{\Omega^2}{\omega^2} \sin\left(\frac{x_{\min}(t)}{\sigma}\right) \cos\left(\frac{x_{\min}(t)}{\sigma}\right). \tag{5.6}$$

We have defined the frequency $\Omega = \sqrt{2\frac{U_0}{\sigma^2 m}}$; this Ω corresponds to the frequency of the harmonic approximation of the well of the lattice. We will also use a time unit T defined by $T = 1/\Omega$. While Eq. (5.6) can not be solved

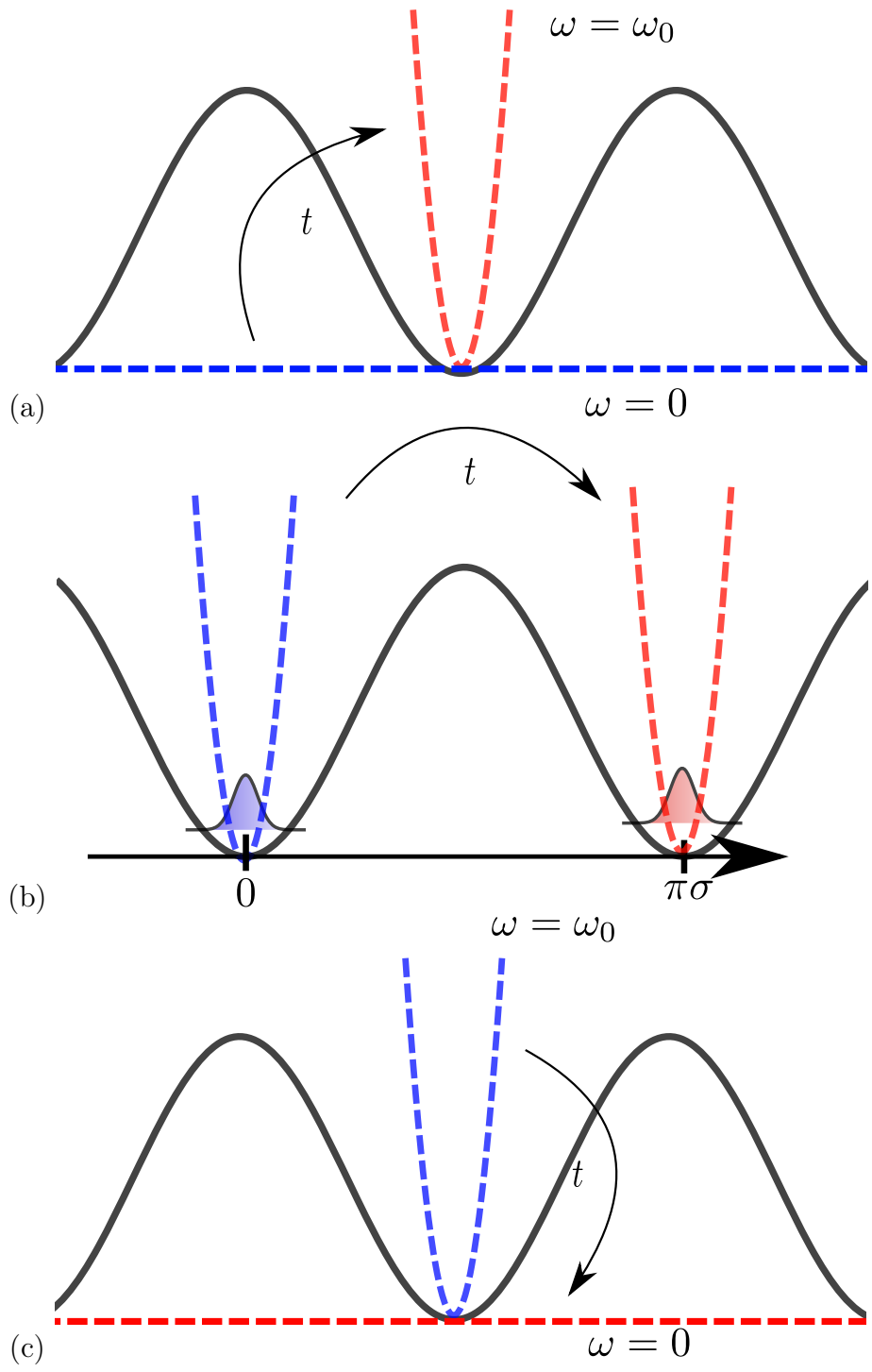

FIGURE 5.1: Schematic of different control tasks: (a) Loading sample into an external harmonic trap (b) Transporting sample across a lattice (c) Unloading sample back onto lattice.

analytically we can solve it numerically to find $x_{\min}$ for a given q_0.

Now that we have this system written in the form of a harmonic trap we can

apply the analysis developed in [8] to develop shortcut schemes for it. We want to start in an eigenstate of the Hamiltonian $H(0)$ and finish in an eigenstate of the the final Hamiltonian $H(t_f)$, either shifted over a lattice site or with the harmonic trap turned on or off. To do this we use the method of inverse engineering using the Lewis-Reisenfeld invariant [15]. A Harmonic potential of the form in Eq. (5.4) has a dynamical invariant (see Chapter 2)

$$I(t) = \frac{1}{2m}\underbrace{[\rho(\hat{p} - mq_c) - m\dot{\rho}(\hat{x} - q_c)]^2}_{=\hat{A}^2} + \frac{1}{2}m\tilde{\omega}(0)^2\underbrace{\left(\frac{\hat{x} - q_c}{\rho}\right)^2}_{=\hat{B}^2}. \tag{5.7}$$

The $\rho(t)$ and q_c functions are auxiliary functions that obey auxiliary equations

$$\rho^3(\ddot{\rho} + \rho\tilde{\omega}^2) - \tilde{\omega}_0^2 = 0, \tag{5.8}$$

$$\ddot{q}_c + \omega^2(q_c - x_{\min}) = 0. \tag{5.9}$$

The Eqs. (5.8) and (5.9) relate the auxiliary functions $\rho(t)$ and q_c to the virtual harmonic trap parameters $x_{\min}(t)$ and $\tilde{\omega}(t)$.

To derive the appropriate boundary conditions on $\rho(t)$ and $q_c(t)$ for high fidelity state transition, we demand that the Hamiltonian $H(t)$ and the invariant $I(t)$ commute at initial and final times *i.e.* $[I(0), H(0)] = [I(t_f), H(t_f)] = 0$. From the resulting expressions, we derive the boundary conditions on the auxiliary functions $\rho(t)$ and $q_c(t)$. Therefore we first calculate the commutator $[I(t), H(t)]$,

$$\begin{aligned}
[I(t), H(t)] &= \frac{1}{4}\Big(1/m^2\left[\hat{A}^2, \hat{p}^2\right] + \tilde{\omega}^2\left[\hat{A}^2, (\hat{x} - x_{min})^2\right] + \tilde{\omega}_0^2\left[\hat{B}^2, \hat{p}^2\right] \\
&\qquad + m^2\tilde{\omega}_0^2\tilde{\omega}^2\underbrace{\left[\hat{B}^2, (\hat{x} - x_{min})^2\right]}_{=0}\Big) \\
&= \frac{\hbar}{2i}\Big\{\dot{\rho}\frac{1}{m}\left(\hat{A}\hat{p} + \hat{p}\hat{A}\right) + \tilde{\omega}^2\rho\left(\hat{A}(\hat{x} - x_{min}) + (\hat{x} - x_{min})\hat{A}\right) \\
&\qquad - \frac{\tilde{\omega}_0^2}{\rho}\left(\hat{B}\hat{p} + \hat{p}\hat{B}\right)\Big\}
\end{aligned}$$

$$
\begin{aligned}
= \frac{i\hbar}{2} \quad \Bigg[\quad & (\hat{x}\hat{p}+\hat{p}\hat{x})\left\{\dot{\rho}^2+\frac{\tilde{\omega}_0^2}{\rho^2}-\tilde{\omega}^2\rho^2\right\}+\hat{p}^2\left\{-2\frac{\rho\dot{\rho}}{m}\right\}+\hat{x}^2\left\{2m\tilde{\omega}^2\dot{\rho}\rho\right\} \\
+ \quad & \hat{p}\left\{2\rho^2\tilde{\omega}^2x_{min}-2\dot{\rho}(q_c\dot{\rho}-\dot{q}_c)-2q_c\frac{\tilde{\omega}_0}{\rho^2}\right\} \\
+ \quad & \hat{x}\left\{2m\tilde{\omega}^2\rho(\dot{q}_c\rho-\dot{\rho}q_c-\dot{\rho}x_{min})\right\}+\left\{2m\tilde{\omega}^2\rho x_{min}(\dot{\rho}q_c-\dot{q}_c\rho)\right\}\Bigg].
\end{aligned}
$$

Now we require everything in the curly brackets to be zero at times $t=0$ and $t=t_f$ and from this we derive the following boundary conditions on $\rho(t)$ and $q_c(t)$

$$
\begin{aligned}
\rho(0)=1; \quad & q_c(0)=x_{min}(0) \\
\rho(t_f)=\sqrt{\frac{\tilde{\omega}(0)}{\tilde{\omega}(t_f)}}; \quad & q_c(t_f)=x_{min}(t_f) \\
\dot{\rho}(0)=0; \quad & \dot{q}_c(0)=0 \\
\dot{\rho}(t_f)=0; \quad & \dot{q}_c(t_f)=0.
\end{aligned}
$$

We further set boundary conditions on the second derivatives, looking again at Eqn. (5.8) for initial and final times

$$
\begin{aligned}
\tilde{\omega}^2(0) &= -\ddot{\rho}(0)+\tilde{\omega}(0)^2 \\
\tilde{\omega}^2(t_f) &= -\ddot{\rho}(t_f)+\tilde{\omega}(t_f)^2.
\end{aligned} \tag{5.10}
$$

From Eqn. (5.9) for initial and final times

$$
\begin{aligned}
x_{\min}(0) &= x_{\min}(0)+\frac{\ddot{q}_c(t)}{\tilde{\omega}(t)^2} \\
x_{\min}(t_f) &= x_{\min}(t_f)+\frac{\ddot{q}_c(t_f)}{\tilde{\omega}(t_f)^2}.
\end{aligned} \tag{5.11}
$$

From Eqs. (5.10) and (5.11) we set the boundary conditions $\ddot{\rho}(0)=\ddot{\rho}(t_f)=0$ and $\ddot{q}_c(0)=\ddot{q}_c(t_f)=0$.

5.2.2 Bose-Einstein System

In the previous subsection we developed a shortcut framework for moving a single particle across a lattice site. In the following we will describe how STA techniques can be applied to a Bose-Einstein condensate; this is based on combining the results of previous work transporting a condensate [11] and varying the trap parameters for a condensate [12]. The initial ground state and final state can be found by solving the relevant time-independent Gross-Pitaevskii equation

$$\mu\psi_0(x) = \Bigg[-\frac{\hbar^2}{2m}\partial_x^2 + \frac{1}{2}m\omega(t)^2(x - x_0(t))^2 + U_0 \sin^2\left(\frac{\hat{x}}{\sigma}\right) + g(t)|\psi_0(x)|^2 \Bigg] \psi_0(x). \tag{5.12}$$

We make the same harmonic approximation as in Eq. (5.4) so that the wavefunction evolves according to

$$i\hbar\partial_t\psi(x,t) = \left(-\frac{\hbar^2}{2m}\partial_x^2 + \frac{1}{2}m\omega(t)^2(x - x_0(t))^2 + g(t)|\psi(x,t)|^2 \right) \psi(x,t). \tag{5.13}$$

We wish to be able to extend the shortcut framework developed for the linear case. To do this we make the wavefunction ansatz for Eq. (5.13)

$$\psi(x,t) = e^{-i\alpha_2(t)x^2 + i\alpha_1(t)x - \beta(t) - i\mu\tau(t)}\phi\left(\frac{x - q_c(t)}{\rho(t)}\right) = e^{f(x,t)}\phi(\tilde{x}) \tag{5.14}$$

with variable transformation $\tilde{x} = \dfrac{x - q_c(t)}{\rho(t)}$. Here $\phi(\tilde{x})$ is a solution of the stationary equation

$$\mu\phi(\tilde{x}) = -\frac{\hbar^2}{2m}\partial_{\tilde{x}}^2\phi(\tilde{x}) + \frac{m\omega_0^2}{2}\tilde{x}^2\phi(\tilde{x}) + g_0\left|\phi(\tilde{x})\right|^2\phi(\tilde{x}). \tag{5.15}$$

We now calculate the derivatives of this ansatz Eq. (5.14)

$$i\hbar\partial_t\psi(x,t) = i\hbar e^{f(x,t)}\Big[(\partial_t f(x,t))\phi(\tilde{x}) + \underbrace{\partial_t\phi(\tilde{x})}_{(\partial_t\tilde{x})\partial_{\tilde{x}}\phi(\tilde{x})}\Big]$$

and

$$\begin{aligned}-\frac{\hbar^2}{2m}\partial_x^2\psi(x,t) &= -\frac{\hbar^2}{2m}e^{f(x,t)}[\{(\partial_x f(x,t))^2 + (\partial_x^2 f(x,t))\}\phi(\tilde{x}) \\ &+ 2(\partial_x f(x,t))(\partial_x\tilde{x}(x,t))(\partial_{\tilde{x}}\phi(\tilde{x})) + (\partial_x\tilde{x}(x,t))^2(\partial_{\tilde{x}}^2\phi(\tilde{x}))\end{aligned}$$

with

$$\partial_x\tilde{x}(x,t) = \frac{1}{\rho(t)}, \qquad \partial_t\tilde{x}(x,t) = -\frac{1}{\rho(t)}(\tilde{x}\dot{\rho}(t) - \dot{q}_c(t)),$$
$$\partial_x f(x,t) = i(\alpha_1(t) - 2x\alpha_2(t)), \qquad \partial_x^2 f(x,t) = -2i\alpha_2(t),$$

$$\partial_t f(x,t) = i(x\dot{\alpha}_1(t) - x^2\dot{\alpha}_2(t) + i\dot{\beta}(t) - \mu\dot{\tau}(t)).$$

We can now insert this into the G-P Eq. (5.15) to get:

$$\begin{aligned}&\frac{1}{2m}\phi(\tilde{x})\Big[\frac{g}{g_0}\Big|e^{f(x,t)}\Big|^2 m(m\omega_0^2\tilde{x}^2 - 2\mu) - m^2\omega^2(x-x_0)^2 \\ &+\hbar\{2im(\partial_t f(x,t))\hbar((\partial_x f(x,t))^2 + (\partial_x^2 f(x,t)))\}\Big] \\ &+\frac{\hbar}{m}\partial_{\tilde{x}}\phi(\tilde{x})\Big[im(\partial_t\tilde{x}) + \hbar(\partial_x f(x,t))(\partial_x\tilde{x})\Big] \\ &+\frac{\hbar^2}{2m}(\partial_{\tilde{x}}^2\phi(\tilde{x}))\Big[(\partial_x\tilde{x})^2 - \frac{g}{g_0}\Big|e^{f(x,t)}\Big|^2\Big] = 0. \qquad (5.16)\end{aligned}$$

We next set the coefficients of $\phi(\tilde{x}), \partial_{\tilde{x}}\phi(\tilde{x})$ and $\partial_{\tilde{x}}^2\phi(\tilde{x})$ to 0. Let us first look at the coefficient of $\partial_{\tilde{x}}^2\phi(\tilde{x})$; this coefficient is zero if $g(t) = \frac{e^{2\beta}g_0}{\rho(t)^2}$. Now looking at the coefficient of $\partial_{\tilde{x}}\phi$ we obtain the following two equations

$$\tilde{x}\dot{\rho} - \dot{q}_x - \frac{\hbar}{m}(\alpha_1 - 2(\tilde{x}\rho + q_c)\alpha_2) = 0,$$

and

$$\tilde{x}\underbrace{(m\dot{\rho}+2\rho\alpha_2\hbar)}_{A}-\underbrace{\hbar(\alpha_1-2q_c\alpha_2)-m\dot{(q)}_c}_{B}=0.$$

Solving $A=0$ and $B=0$ for α_1 and α_2 gives

$$\alpha_2 = -\frac{m\dot{\rho}}{2\rho\hbar}, \tag{5.17}$$

$$\alpha_1 = \frac{m}{\hbar\rho}(\dot{q}_c\rho - q_c\dot{\rho}). \tag{5.18}$$

Finally let us look at the $\phi(\tilde{x})$ term; here we have the same auxiliary equations as in Eqs. (5.8) and (5.9)

$$\frac{1}{2\rho^2}C+\frac{m}{2\rho^2}\tilde{x}^2\underbrace{\{\rho^3(\ddot{\rho}+\rho\omega^2)-\omega_0^2\}}_{D}+m\rho\tilde{x}\underbrace{\{\ddot{q}_c+\omega^2(q_c-x_0)\}}_{E}=0. \tag{5.19}$$

We set $D=0$ and $E=0$; these are the same as the auxiliary equations for the single particle case Eqs. (5.23) and (5.24). The C in Eq. (5.19) is given by

$$\begin{aligned} C=\Big[&2\mu+mq_c^2\dot{\rho}^2-\rho\{\dot{\rho}(i\hbar+mq_c\dot{q}_c)+mq_c^2\ddot{\rho}\} \\ &+\rho^2\{2i\hbar(\dot{\beta}+i\mu\dot{\tau})+m(\omega^2(q_c-x_0)^2+\dot{q}_c^2+2q_c\ddot{q}_c)\}\Big] \end{aligned} \tag{5.20}$$

We see that in Eq. (5.19) we have the same auxiliary equations as in the single particle case allowing us to use the same solutions as in the simpler linear case. Finally we need to set $Im\{C\}=Re\{C\}=0$. $Im\{C\}=0$ results in $\beta(t)=\frac{1}{2}ln(\rho(t))$, and with $Re\{C\}=0$, we solve for $\tau(t)$

$$\begin{aligned} \tau=\frac{1}{2\hbar\mu}\int_0^t\frac{1}{\rho^2(\tilde{t})}\Big(&2\mu+mq_c^2(\tilde{t})\dot{\rho}^2(\tilde{t})-2m\rho(\tilde{t})q_c(\tilde{t})\dot{\rho}(\tilde{t})\dot{q}_c(\tilde{t})+m\rho^2(\tilde{t})\dot{q}_c^2(\tilde{t}) \\ &-m\rho(\tilde{t})q_c^2(\tilde{t})\ddot{\rho}(\tilde{t})+m\rho^2(\tilde{t})q_c(\tilde{t})\ddot{q}_c(\tilde{t})+m\rho^2(\tilde{t})x_0(\tilde{t})\ddot{q}_c(\tilde{t})\Big)d\tilde{t}. \end{aligned}$$

5.2.3 Invariant-based Inverse Engineering

We have control functions for the trap position $q_0(t)$ and trap frequency $\omega(t)$ related to the virtual position $x_{\min}(t)$ and virtual frequency $\tilde{\omega}(t)$ by

$$q_0(t) = x_{\min}(t) + \frac{\Omega^2}{\omega(t)^2} \sin\left(\frac{x_{\min}(t)}{\sigma}\right) \cos\left(\frac{x_{\min}(t)}{\sigma}\right) \tag{5.21}$$

$$\tilde{\omega}(t)^2 = \omega(t)^2 + \Omega^2 \cos\left(\frac{2x_{\min}(t)}{\sigma}\right). \tag{5.22}$$

The virtual position and virtual frequency are then related to the auxiliary functions $\rho(t)$ and $q_c(t)$ through the auxiliary equations

$$\rho^3(\ddot{\rho} + \rho\tilde{\omega}^2) - \tilde{\omega}_0^2 = 0, \tag{5.23}$$

$$\ddot{q}_c + \tilde{\omega}^2(q_c - x_{\min}) = 0, \tag{5.24}$$

$$g(t) = \frac{g_0}{\rho(t)}. \tag{5.25}$$

Feschbach resonance can be used to tune the atom-atom interaction according to Eq. (5.25). We now inverse engineer the Eqs. (5.23) and (5.24) to obtain

$$\tilde{\omega}(t)^2 = -\frac{\ddot{\rho}(t)}{\rho(t)} + \frac{\tilde{\omega}(0)^2}{\rho^3} \tag{5.26}$$

$$x_{\min}(t) = q_c(t) + \frac{\ddot{q}_c}{\tilde{\omega}(t)^2} \tag{5.27}$$

Next we proceed to discuss the different building blocks using the developed shortcuts framework. The different control tasks correspond to changing the boundary conditions on the control and auxiliary functions.

5.3 Building Blocks

5.3.1 Loading particles into harmonic trap

The goal here is to load the particle or condensate from a lattice into an external harmonic trap successfully. We start with the external harmonic trap having a frequency of $\omega(0) = 0$ at initial time $t = 0$ and $\omega(t_f) = \omega_f$ at final time t_f. The position of the trap remains unchanged in a well of the lattice $q_0(t) = 0$. Now considering Eqs. (5.23) and (5.24) we see the auxiliary function $q_c(t)$ can be set $q_c(t) = q_0(0) = 0$. This leaves us with Eq. (5.23); and so $\rho(t)$ must satisfy the following boundary conditions,

$$\rho(0) = 1; \tag{5.28}$$

$$\rho(t_f) = \sqrt{\frac{\tilde{\omega}(0)}{\tilde{\omega}(t_f)}}; \tag{5.29}$$

$$\dot{\rho}(0) = \dot{\rho}(t_f) = 0; \tag{5.30}$$

$$\ddot{\rho}(0) = \ddot{\rho}(t_f) = 0. \tag{5.31}$$

We choose a polynomial of minimal degree that satisfies the above boundary conditions for $\rho(t)$. We can then substitute this $\rho(t)$ to find the virtual frequency $\tilde{\omega}(t)$ as a function of time according to,

$$\tilde{\omega}(t)^2 = -\frac{\ddot{\rho}(t)}{\rho(t)} + \frac{\tilde{\omega}(0)^2}{\rho^3}. \tag{5.32}$$

This approach corresponds to having to tune the external trap frequency according to

$$\omega(t)^2 = \tilde{\omega}(t)^2 + \Omega^2, \tag{5.33}$$

We call this approach the shortcut solution. Note that if the harmonic approximation is exact, then the corresponding shortcut scheme will achieve a fidelity of

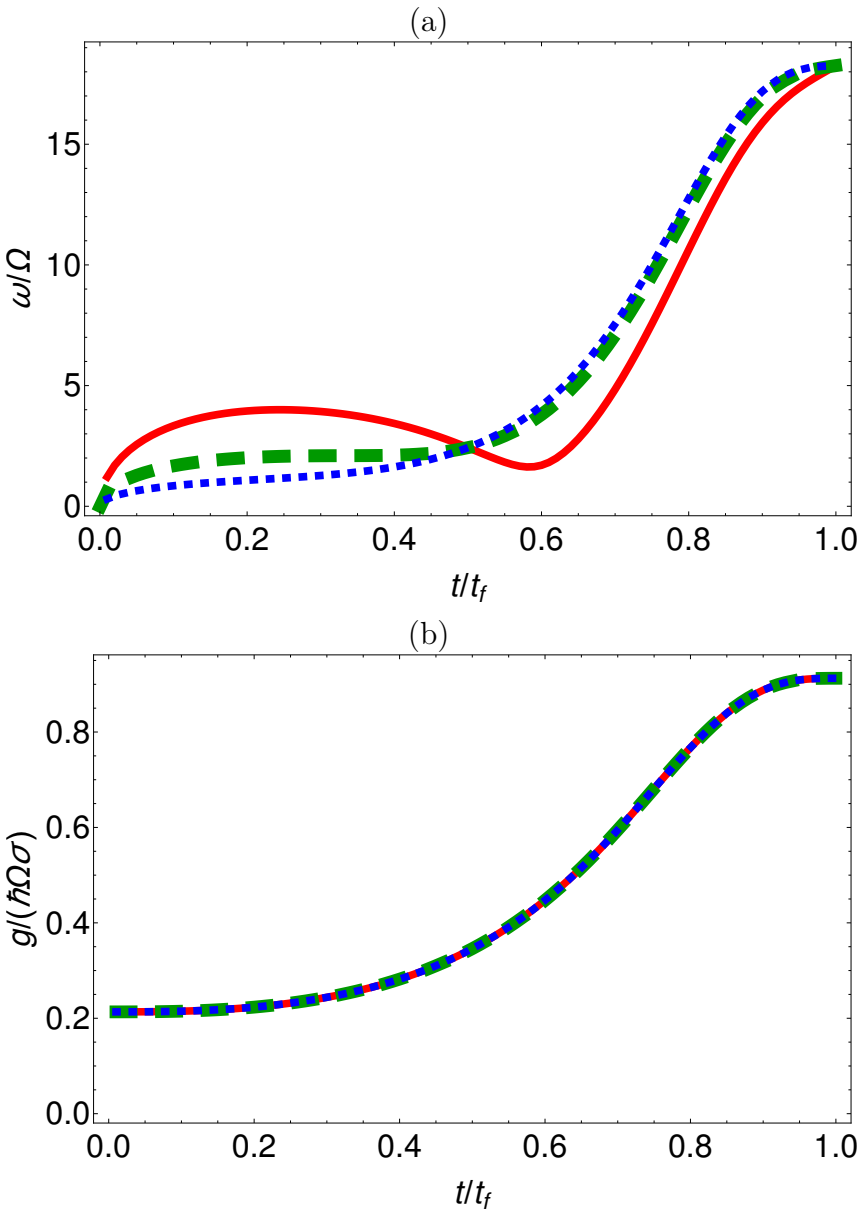

FIGURE 5.2: Loading particles into trap: (a) ω/Ω versus t/t_f, $\omega_0 = 1.219\Omega$ and $\omega_f = 18.257\Omega$; (b) $g/(\hbar\Omega\sigma)$ versus t/t_f, $g_0 = 0.213(\hbar\Omega\sigma)$ and $g_f = 0.913(\hbar\Omega\sigma)$. Final time: $t_f = 0.55T$(red solid line), $t_f = 1.10T$ (green dashed line) $t_f = 2.19T$ (blue dotted line).

$F = 1$ in arbitrarily short timescales. For the case of the Gross-Pitaevskii equation we must also tune the atom-atom interaction according to Eq. (5.25). We now simulate the full Schrödinger and Gross-Piteavskii equations using exact initial states obtained by numerically solving the relevant stationary equations. We set the parameters as follows; the lattice height $U_0/(\hbar\Omega) = 547.7$, the final frequency of the external harmonic trap is chosen as $\omega_f = 18.257\Omega$. In Fig 5.2 we plot the control functions $\omega(t)$ and in the case of STA $g(t)$ for different values of t_f and we see that the $\omega(t)$ function changes for different values of t_f but the $g(t)$ function remains the same; this is because the auxiliary function $\rho(t)$ is a polynomial of t/t_f. In Fig. 5.3 we plot the fidelity F as a function of final time t_f, in (a) for $g = 0.0$ and in (b) for $g_f = 0.913(\hbar\Omega\sigma)$. For comparison we also consider two alternate schemes, first varying the trap frequency $\omega(t)$ adiabatically according to

$$\omega(t) = (\omega(t_f) - \omega(0)) \sin\left(\frac{t\pi}{2t_f}\right)^2 + \omega(0).$$

and second varying the $\omega(t)$ as in the shortcut protocol but with constant atom-atom interaction $g(t) = g_f = 0.91\hbar\Omega\sigma$. We see in Fig. 5.3 that in both scenarios, the shortcut scheme performs very well for both values of g, achieving fidelities of $F \geq 0.99$ for all times. This is to be expected as the harmonic approximation in this case is very good and so the shortcut solution is very close to an exact solution of the problem. The adiabatic scheme however performs poorly in comparison; in the $g = 0$ case it fails to achieve high fidelities having $F < 0.83$ for all time-scales shown. In Fig. 5.3 (b) we see that the third scheme of varying the $\omega(t)$ according to the shortcut protocol but leaving the g fixed doesn't achieve the same high fidelities as the full shortcut protocol but performs better than the adiabatic case. In the case of $g = g_0 = 0.91(\hbar\Omega\sigma)$, we see that both the adiabatic and the fixed g approach are not oscillatory. When considering the atom-atom interaction we see that the adiabatic scheme performs more poorly

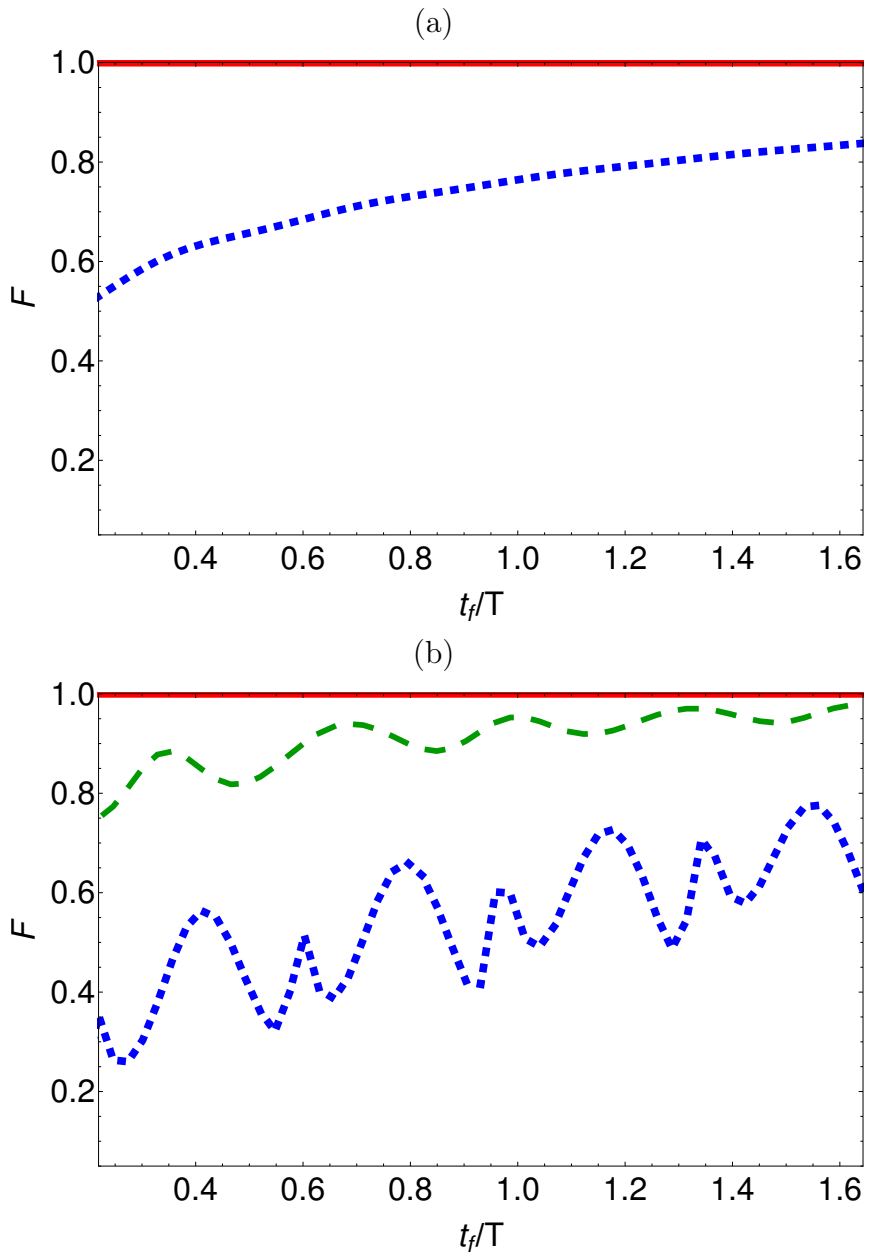

FIGURE 5.3: Loading particles into trap: Fidelity F versus final time t_f; (a) $g(t) = 0$; (b) $g_f = 0.91\ \hbar\Omega\sigma$. The shortcut solution (red solid line), the adiabatic solution (blue dotted line), the constant g solution (green dashed line).

than in the $g = 0$ case; the shortcut scheme however still achieves the high fidelities on all time-scales.

5.3.2 Transport across Lattice Site

In this subsection we want to transport the condensate from one lattice site to its nearest neighbour. This could of course be concatenated to achieve transport of the condensate over a number of lattice sites. The external harmonic trap will thus start at $q_0(0) = 0$ and at final time will be at $q_0(t_f) = \pi\sigma$. In addition the frequency of the external harmonic trap should be the same at initial and final time $\omega_0 = \omega(t_f) = \omega(0)$. We will first discuss a shortcut scheme we call the variable frequency solution, that exactly solves the Eqs. (5.23) and (5.24). The key idea here is to alter the harmonic trap frequency $\omega(t)$ in such a way that the virtual trap frequency stays constant *i.e.* $\tilde{\omega}(t) = \tilde{\omega}(0) = \omega(0)^2 + \Omega^2$. This allows us to solve Eq. (5.23) by setting $\rho = 1$. In the case of a condensate, this has the added benefit that there is no need to tune the atom-atom interaction in time, as $g(t) = g(0)/\rho(t) = g$. The boundary conditions on the auxiliary function $q_c(t)$ are

$$\begin{aligned} q_c(0) &= 0, & q_c(t_f) &= \pi\sigma \\ \dot{q}_c(0) &= 0, & \dot{q}_c(t_f) &= 0 \\ \ddot{q}_c(0) &= 0, & \ddot{q}_c(t_f) &= 0 \end{aligned}$$

We choose a polynomial solution of minimal degree to fulfil these boundary conditions and so we can calculate the position virtual trap centre as

$$x_{\min}(t) = q_c(t) + \frac{1}{\tilde{\omega}^2}\ddot{q}_c(t)$$

and the control function for the actual trap centre is given by

$$\begin{aligned} q_0(t) &= x_{min}(t) \\ &+ \frac{\Omega^2}{\omega(t)^2} \sin\left(\frac{x_{min}(t)}{\sigma}\right) \cos\left(\frac{x_{min}(t)}{\sigma}\right). \end{aligned} \tag{5.34}$$

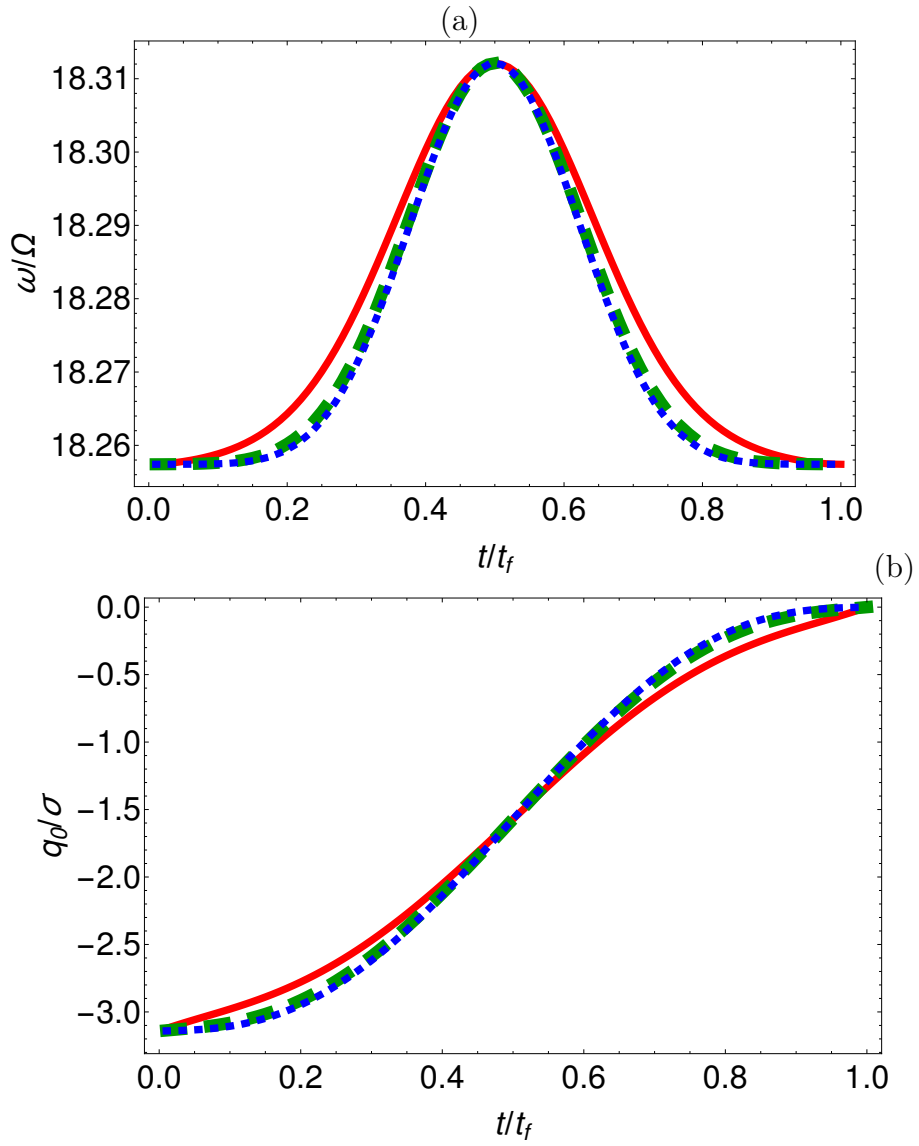

FIGURE 5.4: Transporting particles across a lattice site: (a) ω/Ω versus t/t_f; (b) q_0/σ versus t/t_f. Final time: $t_f = 0.55T$(red solid line), $t_f = 1.10T$ (green dashed line) $t_f = 2.19T$ (blue dotted line).

In addition, for this approach we vary the trap frequency according to

$$\begin{aligned} \omega(t)^2 &= \tilde{\omega}^2 + \Omega^2 \cos\left(\frac{2x_{min}(t)}{\sigma}\right) \\ &= \omega_0^2 + \Omega^2 \left[1 + \cos\left(\frac{2x_m(t)}{\sigma}\right)\right] \end{aligned} \tag{5.35}$$

Fidelities based on full Schrödinger/G-P equation

We now simulate the full Schrödinger and Gross-Pitaevskii equations with an exact initial and final state using these schemes *i.e. we assume first that the previous loading of the particles into the trap had fidelity one.*

Both the trap centre position $q_0(t)$ and trap frequency $\omega(t)$ control functions are shown in Fig. 5.4 with the frequency $\omega(t)$ shown in (a) and the trap centre position $q_0(t)$ shown in (b). The fidelities for different final times t_f are shown in Fig. 5.5 as the red solid line for $g = 0$ in figure (a), for $g = 9.13\ \hbar\Omega\sigma$ in (b) and for $g = 91.3\ \hbar\Omega\sigma$ in (c). This variable frequency solution approach performs very well achieving high fidelities even on very short time-scales. This solution performs the best for both values of g shown. This result however is not surprising as it is the only exact solution to the auxiliary Eqs. (5.23) and (5.24). For a more indepth, look we examine the threshold time $t_{0.99}$ which is defined as the time for which the fidelity $F \geq 0.99$ for all times $t \geq t_{0.99}$. We plot this quantity $t_{0.99}$ for different frequencies ω_0 in Fig. 5.7. We see that the threshold time $t_{0.99}$ decreases as initial trapping frequency ω_0 is increased for all values of g.

Approximated transport schemes

We now consider two approximated transport schemes assuming $\omega_0 \gg \Omega$; in particular we look at these because these two schemes do not require the tuning of the external harmonic frequency $\omega(t)$ during the transport.

The first approximated scheme is achieved by neglecting the Ω^2 term in Eq. (5.35) as $\omega_0 \gg \Omega$ leading to $\omega(t) = \omega(0)$. This means that we are implementing the same $q_{0,A1}(t) = q_0(t)$ function as the variable frequency scheme (seen in Fig. 5.4 (b)), but still keeping the frequency $\omega(t) = \omega(0)$ constant during transport. This we label "first constant frequency approximation".

The second approximation is similar, we also fix $\omega(t) = \omega(0)$ but here we also

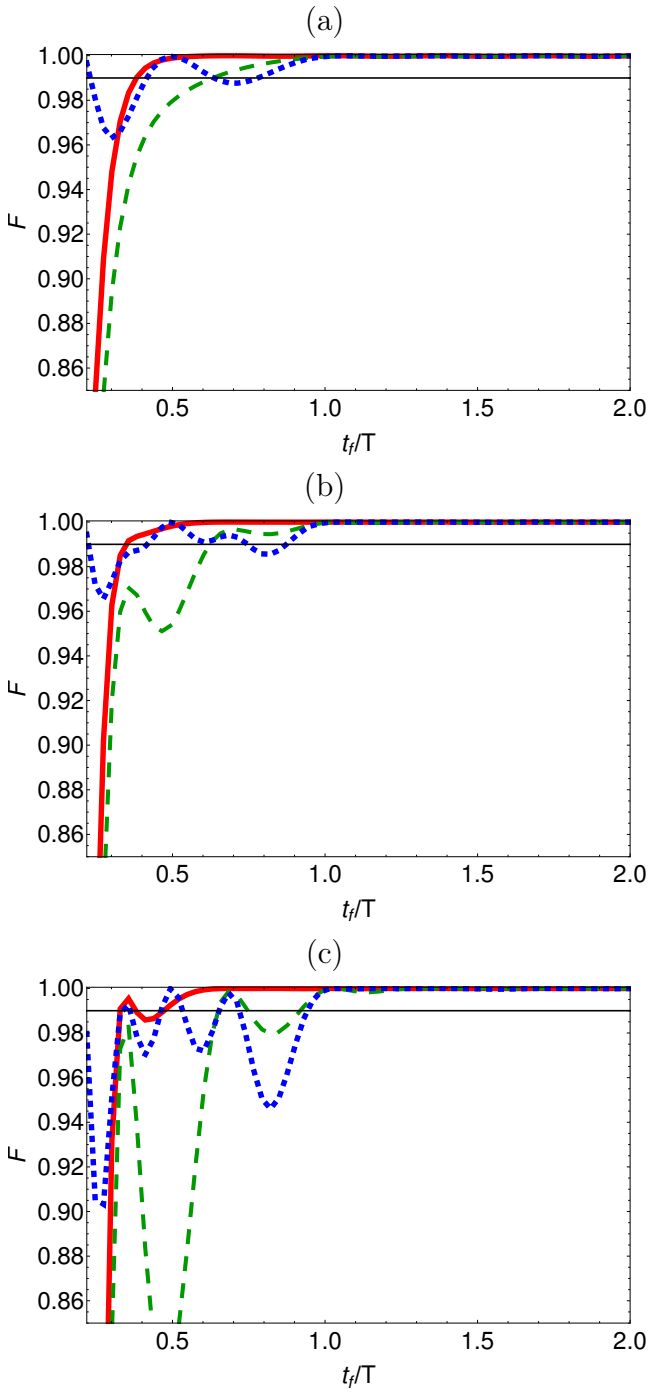

FIGURE 5.5: Transporting particles across a lattice site: Fidelity F versus final time t_f, (a) $g = 0$; (b) $g = 0.91\hbar\Omega\sigma$; (c) $g = 9.1\hbar\Omega\sigma$. The shortcut solution (red solid line), the adiabatic solution (blue dotted line), the constant g solution (green dashed line).

neglect any terms proportional to Ω^2/ω_0^2 in Eq. (5.34), giving us the following

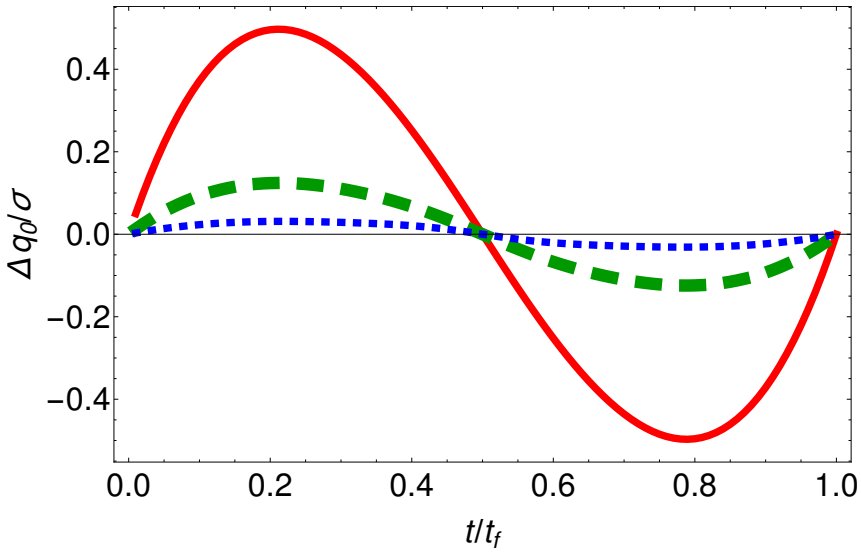

FIGURE 5.6: Transporting particles across a lattice site: Difference between variable frequency solution and "second constant frequency approximation": $\Delta q_0/\sigma$ versus t/t_f. Final time: $t_f = 0.55T$(red solid line), $t_f = 1.10T$ (green dashed line) $t_f = 2.19T$ (blue dotted line).

trap centre function

$$q_{0,A2}(t) = x_{min}(t) = q_c(t) + \frac{1}{\omega_0^2}\ddot{q}_{c,0}(t). \tag{5.36}$$

We call this the "second constant frequency approximation". More details on how this is obtained are available in the Appendix 5.5.1.

The particular strength of the above two approximations is that there is no longer any need to control the trap frequency ω or the atom-atom interaction $g(t)$ during the transport. Instead the only varying function is the trap centre position $q_0(t)$. Both schemes will result in different trap trajectories, the "first constant frequency approximation" will have the same trap trajectory $q_{0,A1}(t)$ as the variable frequency solution derived earlier and shown in Fig. 5.4(b). However the "second constant frequency approximation" is different. The difference between the two trajectories $q_{0,A1}$ and $q_{0,A2}$ is seen in Fig. 5.4 for different final times t_f. We see that with increasing final time t_f, the differences between the two schemes decrease.

Similarly to the previous section, we now solve the exact Schrödinger and Gross-Pitaevskii equations numerically, with exact initial states. We have plotted the fidelities in Fig. 5.5 for both approximations together with the variable frequency scheme. Both approximation schemes result in high fidelities for $g \geq 0$ but perform significantly worse than the variable frequency solution described earlier. They both achieve fidelities of $F \geq 0.99$ later than the variable frequency solution.

We again examine the threshold time $t_{0.99}$ in Fig. 5.7. We see that while the variable frequency solution performs the best, the two approximate solutions still give a threshold time $t_{0.99}$ slightly larger than the variable frequency solution and do not require control of trap frequency $\omega(t)$. This may prove useful in situations where the frequency of the trapping potential is difficult to tune. It appears in Fig. 5.7 (a) and (b) that the "first constant frequency approximation" performs at least as well as the "second constant frequency approximation" and in some circumstances such as lower g and higher ω, it performs better. We see a different behaviour in 5.7 (c) where the "first constant frequency approximation" performs worse than the "second constant frequency approximation" in the case of low ω_0, but as well as it otherwise. In Fig 5.8 we again examine the threshold time $t_{0.99}$, this time against the atom-atom interaction strength g. As with all the previous examples, the variable frequency solution performs best for all values of g. We do however see that there is a range of values for g where the "second constant frequency approximation" is preferable to the "first constant frequency approximation". In a region of values around $0.1 > g\hbar\Omega\sigma > 0.6$ we see that the second approximation performs much better than the first approximation and performs similarly to the variable frequency solution.

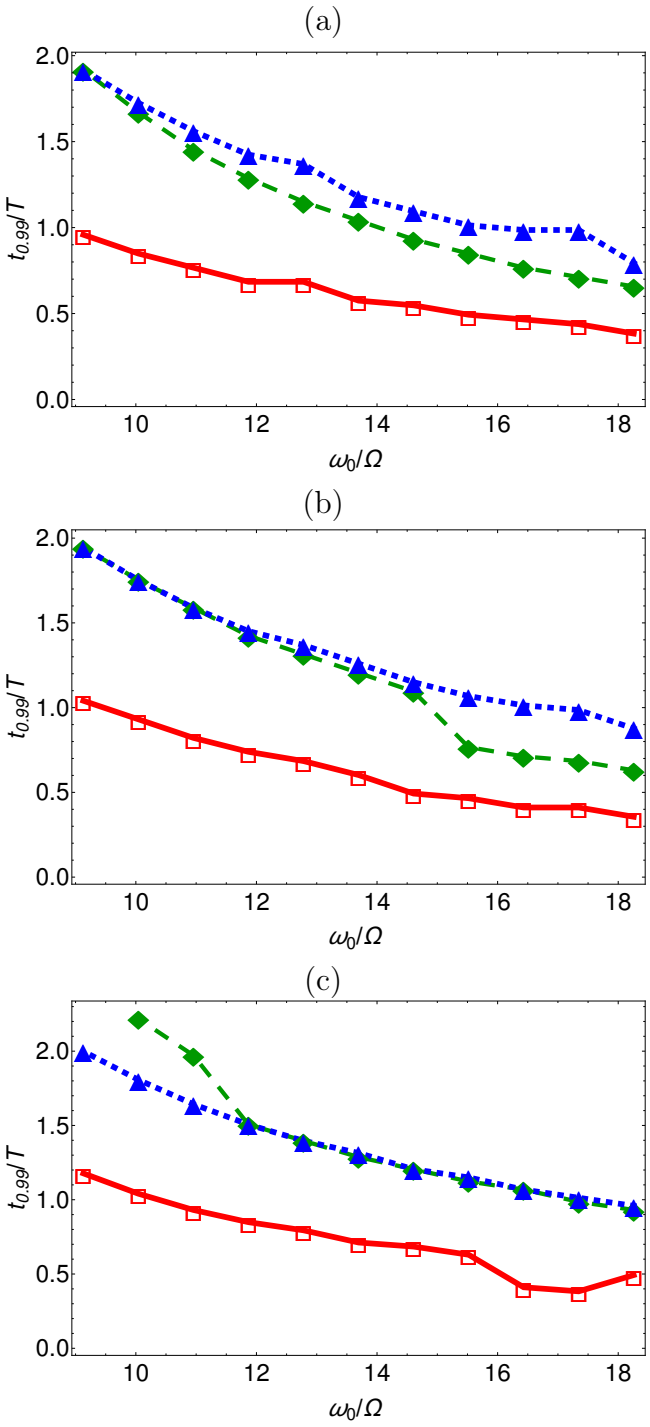

FIGURE 5.7: Transporting particles across a lattice site: Threshold time $t_{0.99}$ versus ω_0 (a) $g = 0$; (b) $g = 0.91\hbar\Omega\sigma$; (c) $g = 9.1\hbar\Omega\sigma$. Exact scheme (red boxes connected with a solid line), first "simplified approximation" (green diamonds connected by a dashed line) second "simplified approximation" (blue triangles connected by a dotted line).

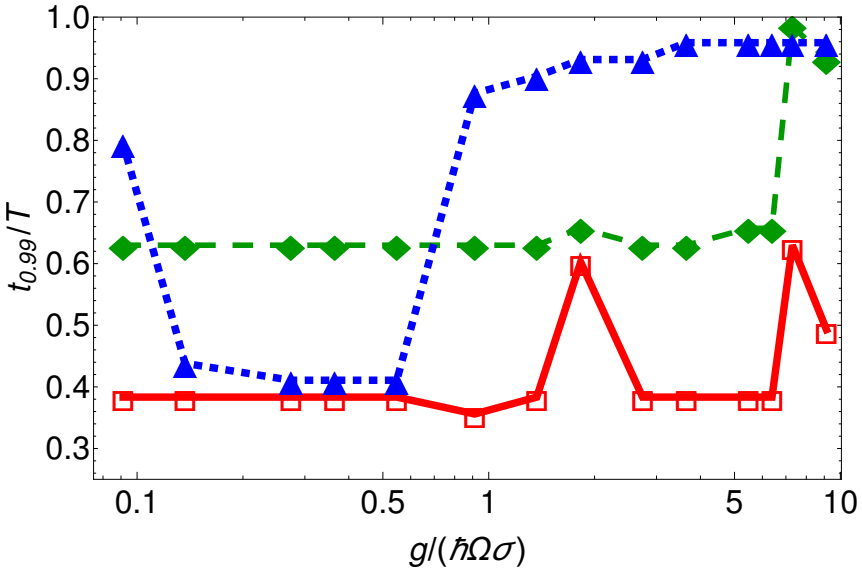

FIGURE 5.8: Transporting particles across a lattice site: Threshold time $t_{0.99}$ versus $g/(\hbar\Omega\sigma)$ for $\omega_0 = 18.257\Omega$. Variable frequency scheme (red boxes connected with a solid line), first "simplified approximation (green diamonds connected by a dashed line) second "simplified approximation" (blue triangles connected by a dotted line).

Robustness

In this subsection we examine the robustness of the exact scheme for transporting the trap. We will consider an error in the position q_0 and later in the frequency ω during the transport. First let us consider an error in the trap position q_0 of the form

$$q_0(t) = q_{0,\text{exact}}(t) + d\epsilon, \qquad 0 < t < t_f \tag{5.37}$$

where ϵ is a small perturbation parameter and $d = \sigma\pi$ is the distance between the two lattice sites. The perturbation only acts during the transportation, at boundary times $q_0(0) = q_{0,\text{exact}}(0)$ and $q_0(t_f) = q_{0,\text{exact}}(t_f)$. The frequency of the external harmonic trap is chosen as $\omega_0 = 18.257\Omega$ and the final time is $t_f = 1.10T$. We have plotted the fidelity F versus the perturbation ϵ in Fig. 5.9(a). We see that the the region close to $\epsilon = 0$ retains high fidelities as

expected showing this variable frequency protocol is stable against this perturbation. We also see that the fidelity F is asymmetric, for $\epsilon > 0$ F is larger than those for $\epsilon < 0$. We see that for the case of $g = 0$ that the transport is more stable against this perturbation.

As a second form of perturbation let us consider an error in the trap frequency ω of the form

$$\omega(t) = \omega_{exact}(t)(1 + \epsilon) \qquad 0 < t < t_f. \tag{5.38}$$

Here ϵ is a small perturbation parameter that changes the frequency of the trap. Again the system is perturbed only during the transport. We have plotted the fidelity F versus the perturbation ϵ in Fig. 5.9 (b). Similar to the case above of perturbation in the trap trajectory q_0, we see an asymmetry in the fidelity, in both the case of $g = 0$ and $g = 0.91\ \hbar\Omega\sigma$ a perturbation of $\epsilon < 0$ is preferable and retains higher fidelities than a perturbation of $\epsilon > 0$. The $g = 0.91\ \hbar\Omega\sigma$ scheme performs better than the $g = 0.0$ for perturbations $\epsilon < 0$, but for perturbations $\epsilon > 0$ the $g = 0.0$ scheme achieves higher fidelities.

5.3.3 Unloading onto lattice

In this section we now attempt to open the external harmonic trap to unload the particles back onto the lattice after transport. We start with the frequency of the harmonic trap $\omega(0) = \omega_0 > 0$ at initial time $t = 0$ and finish with $\omega(t_f) = 0$ at final time t_f. The position of the external trap stays constant in the well of a lattice such that $q_0(t) = n\pi\sigma$ for all $t \geq 0$.

There is no change in position of the trap so the auxiliary function $q_c(t)$ can be chosen to be constant $q_c(t) = q_0(0)$. We can then pick the auxiliary function

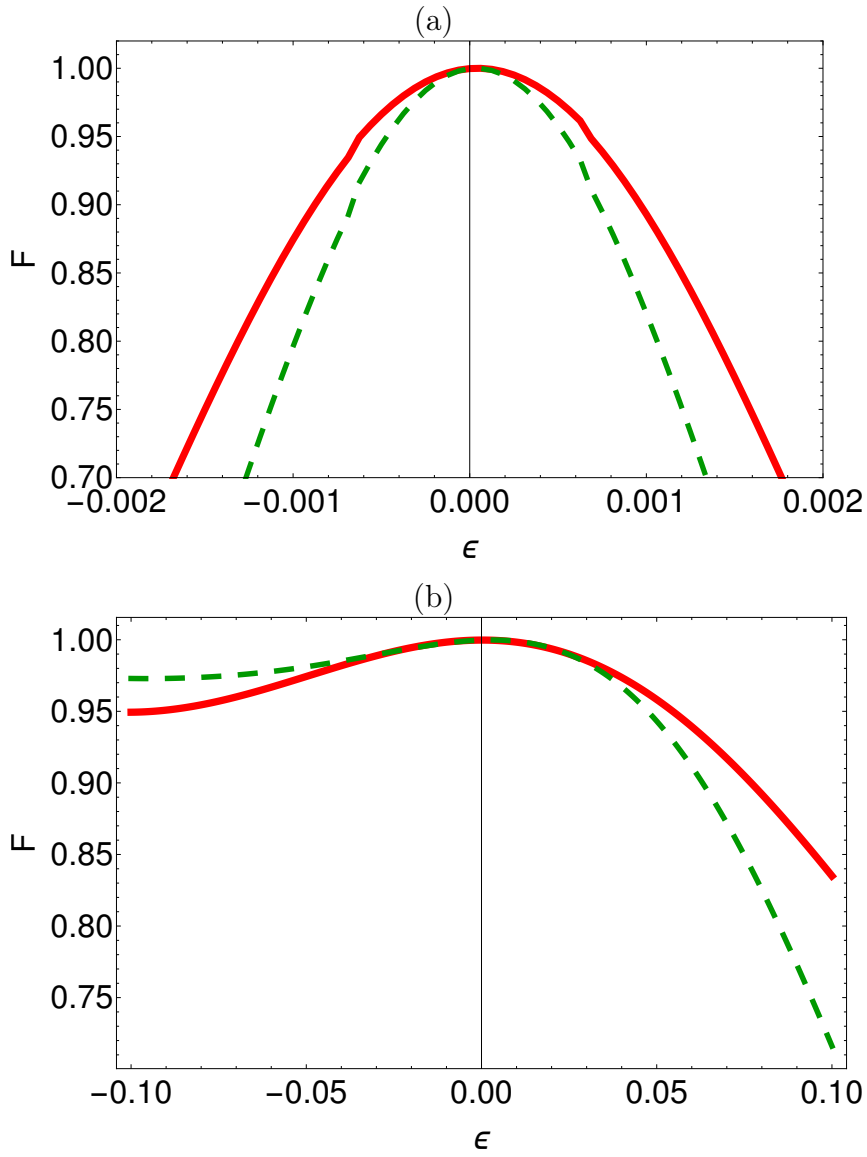

FIGURE 5.9: Transporting particles across a lattice site: Fidelity F versus perturbation ϵ (a) error in $q_0(t)$ (b) error in $\omega(t)$. $g = 0$ (red solid line), $g = 0.91\ \hbar\Omega\sigma$ (green dashed line).

$\rho(t)$ to satisfy the following boundary conditions

$$\begin{aligned} \rho(0) &= 1; \\ \rho(t_f) &= \sqrt{\frac{\tilde{\omega}(0)}{\tilde{\omega}(t_f)}}; \\ \dot{\rho}(0) &= \dot{\rho}(t_f) = 0; \\ \ddot{\rho}(0) &= \ddot{\rho}(t_f) = 0. \end{aligned}$$

Again we choose a polynomial $\rho(t)$ of minimal degree to fulfil these boundary conditions. This approach corresponds to tuning the external harmonic trap frequency as follows

$$\omega(t) = \tilde{\omega}(t) + \Omega^2.$$

In the case of the atom-atom interaction, we tune $g(t)$ according to $g(t) = g_0/\rho(t)$ following from earlier results. The unloading is a direct reverse of the previous loading and in the sense that each of the auxiliary functions $\omega(t)$ and $g(t)$ is the time reversed function from that section. The time dependent functions $\omega(t)$ are shown in Fig. 5.10; these are the time-reversed functions from the earlier loading section. Again if the harmonic approximation is exact the fidelity of the scheme would be $F = 1$ independent of final time t_f. We now, as in previous sections, simulate the full dynamics of the system using the Schrödinger and Gross-Piteavskii equations with an exact initial state. The initial frequency of the harmonic trap is chosen to be $\omega_i = 18.257\Omega$. We have plotted the fidelity F versus final time t in Fig. 5.11 (a) and (b). Fig. 5.11 (a) is the same graph as in the loading section and is presented here for convenience. Similarly to the earlier case of loading particles into the trap, the shortcut scheme achieves a stable fidelity of $F \geq 0.99$ for all times shown. However in the case of unloading particles back onto the lattice, the adiabatic scheme is more stable. In the earlier figure Fig. 5.3(b) we saw that for $g > 0$, the fidelity as a function of time varies more and does not display the almost monotonic behaviour seen in Fig. 5.11(b). However, in both the loading and unloading, the adiabatic protocol doesn't perform well when compared with the shortcut protocol or the constant g protocol.

5.4 Conclusion

We have proposed a method utilizing STA for the fast and robust movement of atoms or a Bose-Einstein condensate across a time dependent optical lattice

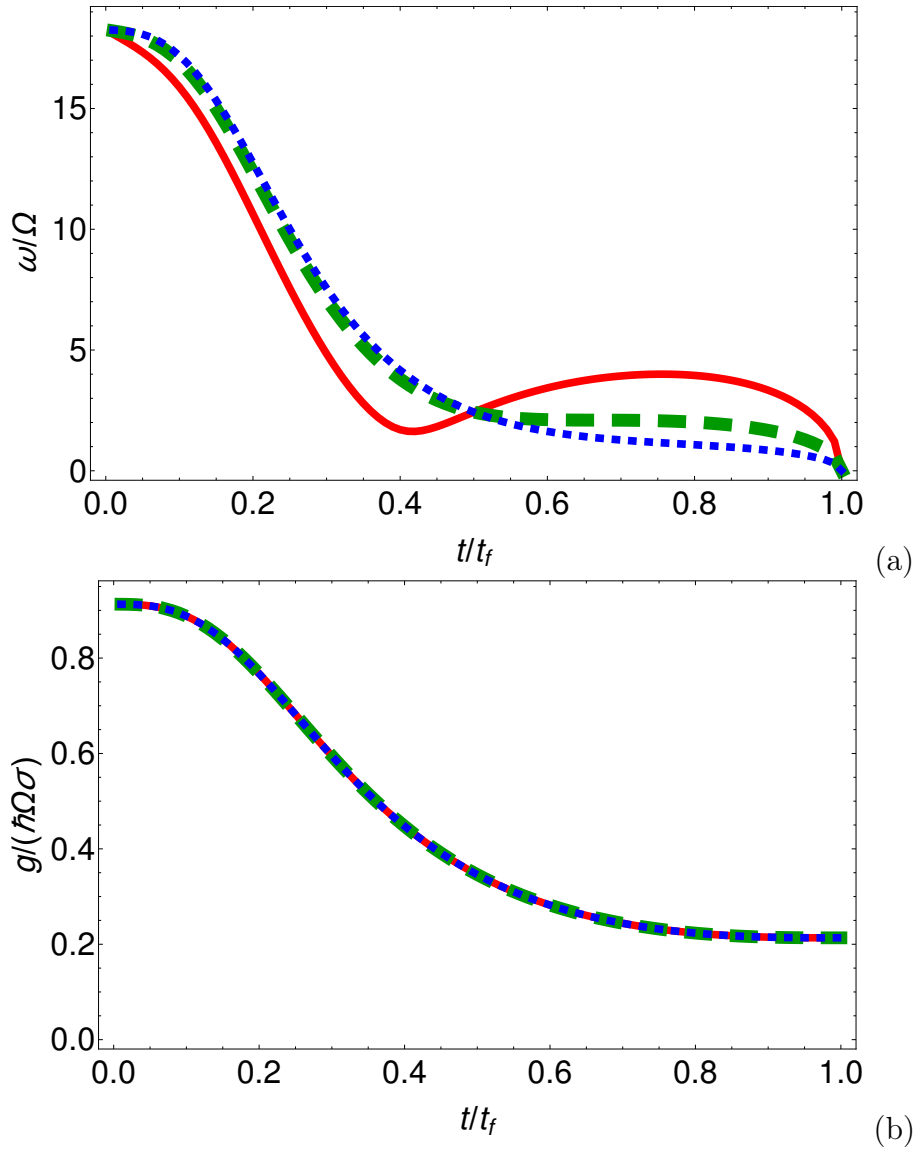

FIGURE 5.10: Unloading particles back onto lattice: Control functions for unloading particle out of external trap: (a)$\omega/Omega$ versus t/t_f; (b) $g/(\hbar\Omega\sigma)$ versus t/t_f.

by using an external trapping potential. To do this we have broken the moving process into three independent building blocks: First loading a particle from a lattice site into an external trapping potential, then transporting the particle across the lattice and finally unloading the particle from the external trapping potential back on to a lattice site. We then applied methods from STA to each of these building blocks to derive control schemes for the external trap. Concatenating all three of the different building blocks we can move particles

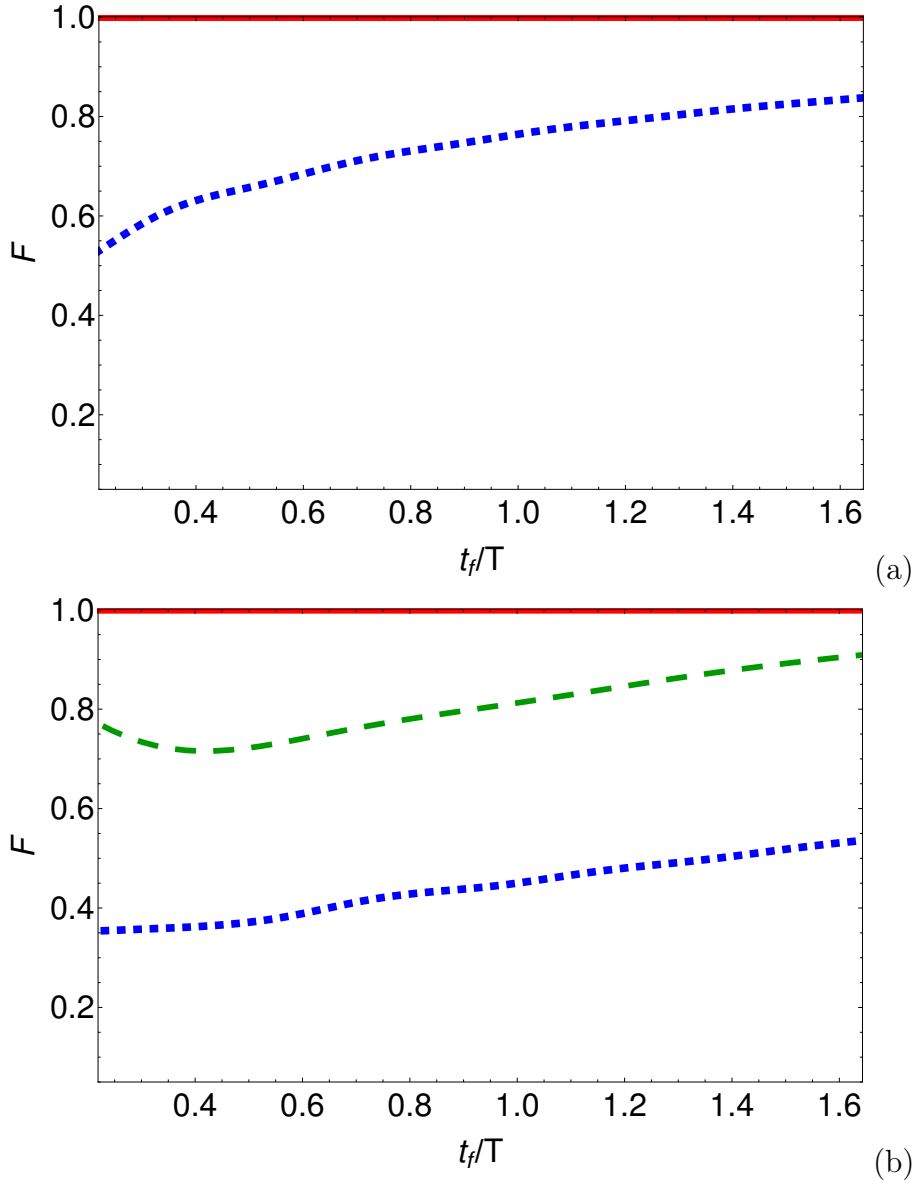

FIGURE 5.11: Unloading particles back onto lattice: Fidelity F versus final time t_f, (a) $g(t) = 0$; (b) $g_0 = 0.91(\hbar\Omega\sigma)$. The shortcut solution (red solid line), the adiabatic solution (blue dotted line), the constant g solution (green dashed line).

from one lattice site, trap them and then transport them to another and finally unload them into the target lattice site. Alternative schemes to achieve similar fidelities but requiring less control were also considered. The sensitivity of the protocols with respect to trap centre control and trapping frequency were investigated and the protocols were shown to be robust against these errors.

5.5 Appendices for chapter 5

5.5.1 Perturbation approach/Series expansion

The auxiliary equations are

$$\rho^3\ddot{\rho} + \tilde{\omega}(t)^2\rho^4 - \tilde{\omega}(0) = 0 \tag{5.39}$$

$$\ddot{q}_c(t) + \tilde{\omega}(t)^2(q_c(t) - x_m(t)) = 0 \tag{5.40}$$

The auxiliary functions can be expanded as

$$\begin{aligned} \rho(t) = \Sigma_{i=0}^{\infty}\epsilon^i\rho_i(t) &\approx \rho_0(t) + \epsilon\rho_1(t) \\ q_c(t) = \Sigma_{i=0}^{\infty}\epsilon^i q_{c,i}(t) &\approx q_{c,0}(t) + \epsilon q_{c,1}(t) \\ x_m(t) = \Sigma_{i=0}^{\infty}\epsilon^i x_{m,i}(t) &\approx x_{m,0}(t) + \epsilon x_{m,1}(t). \end{aligned}$$

The ϵ is a small parameter given by $\epsilon = U_0/\sigma^2 m$, here we only solve up to first order. Substituting these equations into 5.40 we obtain

$$\begin{aligned} \epsilon\Bigg\{ 3\rho_0^2\rho_1\ddot{\rho}_0 + \rho_0^2\ddot{\rho}_1 + 4\rho_0^3\rho_1\omega_0^2 + 2\rho_0^4\cos\left(\frac{2x_{m,0}(t)}{\sigma}\right) \\ - \ 2\cos\left(\frac{2x_{m,0}(0)}{\sigma}\right)\Bigg\} + \left\{\rho_0^3\ddot{\rho}_0 + \omega_0^2\rho_0^4 - \omega_0^2\right\} = 0, \end{aligned} \tag{5.41}$$

and

$$\begin{aligned} \epsilon\Bigg\{ \ddot{q}_{c,1} + 2\cos\left(\frac{2x_{m,0}(t)}{\sigma}\right)[q_{c,0}(t) - x_{m,0}(t)] \\ + \ \omega_0^2(q_{c,1}(t) - x_{m,1}(t)\Bigg\} + \left\{\ddot{q}_{c,0}(t) + \omega_0^2(q_{c,0}(t) - x_{m,0}(t))\right\} = 0. \end{aligned} \tag{5.42}$$

Looking first at order ϵ^0 gives

$$\rho_0^3\ddot{\rho}_0 + \omega_0^2\rho_0^4 - \omega_0^2 = 0$$

$$\ddot{q}_{c,0}(t) + \omega_0^2(q_{c,0}(t) - x_{m,0}(t)) = 0,$$

we can solve the first equation with $\rho_0 = 1$ allowing us to solve for $x_{m,0}(t)$ by

$$x_{m,0}(t) = q_{c,0}(t) + \frac{1}{\omega_0^2}\ddot{q}_{c,0}(t).$$

Now looking at order ϵ^1 we get

$$\ddot{\rho}_1(t) + 4\rho_1(t)\omega_0^2 + 2(\cos\left(\frac{2x_{m,0}(t)}{\sigma}\right) - \cos\left(\frac{2x_{m,0}(0)}{\sigma}\right) = 0$$

$$\ddot{q}_{c,1}(t) + 2\cos\left(\frac{2x_{m,0}(t)}{\sigma}\right)(q_{c,0}(t) - x_{m,0}(t)) + \omega_0^2(q_{c,1}(t) - x_{m,1}(t)) = 0.$$

We can thus solve for $x_{m,1}(t)$

$$x_{m,1}(t) = \frac{1}{\omega_0^2}\left\{\ddot{q}_{c,1}(t) - \frac{2}{\omega_0^2}\ddot{q}_{c,0}\cos\left(\frac{2(q_{c,0}(t) + \frac{1}{w_p^2}\ddot{q}_{c,0}(t)}{\sigma}\right) + q_{c,1}(t)\omega_0^2\right\}.$$

We can then write $x_m(t)$ as

$$x_m(t) = q_c + \frac{1}{\omega_0^2}\ddot{q}_c(t) - \frac{2\epsilon}{\omega_0^4}\ddot{q}_{c,0}\cos\left(\frac{2(q_{c,0}(t) + \frac{1}{w_p^2}\ddot{q}_{c,0}(t))}{\sigma}\right).$$

In principle we can choose a q_c as long as it satisfies the relevant boundary conditions. We can therefore solve for $\rho_1(t)$ as follows

$$\rho_1(t) = \frac{(\cos(2\omega_0 t) + \sin(2\omega_0 t))}{\omega_0}\int_0^t\left(\cos\left(\frac{2x_{m,0}(k)}{\sigma}\right) - \cos\left(\frac{2x_{m,0}(0)}{\sigma}\right)\right)\sin(2\omega_0 k)dk.$$

Initially both 0^{th} and 1^{st} order perturbation solutions were considered, however it was found that the 1^{st} order perturbation solutions were performing poorly, likely as a result of difficulties minimising Eq. (5.5.1) and were abandoned.

5.5.2 Unsuccessful approaches

Originally in this project we attempted many different unsuccessful approaches before we found and settled on the methods discussed in the chapter. The two auxiliary equations that are used are

$$\rho^3(\ddot{\rho} + \rho\omega^2(t)) - \omega_0^2 = 0, \tag{5.43}$$

$$\ddot{q_c} + \omega^2(t)(q_c - x_{\min}) = 0. \tag{5.44}$$

They are coupled through the $\omega(t)$ term present in both of them and it is this which greatly complicates solving them. The first approach was to make some polynomial ansatz for q_c

$$q_c = \sum_{i=0}^{n} a_i t^i$$

where the order of q_c was greater than the number of boundary conditions on it. From the boundary conditions on q_c we could fix the coefficients $a_0, \ldots, a_5$ in terms of a_6, a_7 and a_8. We then put additional conditions on $q_c(t)$ taking certain values for different values of t,

$$q_c\left(\frac{t_f}{4}\right) = b_1$$
$$q_c\left(\frac{t_f}{2}\right) = b_2$$
$$q_c\left(\frac{3t_f}{4}\right) = b_3$$

We proceeded to solve the first auxiliary equation in Eq. (5.44) for $\omega(t)$ and inserted it into the q_c equation. This gave us an expression for $\rho(t)$ and $\rho''(t)$ in terms of the three free parameters b_1, b_2 and b_3. We attempted to solve this expression for $\rho(t)$ numerically using boundary conditions derived earlier for $\rho(t)$

and it's derivatives for different values of b_i. We next defined an error function to represent how well $\rho(t)$ fitted the boundary conditions derived and attempted to minimise this error by varying over the free parameters b_i. Different parameter sets were found that minimised the error in $\rho(t)$ but unfortunately none of them enabled high fidelity transport when the full solution was examined.

After this first attempt, another similar approach was made except that in this case we truncated the process. Instead of trying to transport the particle from $q_0(0) = 0$ to $q_0(t_f) = \pi\sigma$, the process was broken up into a four even segments; otherwise the approach was the same. This produced some new $\rho(t)$ functions but unfortunately these again were unable to satisfy the boundary conditions well enough to enable sufficiently high fidelity transport.

This process was tried with both the case of the harmonic approximation being an accurate picture of the potential and also with some higher order terms included in the expansion.

Chapter 6

Asymmetric scattering by non-hermitian potentials

6.1 Abstract

The scattering of quantum particles by non-hermitian (generally nonlocal) potentials in one dimension may result in asymmetric transmission and/or reflection from left and right incidence. After extending the concept of symmetry for nonhermitian potentials, eight generalized symmetries based on the discrete Klein's four-group (formed by parity, time reversal, their product, and unity) are found. Together with generalized unitarity relations they determine selection rules for the possible and/or forbidden scattering asymmetries. Six basic device types are identified when the scattering coefficients (squared moduli of scattering amplitudes) adopt zero/one values, and transmission and/or reflection are asymmetric. They can pictorically be described as a one-way mirror, a one-way barrier (a Maxwell pressure demon), one-way (transmission or reflection) filters, a mirror with unidirectional transmission, and a transparent, one-way reflector. We design potentials for these devices and also demonstrate that the behavior of the scattering coefficients can be extended to a broad range of incident momenta.

This chapter is based on the following publication:

A. Ruschhaupt, T. Dowdall, M. A. Simón and J. G. Muga

Asymmetric scattering by non-Hermitian potentials,

EPL **120** 20001 (2017)

I performed calculations for the explicit forms of the potentials and produced a number of plots for the paper. I performed a lot of calculations for the explicit forms of the different potentials to achieve different reflection and transmission asymmetries. Further I produced many of the plots in the paper and it's Appendix. All authors contributed in writing the paper.

6.2 Introduction

The current interest to develop new quantum technologies is boosting applied and fundamental research on quantum phenomena and on systems with potential applications in logic circuits, metrology, communications or sensors. Robust basic devices performing elementary operations are needed to perform complex tasks when combined in a circuit.

In this paper we investigate the properties of potentials with asymmetric transmission or reflection for a quantum, spinless particle of mass m satisfying a one-dimensional (1D) Schrödinger equation. If we restrict the analysis to transmission and reflection coefficients (squared moduli of the scattering complex amplitudes) being either zero or one, a useful simplification for quantum logic operations, there are six types of asymmetric devices, see fig. 6.1. These devices cannot be constructed with Hermitian potentials. In fact for all device types with transmission asymmetries, which are four of the six possible devices, the potentials have to be also nonlocal. Therefore, nonlocal potentials play a major role in this paper. They appear naturally when applying partitioning techniques under similar conditions to the ones leading to non-hermitian potentials, namely, as effective interactions for a subsystem or component of the full

wave-function, even if the interactions for the large system are hermitian and local [109].

Symmetries can be used, analogously to their standard application in atomic physics to determine selection rules for allowed/forbidden transitions, to predict whether a certain potential may or may not lead to asymmetric scattering. The concept of symmetry, however, must be generalized when dealing with non-hermitian potentials.

The theory in this paper is worked out for particles and the Schrödinger equation but it is clearly of relevance for optical devices due to the much exploited analogies and connections between Maxwell's equations and the Schrödinger equation, which were used, e.g., to propose the realization of PT-symmetric potentials in optics [110].

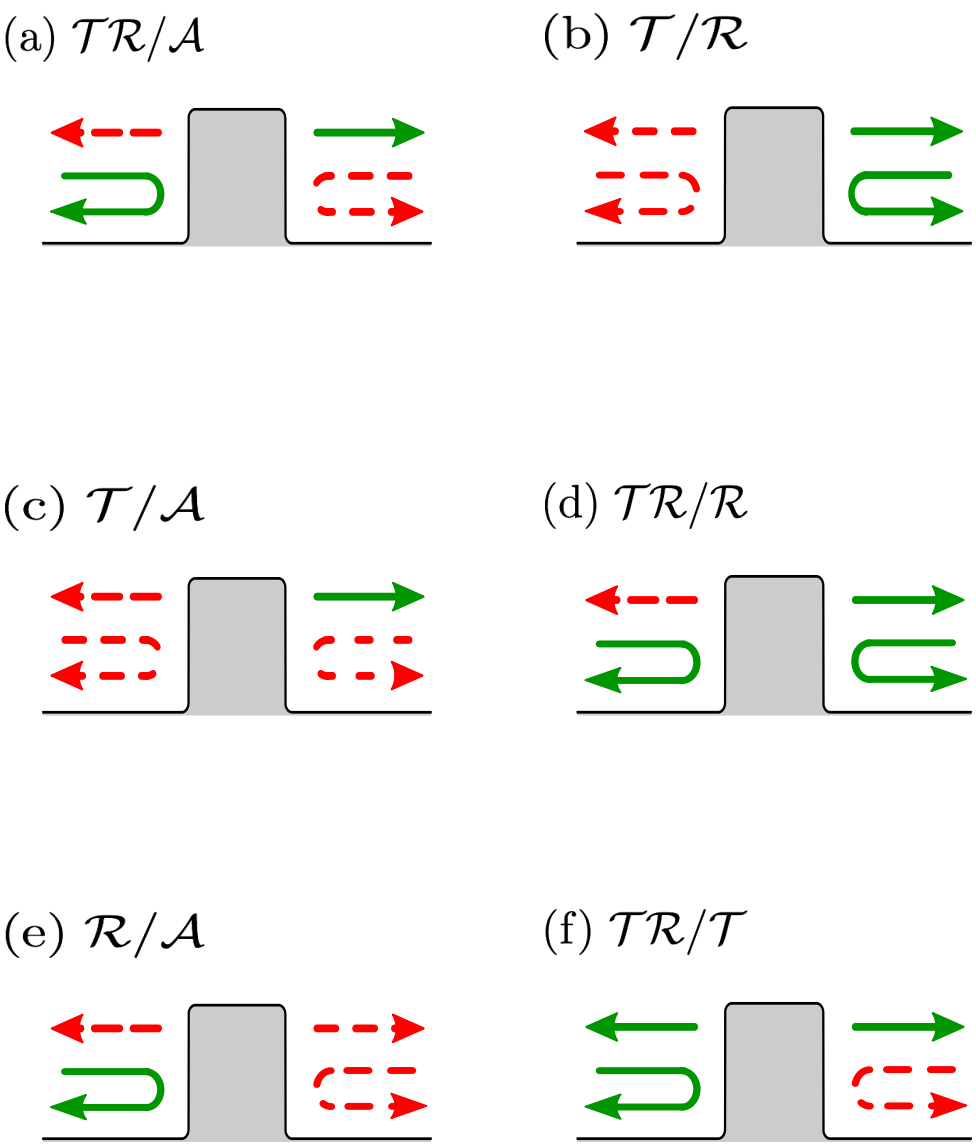

FIGURE 6.1: Devices with asymmetric scattering (limited to scattering coefficients being 0 or 1). The dashed and continuous lines represent respectively zero or one for the moduli of the scattering amplitudes; the bended lines are for reflection amplitudes, and the straight lines for transmission: (a) One-way mirror ($\mathcal{TR}/\mathcal{A}$); (b) One-way barrier ($\mathcal{T}/\mathcal{R}$); (c) One-Way T-filter ($\mathcal{T}/\mathcal{A}$); (d) Mirror & 1-way transmitter ($\mathcal{TR}/\mathcal{R}$); (e) One-way R-filter ($\mathcal{R}/\mathcal{A}$); (f) Transparent, one-way reflector ($\mathcal{TR}/\mathcal{T}$). The letter codes summarize the effect of left and right incidence, separated by a slash "/". $\mathcal{T}$ or $\mathcal{R}$ on one side of the slash indicate a unit transmission or reflection coefficient for incidence from that side, whereas the absence of one or the other letter corresponds to zero coefficients. An $\mathcal{A}$ denotes "full absorption", i.e., both moduli of reflection and transmission amplitudes are zero for incidence from one side. For example, $\mathcal{TR}/\mathcal{A}$ means unit modulus transmission and reflection from the left and total absorption from the right.

TABLE 6.1: Symmetries of the potential classified in terms of the commutativity or pseudo-hermiticity of H with the elements of Klein's 4-group $\{1, \Pi, \theta, \Pi\theta\}$ (second column). The first column sets a simplifying roman-number code for each symmetry. The relations among potential matrix elements are given in coordinate and momentum representations in the third and fourth columns. The fifth column gives the relations they imply in the matrix elements of S and/or $\widehat{S}$ matrices (S is for scattering by H and $\widehat{S}$ for scattering by $H^\dagger$). From them the next four columns set the relations implied on scattering amplitudes. Together with generalized unitarity relations (6.3) they also imply relations for the moduli (tenth column), and phases (not shown). The last two columns indicate the possibility to achieve perfect asymmetric transmission or reflection: "P" means possible (but not necessary), "No" means impossible. In some cases "P" is accompanied by a condition that must be satisfied.

Code	Symmetry	$\langle x\|V\|y\rangle =$	$\langle p\|V\|p'\rangle =$	$\langle p\|S\|p'\rangle =$	$T^l =$	$T^r =$	$R^l =$	$R^r =$	from eq. (6.3) $\|T^r\|=0$	$\|T^l\|=1$ $\|R^r\|=0$	$\|R^l\|=1$
I	$1H = H1$	$\langle x\|V\|y\rangle$	$\langle p\|V\|p'\rangle$	$\langle p\|S\|p'\rangle$	T^l	T^r	R^l	R^r		P	P
II	$1H = H^\dagger 1$	$\langle y\|V\|x\rangle^*$	$\langle p'\|V\|p\rangle^*$	$\langle p\|\widehat{S}\|p'\rangle$	$\widehat{T}^l$	$\widehat{T}^r$	$\widehat{R}^l$	$\widehat{R}^r$	$\|T^l\|=\|T^r\|$, $\|R^l\|=\|R^r\|$	No	No
III	$\Pi H = H\Pi$	$\langle -x\|V\|-y\rangle$	$\langle -p\|V\|-p'\rangle$	$\langle -p\|S\|-p'\rangle$	T^r	T^l	R^r	R^l	$\|T^l\|=\|T^r\|$,$\|R^l\|=\|R^r\|$	No	No
IV	$\Pi H = H^\dagger\Pi$	$\langle -y\|V\|-x\rangle^*$	$\langle -p'\|V\|-p\rangle^*$	$\langle -p\|\widehat{S}\|-p'\rangle$	$\widehat{T}^r$	$\widehat{T}^l$	$\widehat{R}^r$	$\widehat{R}^l$		P, $R^r R^{l*} = 1$	P, $T^r T^{l*} = 1$
V	$\Theta H = H\Theta$	$\langle x\|V\|y\rangle^*$	$\langle -p\|V\|-p'\rangle^*$	$\langle -p'\|\widehat{S}\|-p\rangle$	$\widehat{T}^r$	$\widehat{T}^l$	$\widehat{R}^l$	$\widehat{R}^r$	$\|R^l\| = \|R^r\|$	P, $\|R^{r,l}\| = 1$	No
VI	$\Theta H = H^\dagger\Theta$	$\langle y\|V\|x\rangle$	$\langle -p'\|V\|-p\rangle$	$\langle -p'\|S\|-p\rangle$	T^r	T^l	R^l	R^r	$\|T^l\| = \|T^r\|$	No	P
VII	$\Theta\Pi H = H\Theta\Pi$	$\langle -x\|V\|-y\rangle^*$	$\langle p\|V\|p'\rangle^*$	$\langle p'\|\widehat{S}\|p\rangle$	$\widehat{T}^l$	$\widehat{T}^r$	$\widehat{R}^r$	$\widehat{R}^l$	$\|T^l\| = \|T^r\|$	No	P, $\|T^{r,l}\| = 1$
VIII	$\Theta\Pi H = H^\dagger\Theta\Pi$	$\langle -y\|V\|-x\rangle$	$\langle p'\|V\|p\rangle$	$\langle p'\|S\|p\rangle$	T^l	T^r	R^r	R^l	$\|R^l\| = \|R^r\|$	P	No

6.3 Generalized symmetries

The detailed technical and formal background for the following can be found in a previous review on 1D scattering by complex potentials [109], a companion to this article for those readers willing to reproduce the calculations in detail. The Appendix (Sec. I) provides also a minimal kit of scattering theory formulae that may be read first to set basic concepts and notation. The notation is essentially as in [109], but it proves convenient to use for the potential matrix (or kernel function) in coordinate representation two different forms, namely $\langle x|V|y\rangle = V(x,y)$. "Local" potentials are those for which $V(x,y) = V(x)\delta(x-y)$.

For hermitian Hamiltonians, symmetries are represented by the commutation of a symmetry operator with the Hamiltonian. In scattering theory, symmetry plays an important role as it implies relations among the S-matrix elements beyond those implied by its unitarity, see e.g. [111] and, for scattering in one dimension, Sec. 2.6 in [109].

Symmetries are also useful for non-hermitian Hamiltonians, but the mathematical and conceptual framework must be generalized. We consider that a unitary or antiunitary operator A represents a symmetry of H if it satisfies at least one of these relations,

$$AH = HA, \tag{6.1}$$

$$AH = H^\dagger A. \tag{6.2}$$

For a right eigenstate of H, $|\psi\rangle$, with eigenvalue E, eq. (6.1) implies that $A|\psi\rangle$ is also a right eigenstate of H, with the same eigenvalue if A is unitary, and with the complex conjugate eigenvalue E^* if A is antiunitary. Equation (6.2) implies that $A|\psi\rangle$ is a right eigenstate of $H^\dagger$ with eigenvalue E for A unitary or E^* for A antiunitary, or a left eigenstate of H with eigenvalue E^* for A unitary, or E for A antiunitary. For real-energy scattering eigenfunctions in the

TABLE 6.2: Equivalences among symmetries for the potential elements. Given the symmetry of the upper row, the table provides the equivalent symmetries. For example, if II is satisfied, then III=IV holds. In words, if the potential is hermitian, parity symmetry amounts to parity pseudohermiticity. In terms of the matrix elements of the potential, if $\langle x|V|y\rangle = \langle y|V|x\rangle^*$ *and also* $\langle x|V|y\rangle = \langle -x|V|-y\rangle$, $\forall(x,y)$, then $\langle x|V|y\rangle = \langle -y|V|-x\rangle^*$ holds as well. One may proceed similarly for all other relations. The commutation with the identity (I) is excluded as this symmetry is satisfied by all potentials.

II	III	IV	V	VI	VII	VIII
III=IV	II=IV	II=III	II=VI	II=V	II=VIII	II=VII
V=VI	V=VII	V=VIII	III=VII	III=VIII	III=V	III=VI
VII=VIII	VI=VIII	VI=VII	IV=VIII	IV=VII	IV=VI	IV=V

continuum, the ones we are interested in here, $E^* = E$. When eq. (6.2) holds we say that H is A-pseudohermitian [112]. Parity-pseudohermiticity has played an important role as being equivalent to space-time reflection (PT) symmetry for *local* potentials [112, 113]. A large set of these equivalences will be discussed below. A relation of the form (6.2) has been also used with differential operators to get real spectra beyond PT-symmetry for local potentials [114, 115].

Here we consider A to be a member of the Klein 4-group $K_4 = \{1, \Pi, \Theta, \Pi\Theta\}$ formed by unity, the parity operator Π, the antiunitary time-reversal operator Θ, and their product $\Pi\Theta$. This is a discrete, abelian group. We also assume that the Hamiltonian is of the form $H = H_0 + V$, with H_0, the kinetic energy operator of the particle, being hermitian and satisfying $[H_0, A] = 0$ for all members of the group, whereas the potential V may be non-local in position representation. The motivation to use Klein's group is that the eight relations implied by eqs. (6.1) and (6.2) generate all possible symmetries of a non-local potential due to the identity, complex conjugation, transposition, and sign inversion, both in coordinate or momentum representation, see table 6.1, where each symmetry has been labeled by a roman number. Interesting enough, in this classification hermiticity (symmetry II in table 6.1) may be regarded as 1-pseudohermiticity.

Examples on how to find the relations in the fifth column of table 6.1 of $S-$ and $\widehat{S}$-matrix elements (for scattering by H and $H^\dagger$ respectively) are provided in

ref. [109], where the symmetry types III, VI, and VII where worked out. Similar manipulations, making use of the action of unitary or antiunitary operators of Klein's group on Möller operators, help to complete the table.

From the fifth column in table 1, equivalences among the amplitudes for left and right incidence for scattering by H, $(T^{l,r}, R^{l,r})$ or $H^\dagger$ $(\widehat{T}^{l,r}, \widehat{R}^{l,r})$, are deduced, see the Appendix and the four columns for $T^{l,r}$, and $R^{l,r}$ in table 6.1. Together with the generalized unitarity relations $\widehat{S}^\dagger S = S\widehat{S}^\dagger = 1$, which in terms of amplitudes take the form [109]

$$\begin{aligned}
\widehat{T}^l T^{l*} + \widehat{R}^l R^{l*} &= 1, \\
\widehat{T}^r T^{r*} + \widehat{R}^r R^{r*} &= 1, \\
\hat{T}^{l*} R^r + T^r \widehat{R}^{l*} &= 0, \\
T^l \widehat{R}^{r*} + \widehat{T}^{r*} R^l &= 0,
\end{aligned} \tag{6.3}$$

these equivalences between the amplitudes imply further consequences on the amplitudes' moduli (tenth column of table 6.1) and phases (not shown). The final two columns use the previous results to determine if perfect asymmetry is possible for transmission or reflection. This makes evident that hermiticity (II) and parity (III) preclude, independently, any asymmetry in the scattering coefficients; PT-symmetry (VII) or Θ-pseudohermiticity (VI) forbid transmission asymmetry (all local potentials satisfy automatically symmetry VI), whereas time-reversal symmetry (i.e., a real potential in coordinate space) (V) or PT-pseudohermiticity (VIII) forbid reflection asymmetry. A caveat is that asymmetric effects forbidden by a certain symmetry in the linear (Schrödinger) regime considered in this paper might not be forbidden in a non-linear regime [116], which goes beyond our present scope.

The occurrence of one particular symmetry in the potential (conventionally "first symmetry") does not exclude a second symmetry to be satisfied as well. When a double symmetry holds, excluding the identity, the "first" symmetry

implies the equivalence of the second symmetry with a third symmetry. We have already mentioned that Π-pseudohermiticity (IV) is equivalent to *PT*-symmetry (VII) for local potentials. Being local is just one particular way to satisfy symmetry VI, namely Θ-pseudohermiticity. The reader may verify with the aid of the third column for $\langle x|V|y\rangle$ in table 6.1, that indeed, if symmetry VI is satisfied (first symmetry), symmetry IV has the same effect as symmetry VII. They become equivalent. Other well known example is that for a local potential (symmetry VI is satisfied), a real potential in coordinate space is necessarily hermitian, so symmetries V and II become equivalent. These examples are just particular cases of the full set of equivalences given in table 6.2.

TABLE 6.3: Device types for transmission and/or reflection asymmetry, restricted to 1 or 0 moduli for the scattering amplitudes. The fifth column indicates the symmetries in table 6.1 that forbid the device. Figures S1, S2, S3, S4, and S5 can be found in the Appendix to this chapter.

Device type	Left incidence	Right incidence	Code	Forbidden by	Example
One-way mirror	transmits and reflects	absorbs	$\mathcal{TR}/\mathcal{A}$	II, III, IV, V, VI, VII, VIII	fig. S1
One-way barrier	transmits	reflects	$\mathcal{T}/\mathcal{R}$	II, III, IV, V, VI, VII, VIII	fig. S2
One-way T-filter	transmits	absorbs	$\mathcal{T}/\mathcal{A}$	II, III, IV, V, VI, VII	fig. 6.2, S3
Mirror&1-way transmitter	transmits and reflects	reflects	$\mathcal{TR}/\mathcal{R}$	II, III, VI, VII	fig. S4
One-way R-filter	reflects	absorbs	$\mathcal{R}/\mathcal{A}$	II, III, IV, V, VII, VIII	[117]
Transparent 1-way reflector	transmits and reflects	transmits	$\mathcal{TR}/\mathcal{T}$		

TABLE 6.4: Device types allowed for a given symmetry.

Symmetry	Allowed devices
I	All types
II	None
III	None
IV	$\mathcal{TR}/\mathcal{R}, \mathcal{TR}/\mathcal{T}$
V	$\mathcal{TR}/\mathcal{R}$
VI	$\mathcal{R}/\mathcal{A}, \mathcal{TR}/\mathcal{T}$
VII	$\mathcal{TR}/\mathcal{T}$
VIII	$\mathcal{T}/\mathcal{A}, \mathcal{TR}/\mathcal{R}$

Combining the information of the last two-columns in table 6.1 with the additional condition that all scattering coefficients be 0 or 1 we elaborate table 6.3, which provides the symmetries that do not allow the implementation of the devices in fig. 6.1. The complementary table 6.4 gives instead the symmetries that allow, but do not necessarily imply, a given device type. The device denominations in fig. 6.1 or table 6.3 are intended as short and meaningful, and do not necessarily coincide with some extended terminology, in part because the range of possibilities is broader here than those customarily considered, and because we use a 1 or 0 condition for the moduli. For example, a device with reflection asymmetry and with $T^r = T^l = 1$ would in our case be a particular "transparent, one-way reflector", as full transmission occurs from both sides. This effect has however become popularized as "unidirectional invisibility" [118, 119]. A debate on terminology is not our main concern here, and the use of a code system as the one proposed will be instrumental in avoiding misunderstandings.

6.4 Designing potentials for asymmetric devices

We will show how to design non-local potentials leading to the asymmetric devices. For simplicity we look for non-local potentials $V(x, y)$ with local support that vanish for $|x| > d$ and $|y| > d$.

Inverse scattering proceeds similarly to [120], by imposing an ansatz for the wavefunctions and the potential in the stationary Schrödinger equation

$$\frac{\hbar^2 k^2}{2m}\psi(x) = -\frac{\hbar^2}{2m}\frac{d^2}{dx^2}\psi(x) + \int_{-d}^{d} dy V(x,y)\psi(y). \tag{6.4}$$

The free parameters are fixed making use of the boundary conditions. The form of the wavefunction incident from the left is $\psi_l(x) = e^{ikx} + R^l e^{-ikx}$ for $x < -d$ and $\psi_l(x) = T^l e^{ikx}$ for $x > d$, where $k = p/\hbar$. The wavefunction incident from the right is instead $\psi_r(x) = e^{-ikx}T^r$ for $x < -d$ and $\psi_r(x) = e^{-ikx} + R^r e^{ikx}$ for

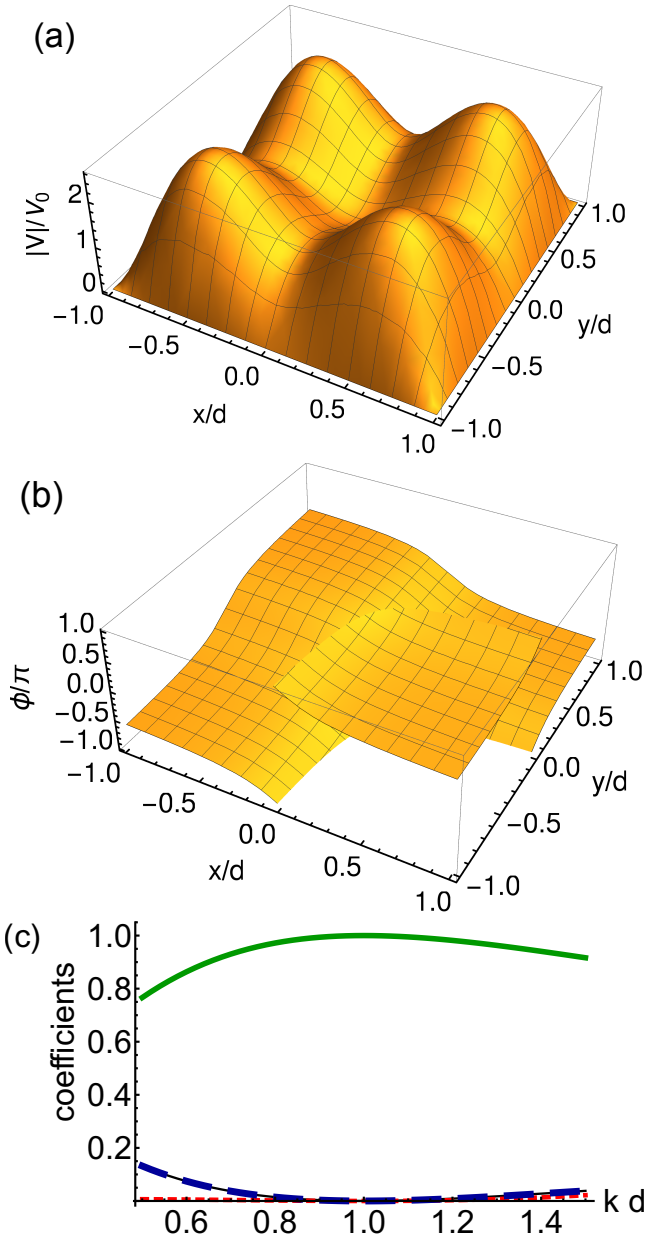

FIGURE 6.2: One-way T-filter ($\mathcal{T}/\mathcal{A}$, $\left|T^l\right| = 1, T^r = R^l = R^r = 0$) with potential $V(x,y) = |V(x,y)|e^{i\phi(x,y)}$ set for $k_0 = 1/d$. (a) Absolute value $|V(x,y)|$; (b) Argument $\phi(x,y)$; (c) Transmission and reflection coefficients: $\left|R^l\right|^2$ (black, solid line), $\left|T^l\right|^2$ (green, solid line), $|R^r|^2$ (blue, tick, dashed line), $|T^r|^2$ (red, dotted line). $V_0 = \hbar^2/(2md^3)$.

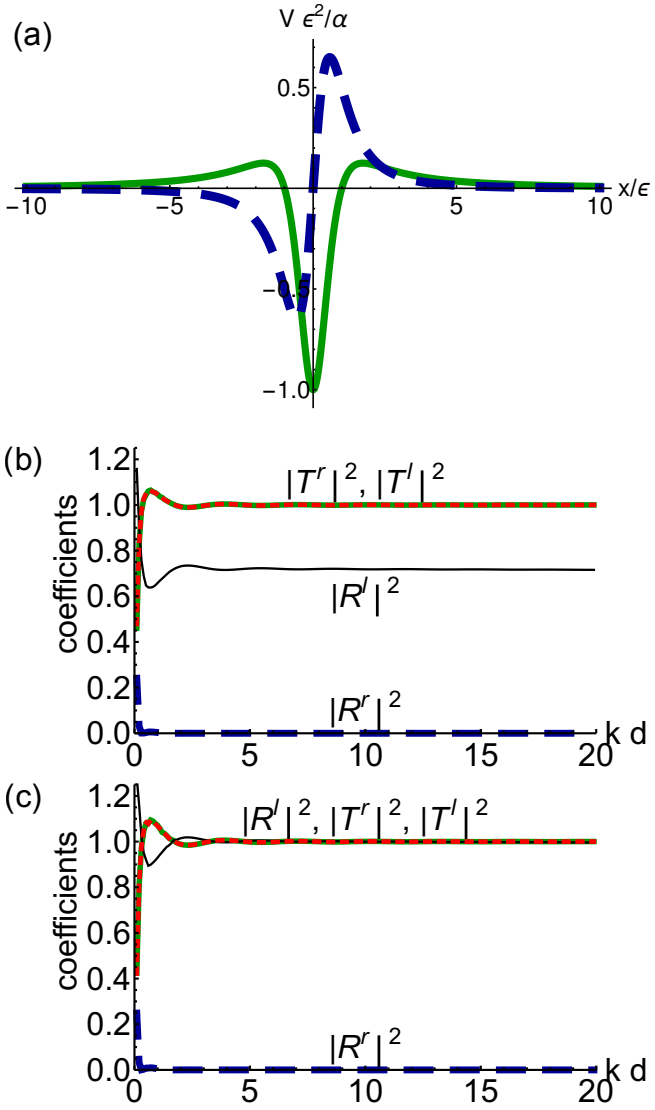

FIGURE 6.3: Transparent 1-way reflector with a local PT potential: (a) Approximation of the potential (6.8), real part (green solid line), imaginary part (blue dashed line). (b,c) Transmission and reflection coefficients versus momentum kd; left incidence: $|R^l|^2$ (black, solid line), $|T^l|^2$ (green, solid line); right incidence: $|R^r|^2$ (blue, tick, dashed line), $|T^r|^2$ (red, dotted line, coincides with green, solid line). $\epsilon/d = 10^{-4}$. (b) $\alpha = 1.0\hbar^2/(4\pi m)$ (c) $\alpha = 1.225\hbar^2/(4\pi m)$ (the black, solid line coincides here mostly with the red, dotted and green, solid lines).

$x > d$.

Our strategy is to assume polynomial forms for the two wavefunctions in the interval $|x| < d$, $\psi_l(x) = \sum_{j=0}^{5} c_{l,j} x^j$ and $\psi_r(x) = \sum_{j=0}^{5} c_{r,j} x^j$, and also a polynomial ansatz of finite degree for the potential $V(x,y) = \sum_i \sum_j v_{ij} x^i y^j$. Inserting these ansatzes in eq. (6.4) and from the conditions that $\psi_{l,r}$ and their derivatives must be continuous, all coefficients $c_{l,j}\,, c_{r,j}$ and v_{ij} can be determined. Symmetry properties of the potential can also be imposed via additional conditions on the potential coefficients v_{ij}. For example we may use this method to obtain a one-way T-filter ($\mathcal{T}/\mathcal{A}$) device (third device in table 6.3) with a nonlocal PT-pseudohermitian potential (symmetry VIII of table 6.1) for a chosen wavevector $k = k_0$. The absolute value and argument of the resulting potential $V(x,y)$ are shown in figs. 6.2(a) and 6.2(b) together with its scattering coefficients as function of the incident wave vector, fig. 6.2(c). As can be seen in fig. 6.2(c) the imposed scattering coefficients are fulfilled exactly for the chosen wavevector. They are also satisfied approximately in a neighborhood of k_0. In the Appendix, Sec. II, we give further details about the construction of this potential and we work out other asymmetric devices of fig. 6.1.

6.5 Extending the scattering asymmetry to a broad incident-momentum domain

The inversion technique just described may be generalized to extend the range of incident momenta for which the potential works by imposing additional conditions and increasing correspondingly the number of parameters in the wavefunction ansatz, for example we may impose that the derivatives of the amplitudes, in one or more orders, vanish at k_0, or 0/1 values for the coefficients not only at k_0 but at a series of grid points k_1, k_2, ... k_N, as in [121, 122, 120, 109].

Here we put forward instead a method that provides a very broad working-window domain. While we make formally use of the Born approximation, the exact numerical computations demonstrate the robustness and accuracy of the approach to achieve that objective by making use of an adjustable parameter in the potential. The very special role of the Born approximation in inverse problems has been discussed and demonstrated in [123, 124, 125]. Specifically we study a transparent one-way reflector $\mathcal{TR}/\mathcal{T}$. Our aim is now to find a local PT-symmetric potential such that asymmetric reflection results, $T^l = T^r = 1, R^r = 0, |R^l| = 1$ for a broad range of incident momenta. A similar goal was pursued in [126] making use of a supersymmetric transformation, without imposing $|R^l| = 1$.

In the Born approximation and for a local potential $V(x)$, the reflection amplitudes take the simple form

$$R^l = -\frac{2\pi i m}{p}\langle -p|V|p\rangle,\ R^r = -\frac{2\pi i m}{p}\langle p|V|-p\rangle. \tag{6.5}$$

Defining the Fourier transform

$$\widetilde{V}(k) = \frac{1}{\sqrt{2\pi}}\int_{-\infty}^{\infty} dx\, V(x)e^{-ikx} \tag{6.6}$$

we get for $k = p/\hbar > 0$:

$$R^l = -\frac{\sqrt{2\pi} i m}{k\hbar^2}\widetilde{V}(-2k),\ R^r = -\frac{\sqrt{2\pi} i m}{k\hbar^2}\widetilde{V}(2k). \tag{6.7}$$

Assuming that the potential is local and PT-symmetrical, we calculate the transition coefficient from them using generalized unitarity as $|T|^2 = 1 - R^{r*}R^l$.

To build a $\mathcal{TR}/\mathcal{T}$ device we demand: $\widetilde{V}(k) = \sqrt{2\pi}\alpha k$ $(k < 0)$ and $\widetilde{V}(k) = 0$ $(k \geq 0)$. By inverse Fourier transformation, this implies

$$\begin{aligned} V(x) = & \quad -\alpha \frac{\partial}{\partial x} \lim_{\epsilon \to 0} \frac{1}{x - i\epsilon} = \alpha \lim_{\epsilon \to 0} \frac{1}{(x - i\epsilon)^2} \\ = & \quad \alpha \lim_{\epsilon \to 0} \left[\frac{x^2 - \epsilon^2}{(x^2 + \epsilon^2)^2} + i \frac{2x\epsilon}{(x^2 + \epsilon^2)^2} \right], \end{aligned} \tag{6.8}$$

which is indeed a local, PT-symmetric potential for α real. α is directly related to the reflection coefficient, within the Born approximation, $R^l = 4\pi i m\alpha/\hbar^2$. As the Born approximation may differ from exact results we shall keep α as an adjustable parameter in the following.

In a possible physical implementation, the potential in eq. (6.8) will be approximated by keeping a small finite $\epsilon > 0$, see fig. 6.3(a). Then, its Fourier transform is $\widetilde{V}(k) = \sqrt{2\pi}\alpha k e^{\epsilon k}$ $(k < 0)$ and $\widetilde{V}(k) = 0$ $(k \geq 0)$. In figs. 6.3(b) and (c), the resulting coefficients for $\epsilon/d = 10^{-4}$ and two different values of α are shown. These figures have been calculated by numerically solving the Schrödinger equation exactly. Remarkably, the Born approximation contains all the information required to build the required potential shape up to a global factor. Such a prominent role of the Born approximation in inverse problems has been noted in different applications [123, 124, 125]. For a range of α, the potential gives $|R^r| \approx 0$, a nearly constant $|R^l|^2$, and $|T^r| = |T^l| \approx 1$ in a broad k-domain, see fig. 6.3(b). Adjusting the value of α, fig. 6.3(c), sets $|R^l| \approx 1$ as desired.

6.6 Discussion

Scattering asymmetries are necessary to develop technologically relevant devices such as one-way mirrors, filters and barriers, invisibility cloaks, diodes, or Maxwell demons. So far much effort has been devoted to build and apply local PT-symmetric potentials but the possible scattering asymmetries with them

are quite limited. We find that six device types with asymmetric scattering are possible when imposing 0 or 1 scattering coefficients. PT-symmetry can only realize one of them, but this symmetry is just one among eight possible symmetries of complex non-local potentials. The eight symmetries arise from the discovery that Klein's four-group $\{1, \Pi, \Theta, \Theta\Pi\}$, combined with two possible relations among the Hamiltonian, its adjoint, and the symmetry operators of the group, eqs. (1) and (2), produce all possible equalities among potential matrix elements after complex conjugation, coordinate inversion, the identity, and transposition. In other words, to have all possible such equalities, the conventional definition of a symmetry A in terms of its commutation with the Hamiltonian H is not enough, and A-pseudohermiticity must be considered as well on the same footing. Extending the concept of what a ÒsymmetryÓ is for complex, non-local potentials is a fundamental, far-reaching step of this work. This group theoretical analysis and classification is not only esthetically pleasing, but also of practical importance, as it reveals the underlying structure and span of the possibilities available in principle to manipulate the asymmetrical response of a potential for a structureless particle.

We provide potentials for the different asymmetric devices including an example that works in a broad domain of incident momenta. Although the present theory is for the scattering of quantum particles, the analogies between quantum physics and optics suggest to extend the concepts and results for optical asymmetric devices.

Interesting questions left for future work are the inclusion of other mechanisms for transmission and reflection asymmetries (for example nonlinearities [116, 127], and time dependent potentials [128, 129]), or a full discussion of the phases of the scattering amplitudes in addition to the moduli emphasized here. In this paper the properties of the scattering amplitudes have been worked out assuming that the operator A in the symmetry relations in eqs. (6.1) and (6.2) is a unitary/antiunitary operator in Klein's group. We may generalize the study

to include more general operators, possibly including differential operators, as was done in [130] for phase transitions of optical potentials, or the operator that swaps internal states or waveguides [131, 132].

We shall also examine in a complementary paper the physical realization of complex nonlocal effective potentials. In a quantum optics scenario, simple examples were provided in [133] based on applying the partitioning technique [134, 135] to the scattering of a particle with internal structure. The experimental realization of all new symmetries and devices may be challenging, e.g. to engineer the nonlocality in optics, but there is much to gain. We may expect progress similar to the successful evolution from theory to actual devices in the sequence from the first mathematical models of PT-symmetric potentials [136], to the proposal of an optical realization [110], and to the actual experiments [137], even if considerable time lapses were needed between the three steps.

6.7 Appendix for chapter 6

6.7.1 I. Scattering amplitudes

We provide a lightning review of scattering amplitudes in 1D. For a more complete account, see [109]. (Citations and table numbers correspond to the main text. Equation and figure numbers in the Appendix material are indicated as S1, S2, etc..) We assume $p > 0$. The amplitudes for scattering by $H = H_0 + V$, may be calculated by

$$R^l = -\frac{2\pi i m}{p}\langle -p|T_{op}(+)|p\rangle, \tag{6.9}$$

$$T^l = 1 - \frac{2\pi i m}{p}\langle p|T_{op}(+)|p\rangle, \tag{6.10}$$

$$R^r = -\frac{2\pi i m}{p}\langle p|T_{op}(+)|-p\rangle, \tag{6.11}$$

$$T^r = 1 - \frac{2\pi i m}{p}\langle -p|T_{op}(+)|-p\rangle, \tag{6.12}$$

where the l/r superscript indicates left or right incidence, and

$$T_{op}(+)|\pm p\rangle = \left[V + V\frac{1}{E_p + i0 - H}V\right]|\pm p\rangle, \tag{6.13}$$

where $E_p = p^2/(2m)$. To find Born-approximation expressions of the scattering coefficients (square moduli of the amplitudes), we take $T_{op} \approx V$ in the expressions of R^l, and R^r. For T^l and T^r we also include the second order in V, which contributes to the square in second order due to the 1 in eqs. (6.10) and (6.12).

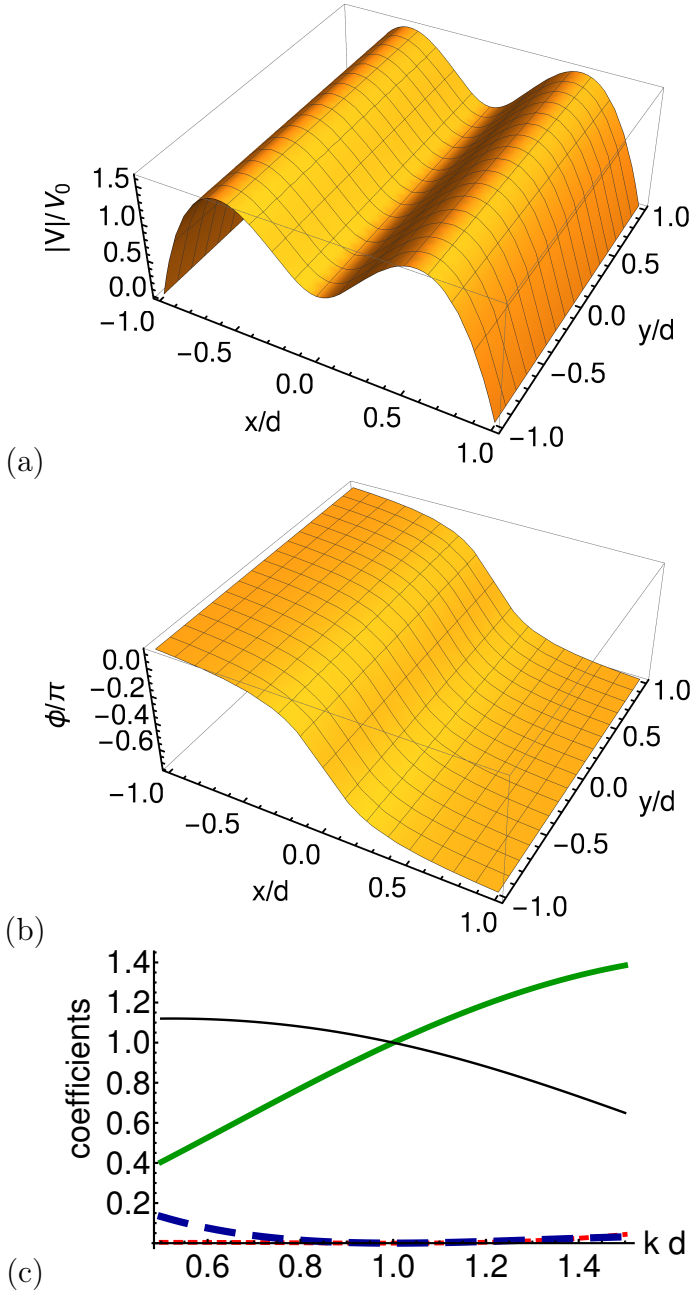

FIGURE 6.4: One-way mirror ($\mathcal{TR}/\mathcal{A}$, $R^l = -1, R^r = 0$) with potential $V(x,y) = |V(x,y)|e^{i\phi(x,y)}$ set for $k_0 = 1/d$. (a) Absolute value $|V(x,y)|$; (b) Argument $\phi(x,y)$; (c) Transmission and reflection coefficients: $\left|R^l\right|^2$ (black, solid line), $\left|T^l\right|^2$ (green, solid line), $|R^r|^2$ (blue, tick, dashed line), $|T^r|^2$ (red, dotted line).

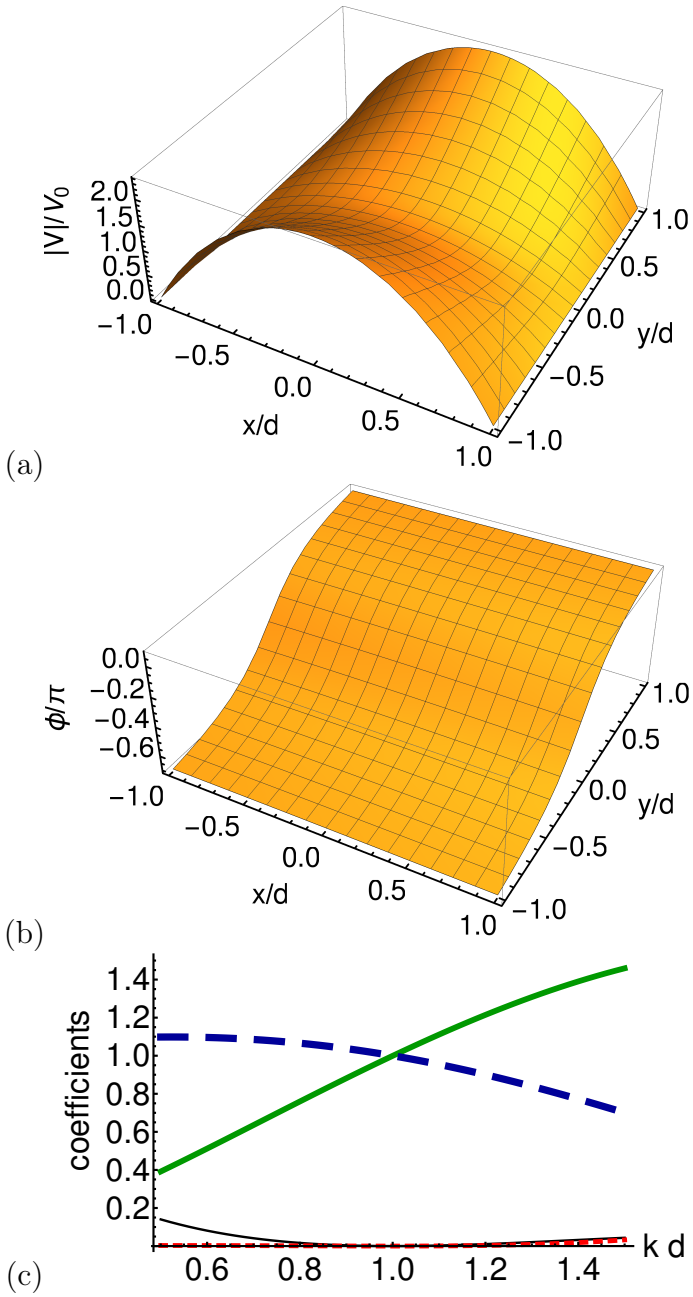

FIGURE 6.5: One-way barrier ($\mathcal{T}/\mathcal{R}$, $R^l = 0, R^r = -1$) with potential $V(x,y) = |V(x,y)|e^{i\phi(x,y)}$ set for $k_0 = 1/d$. (a) Absolute value $|V(x,y)|$; (b) Argument $\phi(x,y)$; (c) Transmission and reflection coefficients: $\left|R^l\right|^2$ (black, solid line), $\left|T^l\right|^2$ (green, solid line), $|R^r|^2$ (blue, tick, dashed line), $|T^r|^2$ (red, dotted line).

The on-shell S matrix, see [109], is formed as

$$\mathsf{S} = \begin{pmatrix} \langle \mathbf{p}|\mathsf{S}|\mathbf{p}\rangle & \langle \mathbf{p}|\mathsf{S}|-\mathbf{p}\rangle \\ \langle -\mathbf{p}|\mathsf{S}|\mathbf{p}\rangle & \langle -\mathbf{p}|\mathsf{S}|-\mathbf{p}\rangle \end{pmatrix} = \begin{pmatrix} T^l & R^r \\ R^l & T^r \end{pmatrix}. \tag{6.14}$$

This on-shell matrix relates to the standard S-matrix elements in momentum representation,

$$\langle p|S|p'\rangle = \delta(p-p') - 2i\pi\delta(E_p - E'_p)\langle p|T_{op}(+)|p'\rangle, \tag{6.15}$$

by factoring out a delta function,

$$\langle p|S|p'\rangle = \frac{|p|}{m}\delta(E_p - E'_p)\langle \mathbf{p}|\mathsf{S}|\mathbf{p}'\rangle.$$

All the above formulae may be reproduced when the particle is scattered instead by $H^\dagger = H_0 + V^\dagger$, giving scattering amplitudes with a hat, $\widehat{T}^r, \widehat{T}^l, \widehat{R}^r, \widehat{R}^l$, and $\widehat{S}$. Hatted and unhatted amplitudes are not independent, they are linked by the generalized unitary relation $\widehat{S}^\dagger S = S\widehat{S}^\dagger = 1$, whose on-shell matrix elements lead to the four relations in Eq. (6.3) of the main text. They can be rearranged to express the transmission amplitudes of $H^\dagger$ in terms of those of H,

$$\begin{aligned} \widehat{T}^{l*} &= \frac{T^r}{T^lT^r - R^lR^r}, \quad \widehat{R}^{l*} = -\frac{R^r}{T^lT^r - R^lR^r}, \\ \widehat{T}^{r*} &= \frac{T^l}{T^lT^r - R^lR^r}, \quad \widehat{R}^{r*} = -\frac{R^l}{T^lT^r - R^lR^r}. \end{aligned} \tag{6.16}$$

6.7.2 II. Examples of potentials for devices with asymmetric-scattering coefficients

IIa. Nonlocal potentials for devices with transmission asymmetry

To construct asymmetric-transmission devices ($|T^l| = 1, |T^r| = 0$, $|R^{r,l}| = 0, 1$) we fix the phases of the transmission amplitudes as $T^l = 1, T^r = 0$, and the reflection amplitudes will be specified in each case. We assume the form $V(x,y) = \sum_{i=0}^{5}\sum_{j=0}^{1} v_{ij}x^iy^j$ for the potential, plug this ansatz in the Schrödinger equation (4), and equate equal powers of x. Moreover we demand that $V(-d,y) = 0 = V(d,y)$ for all y such that the total potential (including

the vanishing potential for $x, y < -d$ and $x, y > d$) is continuous.

We consider first an ideal one-way mirror ($\mathcal{TR}/\mathcal{A}$) with amplitudes $R^l = -1, R^r = 0$. Waves sent from the left are fully reflected, but there is also perfect transmission, whereas waves sent from the right are absorbed. The potential that achieves this for $k = k_0 = 1/d$ is shown in figs. 6.4(a),(b) where $V_0 = \hbar^2/(2md^3)$. Similarly, the potential of a one-way barrier ($\mathcal{T}/\mathcal{R}$) is shown in figs. 6.5 (a),(b) with $R^l = 0, R^r = -1$. Note that the potential matrices or potential kernel functions $V(x, y)$ do not have units of energy but units of a force. In agreement with table 3, these potentials do not satisfy any of the nontrivial symmetries II, III, ...,VIII. The transmission and reflection coefficients around k_0 are also depicted in figs. 6.4 (c) and 6.5 (c), which show that the desired values are achieved exactly at k_0 but also approximately in some neighborhood of k_0. This holds true for all potentials in this Appendix.

IIb. Nonlocal potentials fulfilling symmetry VIII for devices with transmission asymmetry

One-way T-filters ($\mathcal{T}/\mathcal{A}$) and the mirror&1-way transmitters ($\mathcal{TR}/\mathcal{R}$) can be also constructed using the method described in the previous subsection. Nevertheless, unlike the two devices in the previous subsection, these devices can fulfill symmetry VIII. We assume now the form $V(x, y) = \sum_{i=0}^{5}\sum_{j=0}^{5} v_{ij}x^i y^j$ with $v_{ij} = (-1)^{i+j}v_{ji}$. To simplify the potential, we also demand $v_{4,4} = v_{4,5} = v_{5,4} = v_{5,5} = 0$. Moreover we demand that $V(-d, y) = 0 = V(d, y)$ for all y such that the total potential (including the vanishing potential for $x, y < -d$ and $x, y > d$) is continuous. It is also required that $R^l = R^r = R$, consistent with table 1.

In fig. 6.2, the potential for the one-way T-filter ($\mathcal{T}/\mathcal{A}$), with $R = 0, T^l = 1$, is shown, and the potential for the mirror&1-way transmitter ($\mathcal{TR}/\mathcal{R}$), calculated for $R = -1, T^l = 1$, is shown in fig. 6.6 where we have chosen $k_0 = 1/d$. The transmission and reflection coefficients around k_0 are also depicted.

For the first three devices ($\mathcal{TR}/\mathcal{A}, \mathcal{T}/\mathcal{R}$ and $\mathcal{T}/\mathcal{A}$), it follows from the generalized unitarity relations that one or more of the transmission and reflection amplitudes of the corresponding adjoint Hamiltonian will diverge at $k = k_0 = 1/d$ (if the numerator on the right-hand side of these relations stays finite while the corresponding denominator $T^l T^r - R^l R^r = -R^l R^r \to 0$). In the mirror&1-way transmitter, it follows from (6.16) that $\widehat{T}^l = 0, \widehat{R}^l = -1, \widehat{T}^r = -1, \widehat{R}^r = -1$, and therefore the adjoint Hamiltonian provides a mirror&1-way transmitter device with $l \leftrightarrow r$.

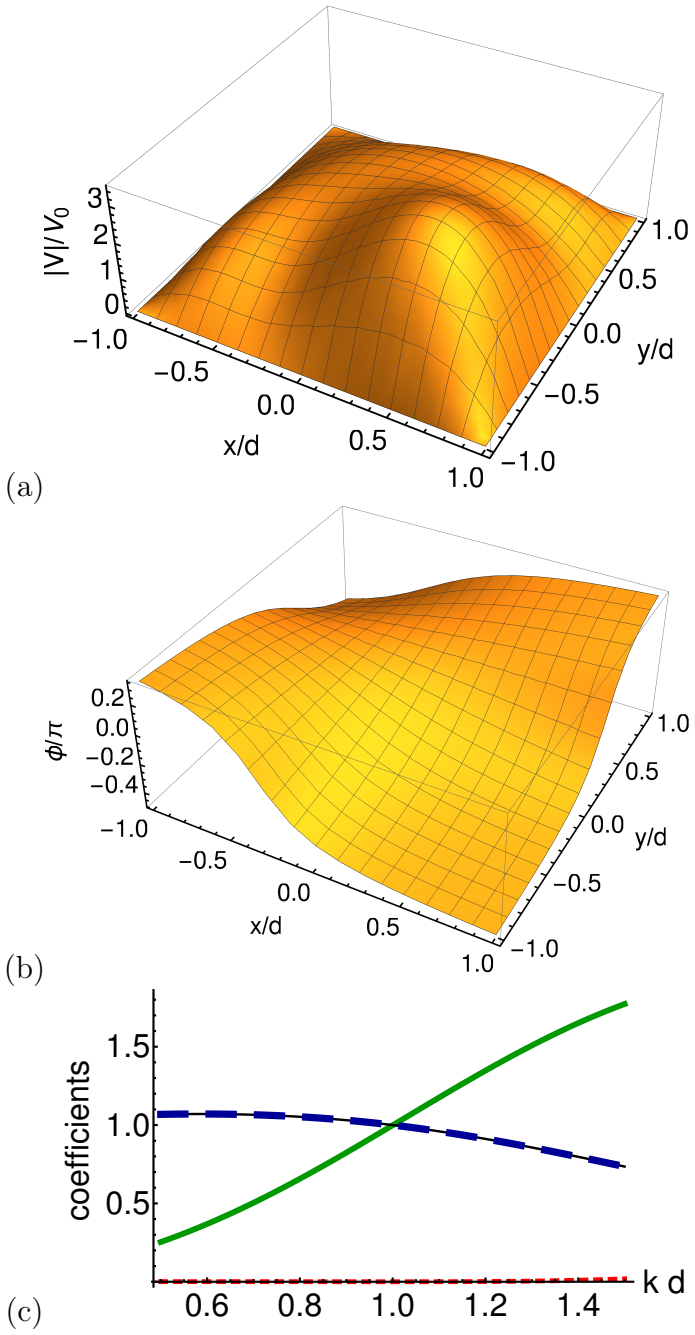

FIGURE 6.6: Mirror&1-way transmitter ($\mathcal{TR}/\mathcal{R}$, $R^l = -1, R^r = -1$) for potential $V(x,y) = |V(x,y)|e^{i\phi(x,y)}$ set for $k_0 = 1/d$. (a) Absolute value $|V(x,y)|$; (b) Argument $\phi(x,y)$; (c) Transmission and reflection coefficients: $\left|R^l\right|^2$ (black, solid line), $\left|T^l\right|^2$ (green, solid line), $|R^r|^2$ (blue, tick, dashed line), $|T^r|^2$ (red, dotted line).

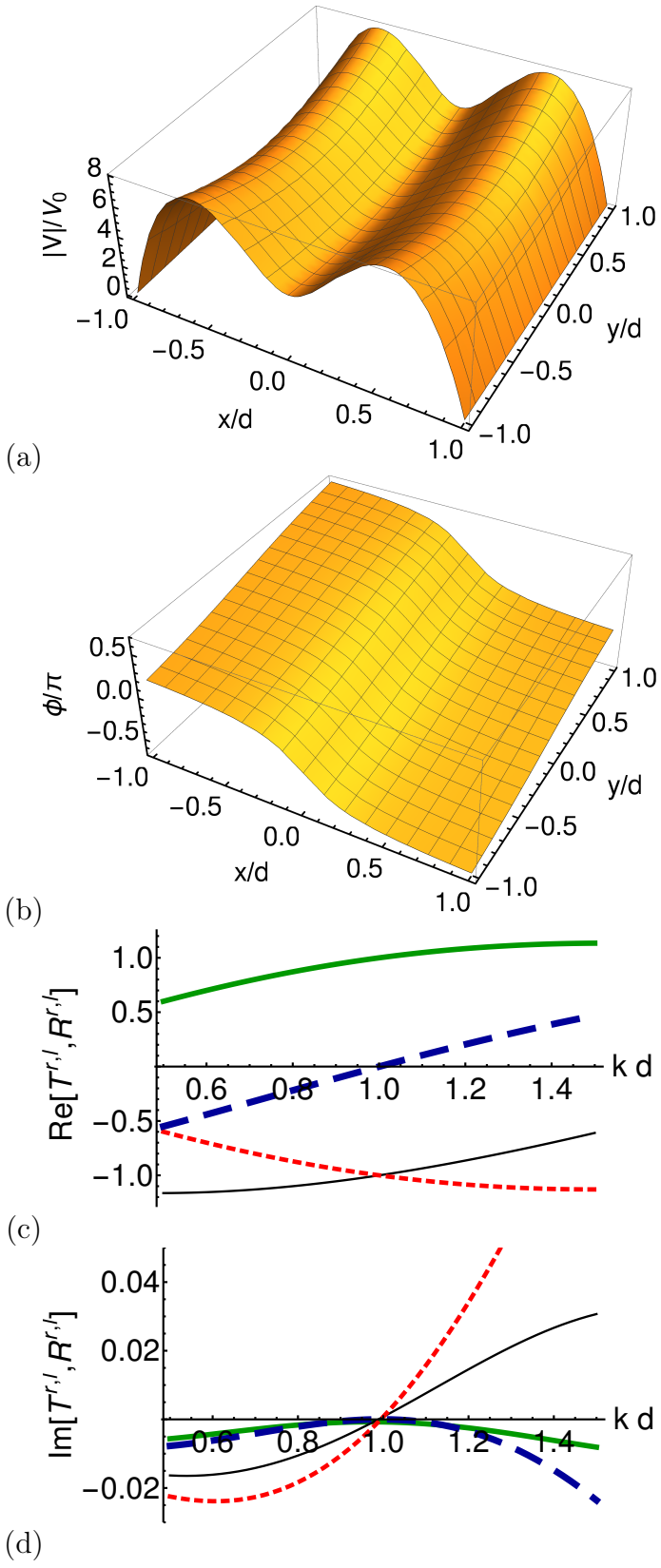

FIGURE 6.7: Transparent, one-way reflector $\mathcal{TR}/\mathcal{T}$ with non-local PT-symmetric potential $V(x,y) = |V(x,y)|e^{i\Phi}$ set for $k_0 d = 1$ so that $T^l = 1, R^l = -1, T^r = -1, R^r = 0$. (a) Absolute value $|V(x,y)|$; (b) Argument ϕ; (c) Real and (d) Imaginary part of the transmission and reflection amplitudes: R^l (black, solid line), T^l (green, solid line), R^r (blue, tick, dashed line), T^r (red, dotted line).

IIc. Devices with asymmetric reflection

In the previous subsections we have already considered two device types with asymmetric reflection coefficients, namely, the one-way mirror ($\mathcal{TR}/\mathcal{A}$), and the one way-barrier ($\mathcal{T}/\mathcal{R}$). These are the only two device types which are simultaneously asymmetrical for transmission and reflection. Two more types are possible which have only reflection asymmetry, namely, the one-way R-filter ($\mathcal{R}/\mathcal{A}$), and the transparent one-way reflector ($\mathcal{TR}/\mathcal{T}$). Both are compatible with symmetry type VI, in particular with local potentials.

A one-way R-filter $\mathcal{R}/\mathcal{A}$ acts as a perfect absorber from one side and as a perfect reflector from the other side. It may thus be constructed by adding an infinite barrier with its edge touching the end of known-perfect absorbers for one-sided incidence [121, 122, 120, 109]. Local, perfect absorbers can be worked out for one or more incident momenta, or for a momentum window. According to table 3, a $\mathcal{R}/\mathcal{A}$ device cannot have PT-symmetry. Indeed experimental realizations in optics imply local non-PT-symmetric potentials [118].

The remaining device is a one-way reflector ($\mathcal{TR}/\mathcal{T}$). Specifically, if we set $T^l = 1, R^l = 1, T^r = -1, R^r = 0$, i.e. $T^l \neq T^r$ but $\left|T^l\right|^2 = |T^r|^2 = 1$, it can be achieved with a PT-symmetric potential, but it must be non-local, see table 1. (If we set $T^l = T^r = 1$, local forms of the potential are also possible, as demonstrated in the main text.) For a nonlocal PT-symmetric potential, $V(x, y) = V(-x, -y)^*$ for all x, y. We assume the form $V(x, y) = \sum_{i=0}^{5} \sum_{j=0}^{1} v_{ij} x^i y^j$ with $v_{ij} = (-1)^{i+j} v_{ij}^*$, in other words, v_{ij} must be real for $i + j$ even and purely imaginary for $i + j$ odd. We also require that $V(-d, y) = V(d, y) = 0$ for all y and follow the same procedure described in previous subsections. The nonlocal PT-potential found can be seen in fig. 6.7 (a),(b) for $k = k_0 = 1/d$. The transmission and reflection coefficients around k_0 are depicted in fig. 6.7 (c),(d).

Chapter 7

Conclusion and Outlook

In this thesis have I focused on using Shortcuts to Adiabaticity along with related techniques and applying them to many particle systems. In this chapter I will discuss the conclusions from the previous chapters and suggest an outlook for possible future work.

Fast and Robust control using Pauli blocking

In chapter 3, we considered a novel method to speed up the adiabatic evolution of a gas of fermions. This method is complementary existing STA methods, however new techniques were required to deal with the anharmonicity of the trapping potential as STA methods do not exist for strong anharmonicity. We used Pauli blocking to induce a large energy gap between fermions in the low energy states and available unoccupied higher energy states. This was done by introducing a layer of buffer fermions on top of the low energy subsystem we were trying to protect.

This method could be used to prepare low energy fermions for different experimental tasks. In this chapter we discussed a number of different manipulations of the fermion gas, we used this method to transport the subsystem, to open or close the trap and further to split the gas into a double well. This method can be applied to a wide range of preparation tasks to provide fast and stable

evolution to the desired state. Temperature effects on the system were investigated and were found to be avoidable by adding increased numbers of fermions to the buffer layer.

As an extension to this paper we could consider further control tasks for preparing many fermion states or combinations of the discussed manipulations, such as splitting a fermion gas during transport. We could also extend the results to two and three dimensional gases which are more computationally complex.

Trapping and cooling with atomic mirror-diode

In chapter 4 we presented a method for trapping and cooling particles using an atom-diode and mirror system. Two different trajectories were studied for the classical case and a strong dependence of the cooling on the trajectory was established. Square root and linear trap trajectories were investigated and the superiority of the linear scheme was deduced. This analysis was then extended to the trapping and cooling of a quantum particle and cooling was again achieved in the quantum case. Several different parameter settings were examined and their effects on the final position and momentum probability distributions were discussed.

As outlook on this it would worth investigating if it were possible to optimise the trajectory of the atom-diode system to produce a desired final distribution. Both atom-diode trajectory and the parameters of the system could be investigated and varied to produce a final distribution for both position and momentum.

Additionally as further outlook this method could be extended to trying to

cool an ensemble of quantum particles. This extension could prove to be particularly useful as a new method for many particle quantum state preparation.

Transport of atoms through an optical lattice

In chapter 5 we presented used the method of invariant-based inverse engineering to transport atoms and Bose-Einstein condensates across an optical lattice by using an external trapping potential. We achieved this by considering three different building blocks, first loading particles into the external harmonic trap, second transporting them across a lattice site and third unloading them back onto the lattice. Different methods were proposed depending on the particular degree of control of trap frequency and and position available. The sensitivity of the protocols with respect to trap centre control and trapping frequency were investigated and the protocols shown to be robust against errors.

A outlook this work could be extended to a more general case for Bose-Einstein condensates across many lattice sites. Fast and robust transport of Bose-Einstein condensates has application in condensate mixing experiments [107]. This might require extended methods to those discussed in chapter 5, as the combination of lattice and external trapping potential is very different across large numbers of lattice sites. Successful mixing would also require an extension of the current analysis.

Further outlook could generalise these methods for two and three dimensional lattices allowing for more general applicability, this should not be particularly difficult to do although would be substantially more time consuming to simulate.

Asymmetric scattering with non-Hermitian potentials

In chapter 6, we investigated devices that produce asymmetries in transmission and reflection coefficients, to achieve this asymmetry we designed a number non Hermitian potentials to achieve reflection-transmission asymmetries. These scattering asymmetries have applications in mirrors, filters, invisibility devices, diodes and Maxwell demon devices.

The discussion is developed for quantum particles but could be extended to the design of asymmetrical optical devices. Another avenue for continuing this work one could consider different ways of producing the desired asymmetries in transmission and reflection, through introducing time dependence into potentials or considering non-linear systems.

As further outlook one could consider ways to physically implement the the non local effective potentials discussed. While physical realization of these potentials would be difficult, the technological prospects are extraordinary.

Bibliography

[1] I. Bloch, J. Dalibard, and W. Zwerger. In: *Rev. Mod. Phys.* **80** (2008), p. 885.

[2] URL: https://www.nobelprize.org/prizes/physics/2001/summary/.

[3] URL: https://www.nobelprize.org/prizes/physics/2012/summary/.

[4] I. M. Georgescu, S. Ashhab, and F. Nori. In: *Rev. Mod. Phys.* **86** (2014), p. 153.

[5] R. P. Feynman. In: *Int. J. Theor. Phys.* **21** (1982), p. 467.

[6] N. V. Vitanov et al. In: *Rev. Mod. Phys.* **89** (2017), p. 015006.

[7] R. Menchon-Enrigh et al. In: *Rep, Prog. Phys* **79** (2016), p. 074401.

[8] E. Torrontegui et al. In: *Adv. At. Mol. Opt. Phys.* **62** (2013), p. 117.

[9] D .Guéry-Odelin et al. In: *Rev. Mod. Phys.* **91** (2019), p. 045001.

[10] M. S. Sarandy, E. I. Duzzioni, and R. M. Serra. In: *Phys. Lett. A* **38** (2011), p. 3343.

[11] E. Torrontegui et. al. In: *New J. Phys.* **14** (2012), p. 013031.

[12] J. G. Muga et al. In: *Journal of Physics B: Atomic, Molecular and Optical Physics* **42** (2009), p. 241001.

[13] M. Born and V. Fock. In: *Zeitschrift für Physik* **51** (1928), p. 165.

[14] G. Rigolin and G. Ortiz. In: *Phys. Rev. Lett.* **104** (2010), p. 170406.

[15] H. R. Lewis and W. B. Riesenfeld. In: *Journal of Mathematical Physics* **8** (1969), p. 1458.

[16] H. R. Lewis and P. G. L. Leach. In: *Journal of Mathematical Physics* **23** (1982), p. 2371.

[17] A. K . Dhara and S. V. Lawande. In: *Journal of Physics A: Mathematical and General* **17** (1984), p. 2423.

[18] X. Chen et al. In: *Phys. Rev. Lett.* **104** (2010), p. 063002.

[19] E. Torrontegui et al. In: *Phys. Rev. A* **83** (2011), p. 013415.

[20] R. Shankar. *Principles of Quantum Mechanics*. Dover, 1994.

[21] W. Pauli. In: *Phys. Rev.* **58** (1940), p. 716.

[22] S. Blundell and K. Blundell. *Concepts in Thermal Physics 2nd Ed.* Oxford University Press, 2009.

[23] M. H. Anderson et al. In: *Science* **269** (1995), p. 198.

[24] C. C. Bradley et al. In: *Phys. Rev. Lett.* **75** (1995), p. 1687.

[25] K. B. Davis et al. In: *Phys. Rev. Lett.* **75** (1995), p. 3969.

[26] C. J. Pethick and H. Smith. *Bose-Einstein Condensation in Dilute Gases 2nd Ed.* Cambridge University Press, 2008.

[27] W. Ketterle and N. J. Van Druten. In: *Adv. At. Mol. Opt. Phys.* **37** (1996), p. 181.

[28] E. P. Gross. In: *J. Math. Phys.* **2** (1963), p. 195.

[29] L. P. Pitaevskii. In: *Sov. Phys. JETP* **13** (1961), p. 451.

[30] I. M. Gelfand and S. V. Fomin. *Calculus of Variations*. Dover, 2000.

[31] M. H. A. Davis. *Markov Models and Optimisation*. Chapman and Hall, 1993.

[32] A. Messiah. *Quantum mechanics*. Elsevier Science B.V., 2016.

[33] S. Guérin, S. Thomasand, and H. R. Jauslin. In: *Phys. Rev. A* **65** (2002), p. 023409.

[34] S. Guérin, V. Hakobyan, and H. R. Jauslin. In: *Phys. Rev. A* **84** (2011), p. 013423.

[35] S. Martínez-Garaot et al. In: *Phys. Rev. A* **92** (2015), p. 043406.

[36] A. Ruschhaupt and J. G. Muga. In: *J. Mod. Optics* **61** (2013), p. 828.

[37] M. Demirplak and S. A. Rice. In: *J. Phys. Chem. A* **107** (2003), p. 9937.

[38] M. V. Berry. In: *J. Phys. A* **42** (2009), p. 365303.

[39] X. Chen et al. In: *Phys. Rev. Lett.* **105** (2010), p. 123003.

[40] P. W. Anderson. In: *Phys. Rev. Lett.* **18** (1967), p. 1049.

[41] G. D. Mahan. *Many Particle Physics*. Springer-Verlag, Berlin/New York, 2000.

[42] P. Nozières and C. T. De Dominicis. **178**. 1969, p. 1097.

[43] J. Goold et al. In: *Phys. Rev. A* **84** (2011), p. 063632.

[44] S. Campbell et al. In: *Phys. Rev. A* **90** (2014), p. 013617.

[45] Th. Busch et al. In: *Europhys. Lett.* **44** (1998), p. 1.

[46] G. Ferrari. In: *Phys. Rev. A* **59** (1999), R4125(R).

[47] B. DeMarco, S. B. Papp, and D. S. Jin. In: *Phys. Rev. Lett.* **86** (2001), p. 5409.

[48] B. O'Sullivan and Th. Busch. In: *Phys. Rev. A* **79** (2009), p. 033602.

[49] A. Omran et al. In: *Phys. Rev. Lett.* **115** (2015), p. 263001.

[50] F. Serwane et al. In: *Science* **332** (2011), p. 336.

[51] A. del Campo and J. G. Muga. In: *Phys. Rev. A* **78** (2008), p. 023412.

[52] M. Pons et al. In: *Phys. Rev. A* **79** (2009), p. 033629.

[53] W. Ketterle and N. J. V. Druten. "Evaporative Cooling of Trapped Atoms". In: *Advances In Atomic, Molecular, and Optical Physics, Academic Press* **37** (1996), p. 181.

[54] W. Ketterle and M.W. Zwierlein. "Ultracold Fermi Gases, Proceedings of the International School of Physics Enrico Fermi, Course CLXIV, Varenna". In: *IOS Press, Amsterdam* (2008).

[55] B. DeMarco and D.S. Jin. In: *Science* **285** (1999), p. 1703.

[56] G.B. Partridge et al. In: *Science* **311** (2006), p. 503.

[57] Y. Shin et al. In: *Nature* **451** (2008), p. 689.

[58] S. Giorgini, L.P. Pitaevskii, and S. Stringari. In: *Rev. Mod. Phys.* **80** (2008), p. 1215.

[59] E. Torrontegui et al. In: *Phys. Rev. A.* **85** (2012), p. 033605.

[60] E. Torrontegui et al. In: *New J. Phys.* **14** (2012), p. 013031.

[61] Qi Zhang et al. In: *J. Phys. B: At. Mol. Opt. Phys.* **49** (2016), p. 125503.

[62] E. Torrontegui et al. In: *Phys. Rev. A.* **87** (2013), p. 033630.

[63] S. Martínez-Garaot et al. In: *Phys. Rev. Lett.* **111** (2013), p. 213001.

[64] A. Couvert et al. In: *Europhys. Lett.* **83** (2008), p. 13001.

[65] Q. Zhang, X. Chen, and D. Guéry-Odelin. In: *Phys. Rev. A* **92** (2015), p. 043410.

[66] H. J. Metcalf and P. v. d. Straten. *Laser Cooling and Trapping*. 1999.

[67] A. M. Dudarev et al. In: *Europhys. Lett.* **70** (2005), p. 761.

[68] A. Ruschhaupt, J. G. Muga, and M. G. Raizen. In: *J. Phys. B* **39** (2006), p. 3833.

[69] M. G. Raizen. In: *Science* **324** (2009), p. 1403.

[70] A. Ruschhaupt and J. G. Muga. In: *Phys. Rev. A* **70** (2004), 061604(R).

[71] M. G. Raizen et al. In: *Phys. Rev. Lett.* **94** (2005), p. 053003.

[72] A. Ruschhaupt and J. G. Muga. In: *Phys. Rev. A* **73** (2006), p. 013608.

[73] A. Ruschhaupt, J. G. Muga, and M. G. Raizen. In: *J. Phys. B* **39** (2006), p. L133.

[74] A. Ruschhaupt and J. G. Muga. In: *Phys. Rev. A* **76** (2007), p. 013619.

[75] A. Ruschhaupt and J. G. Muga. In: *Eur. Phys. J. Spec. Top.* **159** (2008), p. 127.

[76] J. J. Thorn et al. In: *Phys. Rev. Lett.* **100** (2008), p. 240407.

[77] J. J. Thorn et al. In: *Phys. Rev. A* **79** (2009), p. 063402.

[78] A. Steyerl et al. In: *Phys. Lett. A.* **116** (1986), p. 347.

[79] C.S. Adams, M. Sigel, and J. Mlynek. In: *Phys. Rep.* **240** (1994), p. 143.

[80] A.D. Cronin, J. Schmiedmayer, and D.E. Pritchard. In: *Rev. Mod. Phys.* **81** (2009), p. 1051.

[81] A. Steane et al. In: *Phys. Rev. Lett.* **74** (1995), p. 4972.

[82] M. Arndt et al. In: *Phys. Rev. A* **53** (1996), p. 3369.

[83] P. Szriftgiser et al. In: *Phys. Rev. Lett.* **77** (1996), p. 4.

[84] Y. Colombe et al. In: *Phys. Rev. A.* **72** (2005), p. 061601.

[85] S. Rosenblum et al. In: *Phys. Rev. Lett.* **112** (2014), p. 120403.

[86] T. M. Roach et. al. In: *Phys. Rev. Lett.* **75** (1995), p. 629.

[87] G. Reinaudi et al. In: *Eur. Phys. J. D.* **40** (2006), p. 4015.

[88] B. Holst and W. Allison. In: *Nature* **390** (1997), p. 244.

[89] K. Fladischer et al. In: *New J. Phys.* **12** (2010), p. 033018.

[90] G. Anemone et al. In: *Phys. Rev. B.* **95** (2017), p. 205428.

[91] A. Libson et al. In: *New J. Phys.* **8** (2006), p. 77.

[92] E. Narevicius et al. In: *Phys. Rev. Lett.* **98** (2007), p. 103201.

[93] S. Schmidt, J. G. Muga, and A. Ruschhaupt. In: *Phys. Rev. A* **80** (2009), p. 023406.

[94] S. Schmidt. *Quantum-Optical Control Techniques for Atomic Motional States, (Doctoral thesis)*. 2012.

[95] G.C. Hegerfeldt, and T. S. Wilser 1992. "Classical and Quantum Systems, Proceedings of the Second International Wigner Symposium". In: Singapore: World Scientific, 1992.

[96] G. C. Hegerfeldt. In: *Phys. Rev. A* **47** (1993), p. 449.

[97] H. Carmichael. *An Open Systems Approach to Quantum Optics*. Springer-Verlag, Berlin, 1993.

[98] J. Dalibard, Y. Castin, and K. Mölmer. In: *Phys. Rev. Lett.* **68** (1992), p. 580.

[99] D. Barredo et al. In: *Science* **354** (2016), p. 1021.

[100] D. Barredo et al. In: *Nature* **561** (2018), p. 79.

[101] J. Beugnon, C. Tuchendler, and H. Marion et al. In: *Nature Phys* **3** (2007), p. 696.

[102] A. Couvert et al. In: *EPL (Europhysics Letters)* **1** (2008), p. 13001.

[103] M. Endres et al. In: *Science* **6315** (2016), p. 1024.

[104] S. Murmann et al. In: *Phys. Rev. Lett.* **115** (2015), p. 215301.

[105] A. M. Kaufmann et al. In: *Nature* **527** (2015), p. 208.

[106] A. Kumar et al. In: *nature* **561** (2018), p. 83.

[107] L. Reichsöllner et al. In: *Phys. Rev. Lett.* **118** (2017), p. 073201.

[108] M-G. Hu et al. In: *Phys. Rev. Lett.* **5** (2016), p. 6.

[109] J.G. Muga et al. In: *Phys. Rep.* **395** (2004), p. 357.

[110] A. Ruschhaupt, F. Delgado, and J. G. Muga. In: *J. Phys. A: Math. Gen.* **38** (2005), p. L171.

[111] J. R. Taylor. *Scattering Theory*. 1972.

[112] A. Mostafazadeh. In: *Int. J. Geom. Methods Mod. Phys.* **07** (2010), p. 1191.

[113] M. Znojil. *Non-Selfadjoint Operators in Quantum Physics*. Wiley, Hoboken (New Jersey), 2015, p. 7.

[114] S. Nixon and J. Yang. In: *Phys. Rev. A* **93** (31802(R)), p. 2016.

[115] S. Nixon and J. Yang. In: *Opt. Lett.* **41** (2016), p. 2747.

[116] Y.-L. Xu et al. In: *IEEE Photonics J.* **6** (2014), p. 0600507.

[117] Y. Huang, C. Min, and G. Veronis. In: *Opt. Exp.* **24** (22219), p. 2017.

[118] Z. Lin et al. In: *Phys. Rev. Lett.* **106** (213901), p. 2011.

[119] X. Yin and X. Zhang. In: *Nat. Mater.* **12** (2013), p. 175.

[120] J. P. Palao, J. G. Muga, and R. Sala. In: *Phys. Rev. Lett.* **80** (1998), p. 5469.

[121] S. Brouard, D. Macías, and J. G. Muga. In: *J. Phys. A* **27** (1994), p. L439.

[122] J. P. Palao and J. G. Muga. In: *Chem. Phys. Lett.* **292** (1998), p. 1.

[123] R. Snieder. In: *Inverse Probl.* **6** (1990), p. 247.

[124] A. Mostafazadeh. In: *Phys. Rev. A* **89** (2014), p. 012709.

[125] S. A. R. Horsley, M. Artoni, and G. C. La Rocca. In: *Nat. Phot.* **9** (2015), p. 436.

[126] S. Longhi. In: *J. Phys. A: Math. Theor* **47** (2014), p. 485302.

[127] V. V. Konotop, J. Yang, and D. A. Zezyulin. In: *Rev. Mod. Phys.* **88** (2016), p. 035002.

[128] Z. Yu and S. Fan. In: *Nat. Photon.* **3** (2009), p. 91.

[129] S. Longhi. In: *EPL* **118** (2017), p. 20004.

[130] V. V. Konotop and D. A. Zezyulin. In: *Opt. Lett.* **42** (2017), p. 5206.

[131] Y. V. Kartashov, V. V. Konotop, and D. A. Zezyulin. In: *EPL* **107** (2014), p. 50002.

[132] D. A. Zezyulin and Y. V. Kartashovand V. V. Konotop. In: *Opt. Lett.* **42** (2017), p. 1273.

[133] A. Ruschhaupt et al. In: *EPL* **67** (2004), p. 1.

[134] H. Feshbach. In: *Ann. Phys. (N.Y.)* **5** (1958), p. 357.

[135] H. Feshbach. In: *Ann. Phys. (N.Y.)* **19** (1962), p. 287.

[136] C. M. Bender and S. Boettcher. In: *Phys. Rev. Lett.* **80** (1998), p. 5243.

[137] A. Guo et al. In: *Phys. Rev. Lett.* **103** (2009), p. 093902.